Évolution de l'industrie de la chaussure : vers des pratiques durables grâce à la fabrication avancée

par

Chahine GHIMOUZ

MÉMOIRE PAR ARTICLES PRÉSENTÉ À L'ÉCOLE DE TECHNOLOGIE SUPÉRIEURE COMME EXIGENCE PARTIELLE À L'OBTENTION DE LA MAÎTRISE AVEC MÉMOIRE EN GÉNIE MÉCANIQUE
M. Sc. A.

MONTRÉAL, LE 10 DÉCEMBRE 2023

ÉCOLE DE TECHNOLOGIE SUPÉRIEURE
UNIVERSITÉ DU QUÉBEC

PRÉSENTATION DU JURY

CE MÉMOIRE A ÉTÉ ÉVALUÉ

PAR UN JURY COMPOSÉ DE :

M. Lucas A. Hof, directeur de mémoire
Département de Génie mécanique à l'École de technologie supérieure

M. Jean-Pierre Kenné, codirecteur de mémoire
Département de Génie mécanique à l'École de technologie supérieure

M. Éric Wagnac, président du jury
Département de Génie mécanique à l'École de technologie supérieure

Mme Nicole Demarquette, membre du jury
Département de Génie mécanique à l'École de technologie supérieure

IL A FAIT L'OBJET D'UNE SOUTENANCE DEVANT JURY ET PUBLIC

LE 06 DECEMBRE 2023

À L'ÉCOLE DE TECHNOLOGIE SUPÉRIEURE

REMERCIEMENTS

Évolution de l'industrie de la Chaussure : vers des pratiques durables grâce à la fabrication avancée

CHAHINE GHIMOUZ

RÉSUMÉ

À une époque où notre planète fait face à des défis environnementaux sans précédent, tels que la surexploitation des ressources naturelles et l'augmentation des émissions de gaz à effet de serre, il devient impératif de prendre des mesures pour opérer une transition écologique dans nos pratiques industrielles et de consommation. Cette situation a engendré un appel mondial pressant à repenser notre approche de la production de biens de consommation, incitant les industries à adopter des modèles plus durables et respectueux de l'environnement. C'est dans ce contexte que la présente étude explore les opportunités offertes par l'économie circulaire dans la fabrication de chaussures à talons hauts, en tirant parti des technologies avancées.

Deux objectifs distincts ont été poursuivis avec succès. Le premier a conduit à la création d'un prototype de chaussures fabriquées par impression 3D, incarnant les principes de l'écoconception et de l'économie circulaire grâce à l'utilisation de la fabrication additive. Cette approche a permis de réduire le nombre de composants et d'assembler les chaussures sans recours à des colles, transformant ainsi le processus de conception de produits. Le deuxième objectif a impliqué une analyse approfondie du vieillissement des polymères imprimés en 3D face à des conditions environnementales variables. Cette démarche vise à modéliser le processus de vieillissement des polymères et à fournir des informations cruciales pour évaluer la durabilité des chaussures dans une économie circulaire.

Les résultats de cette étude posent les fondations d'une approche novatrice pour la fabrication de produits respectueux de l'environnement, tout en répondant aux normes élevées de qualité. Pour renforcer davantage ces résultats, des essais pratiques étendus sont vivement recommandés, en favorisant une collaboration continue entre les domaines de la technologie des matériaux, de la conception et de la fabrication. En dernière analyse, cette étude met en

VIII

lumière la convergence entre l'innovation technologique et les principes de l'économie circulaire. Elle démontre comment cette synergie peut agir comme un catalyseur, favorisant une transformation positive au sein de l'industrie. Ces conclusions ouvrent des perspectives prometteuses pour des produits plus durables et respectueux de l'environnement.

Evolution of the Footwear Industry: Towards Sustainable Practices through Advanced Manufacturing

CHAHINE GHIMOUZ

ABSTRACT

At a time when our planet is facing unprecedented environmental challenges, such as the overexploitation of natural resources and the increase in greenhouse gas emissions, it is becoming imperative to take steps to make an ecological transition in our industrial and consumer practices. This situation has given rise to an urgent global call to rethink our approach to the production of consumer goods, encouraging industries to adopt more sustainable and environmental respectful models.

It is against this backdrop that the present study explores the opportunities offered by the circular economy in high-heeled shoe manufacturing, taking advantage of advanced technologies. Two distinct objectives were successfully pursued. The first led to the creation of a prototype of shoes manufactured by 3D printing, embodying the principles of eco-design and the circular economy using additive manufacturing. This approach made it possible to reduce the number of components and assemble the shoes without the use of adhesives, thus transforming the product design process. The second objective involved an in-depth analysis of the aging of 3D-printed polymers in the face of varying environmental conditions. This aims to model the aging process of polymers and provide crucial information for assessing the sustainability of footwear in a circular economy.

The results of this study lay the foundations for an innovative approach to manufacturing products that are environmentally friendly, while meeting high quality standards. To further strengthen these results, extensive practical testing is strongly recommended, fostering ongoing collaboration between the fields of materials technology, design, and manufacturing. In the final analysis, this study highlights the convergence between technological innovation and the principles of the circular economy. It demonstrates how this synergy can act as a

X

catalyst, fostering positive transformation within the industry. These findings open up promising prospects for more sustainable, environmentally friendly products.

XII

LISTE DES TABLEAUX

Page

LISTE DES FIGURES

LISTE DES ABRÉVIATIONS, SIGLES ET ACRONYMES

CE	Circular Economy
EC	Économie Circulaire
AM	Additive Manufacturing
FEA	Finite Element Analysis
TPU	Thermoplastic PolyUrethane
PA12	PolyAmide 12
ASTM	American Society for Testing and Materials
SLS	Selective Laser Sintering
MJF	Multi Jet Fusion
TPMS	Triply Periodic Minimal Surface
FA	Fabrication Additive
DfA	Design for Assembly
DfD	Design for Disassembly
DfAM	Design for Additive Manufacturing
GHG	Greenhouse Gases
CM	Circular Manufacturing

LISTE DES SYMBOLES ET UNITÉS DE MESURE

H_{max}	Déflection maximale [mm]
H	Déflection [mm]
ε_{max}	Déformation maximale [mm/mm]
Y	Module de Young [MPa]
UTS	Ultimate Tensile Strength [MPa]
E	Allongement à la rupture [%]
G	Coefficient de Cisaillement [MPa]
v	Coefficient de Poisson [/]
l	Longueur des tiges du snapfit [mm]
r	Rayon extérieure des tiges du snapfit [mm]
J	Moment d'inertie [mm^4]
α1	Angle d'attaque du snapfit [deg]
μ	Coefficient de frottement [/]
E_s	Module d'élasticité sécant [MPa]
A	Surface sujette au cisaillement [mm^2]
τ_b	60% de la contrainte ultime du matériau [MPa]
F1	Force nécessaire à l'assemblage du snapfit [N]
F2	Force nécessaire au désassemblage du snapfit [N]
k	Constante de raideur du ressort monté sur le duromètre [/]
F_0	Constante liée au duromètre [N]
p_0	Constante liée au duromètre [cm]
Mi	Indentabilité mécanique du duromètre
T1	Big toe
T2-5	Small toes
M1	First Metatarsal
M23	Central Forefoot
M45	Lateral Forefoot
MF	Midfoot

XXII

MH	medial Heel
LH	Lateral Heel

INTRODUCTION

En ce XXIe siècle, la consommation mondiale de ressources naturelles est en constante augmentation. Actuellement, les quantités de ressources naturelles consommées annuellement dans le monde sont tellement excessives que les ressources naturelles sont épuisées à un rythme supérieur à celui nécessaire à leur régénération par la planète selon la fondation World Wildlife Fund (WWF, 2012). À l'heure actuelle, il faut à la planète 1,7 an pour régénérer toutes les ressources consommées en un an (Overshoot, 2021). En 2010, 72 milliards de tonnes de matières premières ont été extraites et consommées, soit le double par rapport aux quantités extraites en 1980, selon un rapport de l'Organisation de coopération et de développement économiques publié en 2015 (OCDE, 2015). Avec la croissance économique actuelle, la consommation annuelle atteindra la barre symbolique des 100 milliards de tonnes vers 2030 (Bleischwitz, Welfens, & Zhang, 2009). Cependant l'activité humaine émet de plus en plus de gaz à effet de serre chaque année, ce chiffre dépasse les 48.9 giga tonnes d'équivalent CO2 en 2018 selon Climate Watch Data (CLIMATEWATCH, 2019) dont 1.7 giga tonnes équivalent CO2 sont émises uniquement par l'industrie du textile en 2015 et si la tendance continue le BCG Retail value project prévoit 2.7 giga tonnes d'équivalent CO2 émises en 2030 (Eder-Hansen et al., 2017); soit une augmentation de 63%. De plus pour les déchets de l'industrie du vêtement et de la chaussure qui passeront de 92 méga tonnes en 2015 à 148 méga tonnes en 2030 selon la même source. Sachant qu'uniquement 5% des chaussures sont recyclées dans le monde (Lee & Rahimifard, 2012), il est donc très important d'agir sur ce levier afin d'en limiter les dégâts.

Cette accélération de la consommation de matières premières et des émissions de gaz à effet de serre est en partie due au système économique dans lequel nous avons évolué au cours du siècle dernier. Ce système est un modèle linéaire (Prendre, Fabriquer, Utiliser et Jeter), également appelé "économie linéaire". Afin de surmonter ce problème de surconsommation et le déclin environnementale que connaît la planète, un modèle plus durable, celui de "l'économie circulaire (EC)", a été proposé. Cette nouvelle façon d'aborder l'économie est présentée comme l'état d'esprit des entreprises qui permettra d'évoluer vers un développement durable à long terme (McDowall et al., 2017). Le modèle de la fabrication circulaire s'impose

donc comme une des solutions à considérer. La conception du produit, les matériaux utilisés et sa fabrication jouent un rôle clé dans sa recyclabilité (Ellen MacArthur Foundation & IDEO, 2018). La conception circulaire consiste à penser le produit non pas pour son utilisateur mais pour le système complexe où le produit va exister, augmentant ainsi sa recyclabilité ou sa réutilisation et faciliter sa réinsertion dans une boucle de fabrication fermée (Ellen MacArthur Foundation, 2017).

Ce mémoire est subdivisé en trois chapitres. Le chapitre 1, présente une revue de littérature centré sur le modèle d'économie circulaire , une nouvelle manière de penser notre fabrication de biens de consommation afin de réduire l'impact écologique que nous avons sur notre planète. La fabrication additive en tant que composante de la solution pour une transition vers un modèle de fabrication en boucle fermée dite fabrication circulaire. La dégradation des polymères ainsi que l'importance de la compréhension des mécanismes en jeu et leurs conséquences pour une meilleure anticipation du vieillissement du matériau , par conséquent une amélioration de la durée de vie des biens de consommation. Un aperçu des matériaux architecturé est aussi proposé dans ce chapitre, leur classification, et les avantages qu'ils proposent au monde de la conception. Ce chapitre, sera conclus par une conclusion de la revue de littérature réalisée. Le chapitre 2 présente la problématique les objectifs de cette étude ainsi que la méthodologie adoptée. Dans le chapitre 3, un cas d'application est proposé en adoptant les méthodes de « design for circularity » pour démontrer la faisabilité de l'intégration de la fabrication additive pour un objectif de facilitation d'introduction du produit dans une boucle de fabrication circulaire par la conception. Dans le chapitre 4, il est proposé une étude du vieillissement du PA12 (utilisé dans le cas d'étude dans le chapitre 3) en fonction de multiples facteurs, afin d'anticiper la dégradation du matériau et ainsi améliorer la longévité des pièces conçues. L'étude du vieillissement sera basée sur une approche statistique, et intègrera un plan d'expérience multifactoriel pour mieux comprendre l'effet individuel des facteurs environnementaux ainsi que l'effet d'interactions binaires de ces facteurs. Le chapitre 3 est présenté sous forme d'article de revue scientifique avec comité de lecture publié dans le journal « Materials & Design » qui peut être consulté sous Material & Design volume 233 article number 112224 (https://doi.org/10.1016/j.matdes.2023.112224) , le chapitre 4 est aussi

présenté sous forme d'article de revue scientifique avec comité de lecture soumis pour publication dans le journal « Additive Manufacturing ».

CHAPITRE 1

REVUE DE LITTÉRATURE

1.1   Introduction

Le mémoire s'ouvre sur un chapitre d'une importance capitale, dédié à une revue de littérature approfondie. Ce premier volet constitue une exploration minutieuse de divers aspects qui sous-tendent le présent travail, offrant ainsi une toile de fond complète et éclairante. Les multiples facettes abordées dans ce chapitre inaugural sont essentielles pour cerner le contexte global dans lequel s'inscrit la recherche en question.

- **L'économie circulaire**, en tant que premier pilier abordé, constitue un concept pivot dans la perspective contemporaine de durabilité et de gestion responsable des ressources. Son influence sur les approches de production, de consommation et d'élimination des biens servira de toile de fond pour contextualiser le travail à venir.

- **La fabrication additive** également connue sous le nom d'impression 3D, occupe une place centrale dans la réflexion sur les nouvelles méthodes de production. Son potentiel pour transformer les pratiques de fabrication en réduisant les déchets et en permettant une personnalisation accrue offre des perspectives innovantes pour le développement durable.

- **Les matériaux architecturaux** en tant que troisième aspect examiné, jouent un rôle crucial dans la conception responsable. Le choix approprié de matériaux influe sur divers aspects de la durabilité, de la performance énergétique à l'empreinte carbone, ce qui en fait un élément essentiel de cette étude.

- **La dégradation des polymères** constitue un autre point de discussion clé. Comprendre comment les matériaux interagissent avec leur environnement et comment ils évoluent au fil du temps est d'une importance primordiale pour concevoir des produits durables, capables de résister aux contraintes environnementales.

- **Fabrication dans l'industrie de la chaussure**, une revue des approches de conception de chaussures durables, basée sur la fabrication additive, complétera cette introduction. Les chaussures servent d'exemple concret pour aborder les défis de conception durable

dans l'industrie de la mode, et cette section mettra en lumière les stratégies et les idées qui ont émergé dans ce domaine.

1.2 Modèle d'Économie circulaire (EC)

Une présentation du modèle d'Économie circulaire ainsi que ses piliers sont présentées dans cette section.

1.2.1 Présentation du modèle

L'économie circulaire est un concept qui a gagné du terrain ces dernières années en raison de son potentiel à créer un système économique plus durable et plus efficace (Sassanelli, Rosa, Rocca, & Terzi, 2019). En effet, elle permet de réduire l'impact environnemental de notre économie tout en contribuant au bien-être des individus et des collectivités. Elle est ainsi décrite comme «an economy that is restorative and regenerative by design» (Ellen MacArthur Foundation). Historiquement, l'idée d'une économie circulaire remonte aux années 1960, avec l'émergence du mouvement écologiste. Toutefois, ce n'est qu'au début des années 2000 que le concept a reçu une attention particulière, avec la publication d'un rapport de la Fondation Ellen MacArthur en 2013 intitulé « Towards the Circular Economy : Economic and Business Rationale for an Accelerated Transition » (Ellen MacArthur Foundation, 2015).

La Figure 1.1 représente les différentes boucles constituant l'EC d'après la fondation Ellen MacArthur, le schéma montre le flux des matières premières ainsi que les sources d'énergies qui entrent dans la fabrication des biens et des services.
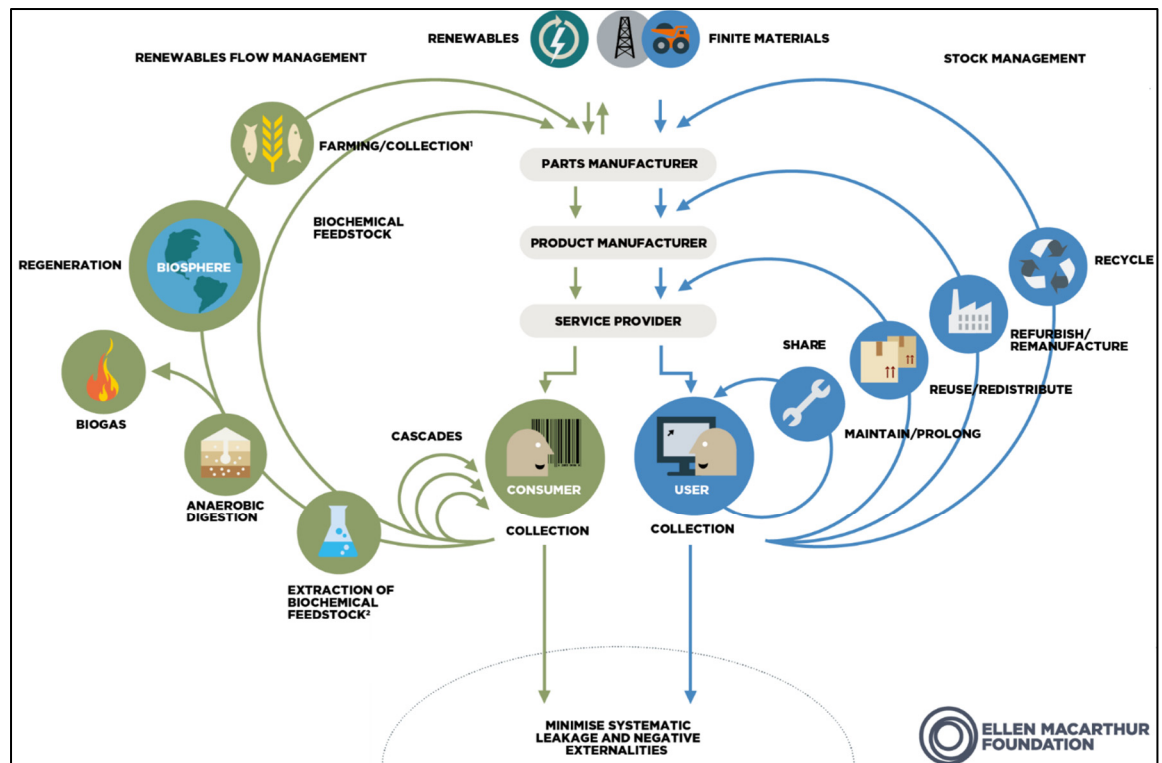
Figure 1.1 Schéma représentant les différentes boucles de l'Économie Circulaire (EC)
Tirée de Ellen MacArthur Foundation (2015, p.06)

1.2.2　Les piliers de l'Économie circulaire

L'économie circulaire se caractérise par une série de principes visant à promouvoir l'utilisation efficace des ressources, à réduire les déchets et à créer de la valeur à partir des déchets. Les sept piliers de l'économie circulaire selon (Agence de l'Environnement et de la Maîtrise de l'Énergie) sont présentés dans la Figure 1.2.
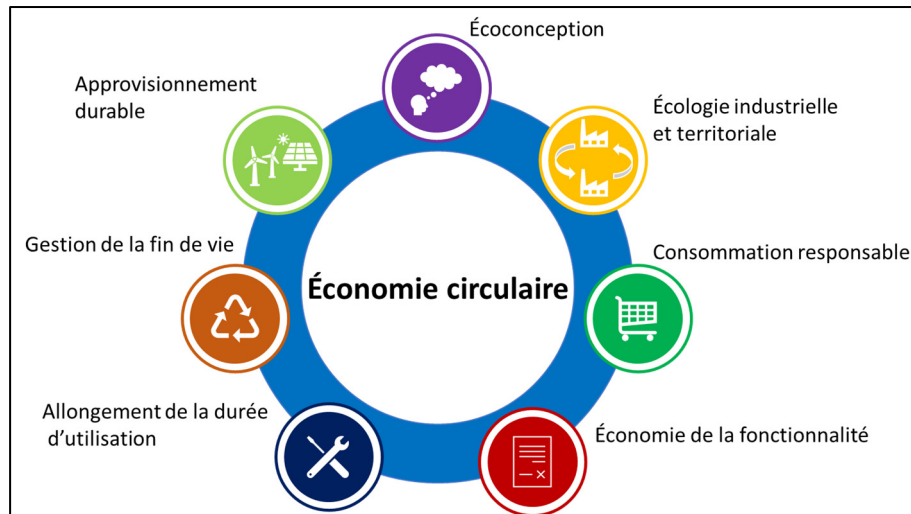
Figure 1.2 Les 7 piliers de l'Économie Circulaire (EC)

- Tout d'abord, l'approvisionnement durable concerne les méthodes d'exploitation et d'achat responsables, qui visent à optimiser l'utilisation des ressources tout en limitant leur impact environnemental. Cette approche est applicable à divers secteurs, tels que les mines, les carrières, l'agriculture, la foresterie et les énergies renouvelables.

- L'écoconception consiste à concevoir des processus, des biens et des services en prenant en compte leur cycle de vie complet afin de minimiser leur impact environnemental. Cette approche est particulièrement importante car elle permet de réduire les impacts dès la conception du produit, plutôt qu'en fin de vie.

- L'écologie industrielle et territoriale, également appelée symbiose industrielle, est un modèle d'organisation interentreprises qui favorise l'échange de flux ou la mutualisation des besoins. Cette approche, qui s'inspire du fonctionnement des écosystèmes naturels, vise à optimiser l'utilisation des ressources dans un territoire donné, qu'il s'agisse d'énergies, d'eau, de matières, de déchets ou d'expertises.

- L'économie de la fonctionnalité privilégie l'usage à la possession, en vendant des services liés aux produits plutôt que les produits eux-mêmes. Cette approche favorise l'utilisation optimale des ressources et encourage les entreprises à concevoir des produits durables.

- La consommation responsable implique de prendre en compte l'impact environnemental à toutes les étapes du cycle de vie d'un produit, que ce soit en tant qu'entreprise ou en tant

que consommateur citoyen. Cette approche encourage les acheteurs à choisir des produits durables et respectueux de l'environnement.

- L'allongement de la durée d'utilisation d'un produit peut être favorisé par la réparation, la vente ou le don d'occasion, ainsi que par l'achat d'occasion dans le cadre du réemploi ou de la réutilisation. Cette approche permet de réduire le gaspillage et d'optimiser l'utilisation des ressources.

- Enfin, la gestion de la fin de vie, ce qui consiste à valoriser au maximum la matière en établissant des stratégies basées sur le principe des 6-R telles que: Reduce, Reuse. Recycle, Recover, Redesign Remanufacture (Jawahir & Bradley, 2016).

Les avantages de l'économie circulaire sont nombreux. Elle permet notamment de réduire les déchets et l'utilisation de nouvelles ressources, favorise la création d'emplois (Lavery, Pennell, & Evans, 2014), l'innovation et la croissance économique (Lacy & Rutqvist, 2015). En effet, de nouveaux modèles d'entreprise et de nouvelles technologies sont développés pour soutenir ce système économique durable. Cependant, l'économie circulaire présente également des défis plus ou moins difficiles à surmonter. L'une des principales critiques est que sa mise en œuvre nécessite des investissements et des infrastructures importants (Gedam, Raut, Lopes de Sousa Jabbour, Tanksale, & Narkhede, 2021), ce qui peut être difficile pour les petites entreprises et les pays moins développés d'adopter le modèle de l'économie circulaire (Badhotiya, Avikal, Soni, & Sengar, 2022). En outre, l'économie circulaire exige un changement significatif du comportement des consommateurs, ce qui peut être difficile à réaliser. Cependant, ces défis ne doivent pas décourager les entreprises et les gouvernements de travailler ensemble pour créer un système économique plus durable et plus efficace.

1.3 Fabrication additive (FA) des polymères

Dans cette section il est présenté le principe de la FA ainsi que les principales technologies existantes se basant sur des polymères, une comparaison entre les deux technologies les plus rependues dans l'industrie *Selective Laser Sintering* (SLS) et *Multi Jet Fusion* (MJF).

1.3.1 Présentation de la technologies FA

Ce que nous appelons communément plastiques sont une classe de matériaux développé et étudié de manière intensive depuis le début du 20ieme siècle et sont produits en masse depuis maintenant presque cent ans (Gewert, Plassmann, & MacLeod, 2015). Leurs masses peu élevées, leurs propriétés mécaniques flexibles leurs procure un vaste champ d'application dans le domaine de l'ingénierie. En comparaison avec les procédés de fabrication comme l'injection moulée, l'extrusion ou le thermoformage, la fabrication additive (FA) est un procédé de fabrication très jeune qui n'a toujours pas atteint sa maturité, ce procédé a fait ses débuts dans les années 1980.
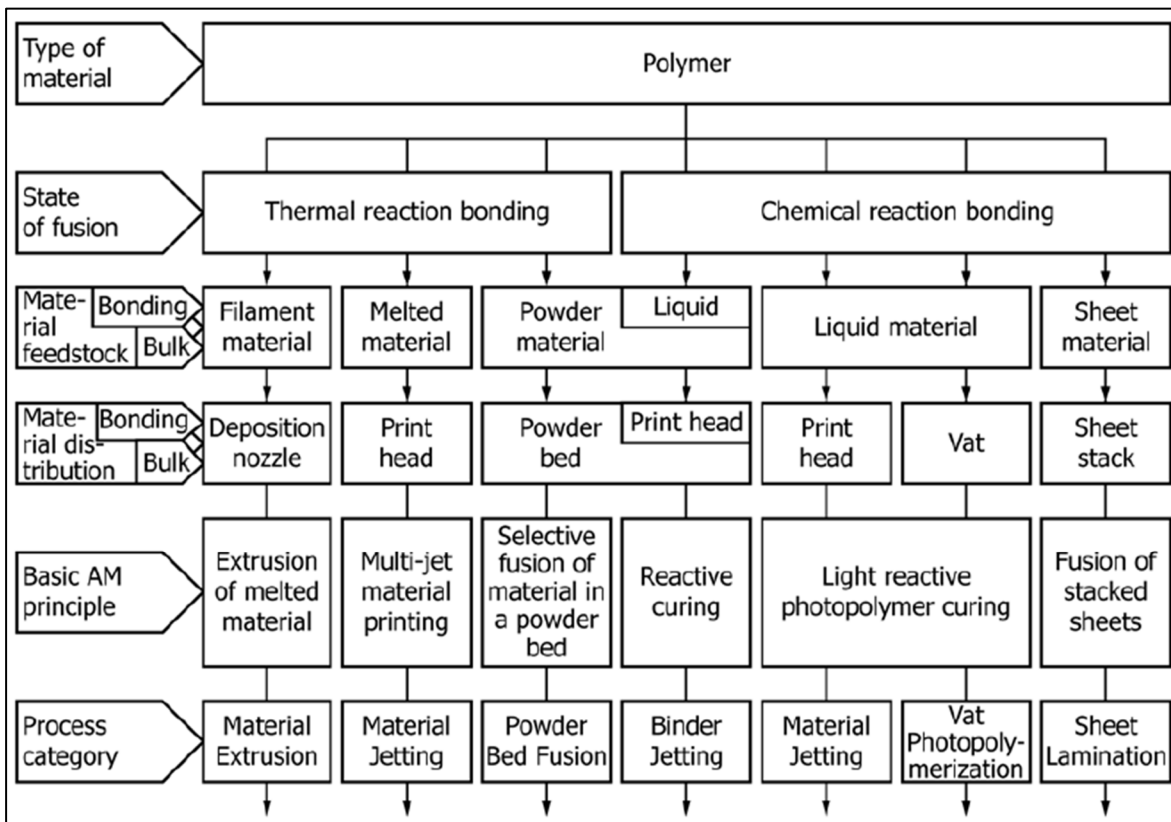
Figure 1.3 Vue d'ensemble des principes de traitement par FA en une seule étape pour les matériaux polymères

Tiré de ISO/ASTM (2022, p.08)

La Figure 1.3 tirée de la norme ISO/ASTM 52900:22 (ISO/ASTM, 2022) résume l'entièreté des technologies existante à ce jour utilisant les polymères comme matériaux pour la FA. Les technologies présentées sont classées selon le type de polymère (thermoformable ou thermodurcissable) ainsi que la forme que peut prendre la matière première pour ce procédé de fabrication. Parmi les sept technologies de FA présentées dans la Figure 1.3 définit dans la norme ISO/ASTM 52900:22 (ISO/ASTM, 2022), la fusion sur lit de poudre du polyamide 12 (Nylon 12 ou PA12) est considérée comme la catégorie plus mature pour des utilisation de pièces industriels (Tan, Zhu, & Zhou, 2020). Les technologies les plus utilisés pour la fusion de lit de poudre, sont *Multi Jet Fusion* (MJF) et *Selective Laser Sintering* (SLS).

1.3.2 Multi Jet Fusion (MJF) vs Selective Laser Sintering (SLS)

Les deux technologies MJF et SLS consistent à chauffer les particules de poudre pour les faire fondre et les consolider couche par couche afin de former un objet tri-dimensionnel. La Figure 1.4 tirée du travail de (Sillani, Kleijnen, Vetterli, Schmid, & Wegener, 2019) présente explicitement la différence entre les deux technologies, en SLS un rouleau vient déposer les particules de poudre de manière uniforme sur le plateau couche après couche pendant qu'un laser vient scanner la surface afin de faire fritter la poudre et ainsi solidifier la couche dans la forme désirée. Cependant, la technologie MJF, propriété de Hewlett Packard (Kabalnov, Wright, & Kasperchik, 2015), consiste à utiliser une stratégie différente de l'étalement de la poudre avec un lame. De plus la technologie choisie ici est de déposer des gouttelettes de liant (binder) et de scanner la surface avec une lampe à infrarouge afin de polymériser le liant et ainsi solidifier la couche et par conséquent le volume de la pièce.

12
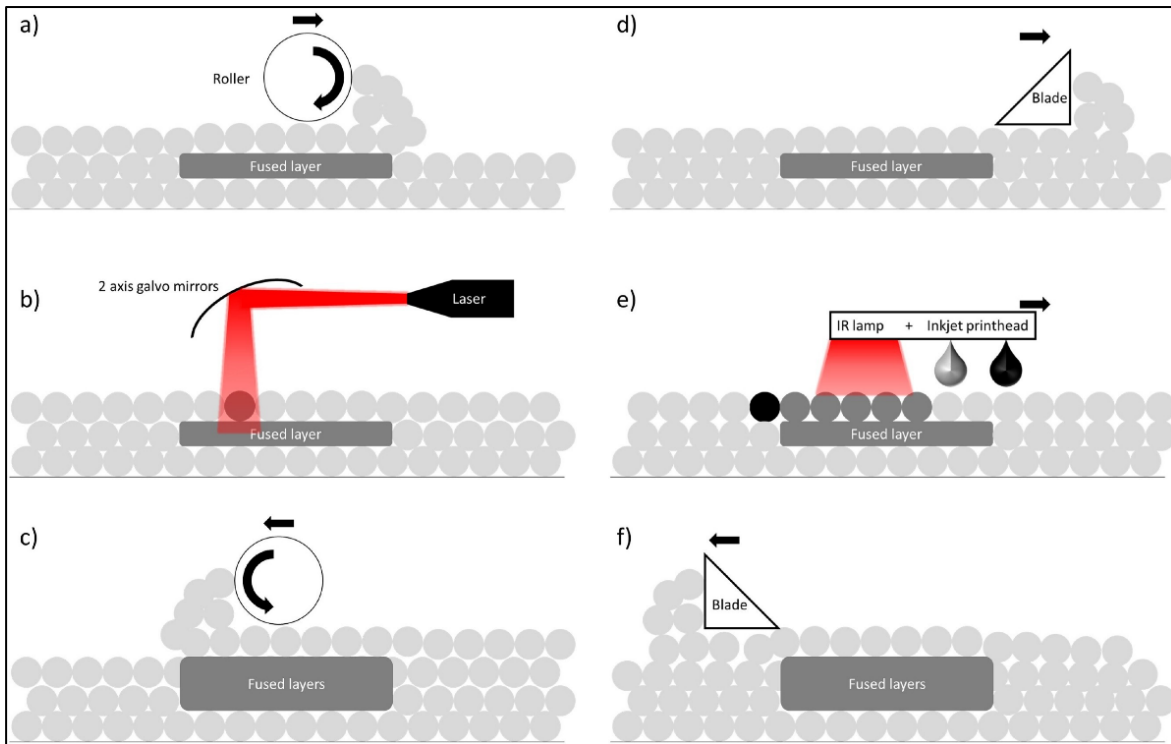
Figure 1.4 Schéma représentant les deux technologies de fabrication additive par fusion sur lit de poudre SLS (a-c) vs. MJF (d-f)

Tirée de Sillani (2019)

En comparaison avec la fabrication conventionnelle, FA donne une très grande liberté géométrique dans la conception et la fabrication (Gibson, Rosen, & Stucker, 2014). Les avantages de la FA en fusion sur lit de poudre sont nombreux, comme la personnalisation de masse, la réduction de masse, la texturation des surfaces et précision dimensionnelle. À ce jour, la FA de polymères est utilisée dans de nombreuses applications par exemple dans l'industrie médicale (Salmi, 2021), dans l'industrie automobile (Gibson et al., 2014), dans des applications aérospatiales, et comme pièces de rechange (Khajavi, Partanen, & Holmström, 2014).

La FA est une technologie qui s'inscrit parfaitement dans l'arsenal des manufacturiers afin de transiter vers une fabrication circulaire, la FA peut être utilisée comme un processus de recyclage, en exploitant des matériaux constitués de composants recyclables, avec des avantages à la fois environnementaux et économiques (Alkadi, Lee, Yeo, Hwang, & Choi,

2019). D'un point de vue logistique, la réussite de la mise en œuvre d'un programme de recyclage dépend de la taille et de l'emplacement de l'installation de production, la FA a le potentiel de les décentraliser, d'augmenter la flexibilité globale, de réduire les coûts logistiques et les délais de livraison, tout en réduisant incidence sur l'environnement (Giurco, Littleboy, Boyle, Fyfe, & White, 2014; Santander, Sanchez, Boudaoud, & Camargo, 2020).

1.4 Matériaux architecturaux (structure lattice)

1.4.1 Présentation du concept

Les matériaux cellulaires naturels tels que le bois, le liège et l'os sont couramment utilisés depuis des siècles et leur structure a été imitée dans des matériaux d'ingénierie modernes tels que les nids d'abeilles et les mousses, leur conférant des propriétés mécaniques uniques à leur porosité. Ce champ d'étude particulier ouvre de nombreuses voies dans le domaine de l'ingénierie et permet la création de matériaux de architecturés tels que l'utilisation de structures en treillis dites lattice. La FA ou plus précisément le SLS est très bien adaptée à la fabrication de ce type de structure, et un certain nombre d'études très importantes ont été menées sur ce sujet. Une structure en lattice est un arrangement périodique tridimensionnel de cellules unitaires qui donne un matériau cohérent et homogène avec des propriétés mécaniques et thermiques spécifiques. Les cellules unitaires de ce type peuvent être divisées en trois classes principales : 1) Strut based lattices, 2) Skeletal-TPMS based lattices and 3) Sheet-TPMS based lattices, qui ont bien sûr des comportements mécaniques très différents. L'acronyme TPMS signifie Triply Periodic Minimal surface. La Figure 1.5 tirée de (Al-Ketan, Rowshan, & Abu Al-Rub, 2018) illustre quelques différentes topologies cellulaires de chaque classe de structures lattices, il est visible dans cette figure qu'à partir d'un même type de cellule unitaire tel que le « *diamant* » il est possible de créer des formes très complexes et de topologies différentes en fonction de l'approche adoptée (voir la Figure 1.5 (a), (b) et (c)).

14
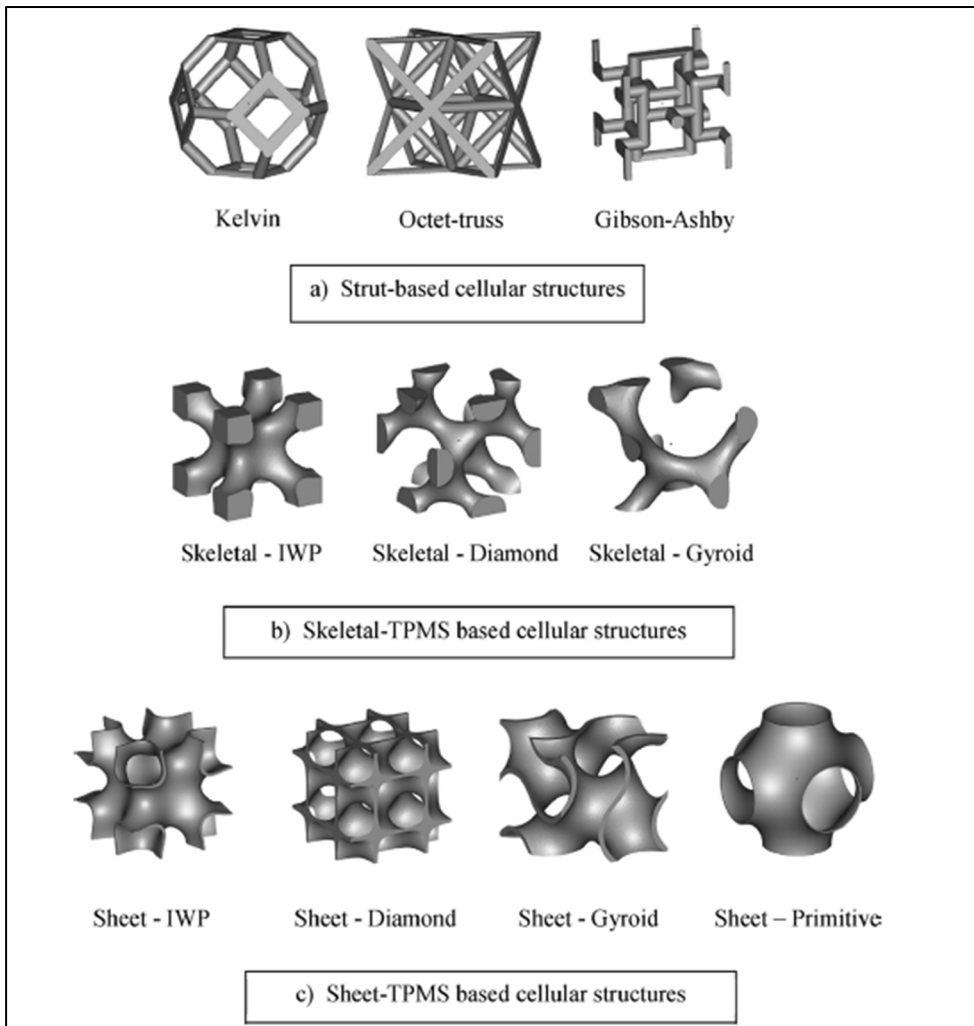
Figure 1.5 Cellule unitaire de différentes topologies cellulaires. a) Strut based structures, b) Skeletal-TPMS based structures, c) Sheet-TPMS based structures

Tirée de Al-Ketan (2018)

Les propriétés mécaniques de ce genre de structure dépendent fortement de certains paramètres de conception de celles-ci telles que la classe et le type de structure, les épaisseurs des murs et des poutres, la densité de la structure l'orientation dans laquelle nous examinons les propriétés, les dimensions de la cellule unitaire et finalement le matériau utilisé pour la construction de ces structures.

1.4.2   Application des structure lattice en ingénierie

Une application majeure des structures en lattice dans le secteur biomédical se concentre sur la conception d'implants, où le défi consiste à contrôler les propriétés mécaniques, c'est-à-dire le module d'Young, afin de se rapprocher le plus possible du comportement des os pour des raisons médicales. La deuxième raison repose sur la capacité optimale d'ostéointégration (Dumas, Terriault, & Brailovski, 2017). L'industrie aérospatiale est très intéressée par ce type de matériau architecturé en cause de leur capacité thermique élevée et, bien sûr, le nombre de pièces qu'il est possible de réduire tout en conservant une résistance mécanique similaire (Frulloni, Kenny, Conti, & Torre, 2007). L'une des limites des structures cellulaires est leur comportement sous chargement cyclique (Helou & Kara, 2018). Les structures en treillis échouent en moins de cycles que les matériaux en vrac car le comportement à la fatigue est directement lié à la densité du matériau (Maconachie et al., 2019).

Les matériaux architecturés offrent une très large gamme de propriétés mécaniques comme cité plus haut, l'utilisation de ce genre de structure dans la conception de pièce permet la réduction de la masse des pièces et par conséquent la quantité de matière utilisée et l'énergie nécessaire pour le transport de celle-ci.

1.5   Dégradation des polymères

Comme il a été précédemment mentionné, les polymères sont un type de matériau très répandu qui a vu sa production quadrupler en l'espace de 30 ans, sous l'impulsion de la croissance des marchés émergents (OCDE, 2022). En raison de leurs propriétés mécaniques et électriques, les polymères sont utilisés dans pratiquement toutes les disciplines de l'ingénierie. Toutefois, un phénomène de vieillissement survient durant la phase de fabrication et d'exploitation des polymères, ce qui justifie une étude plus approfondie des mécanismes intrinsèques qui en sont responsables, afin de mieux anticiper ce phénomène.

1.5.1   Principes du vieillissement des polymères

Le vieillissement correspond à une évolution lente et irréversible d'une ou de plusieurs propriétés du matériau à partir d'un point de référence, généralement pris dès la fin du cycle de fabrication (Fayolle & Verdu, 2005). Cette évolution peut résulter en de modifications de la structure des macromolécules qui assurent leur cohésion mécanique, de leur composition ou de sa morphologie. Le vieillissement se traduit par une altération des propriétés fonctionnelles du matériau ce qui écourte la durée de vie des pièces en opération.

1.5.2   Classification des mécanismes de vieillissement des polymères

Il existe généralement trois grandes classes de vieillissement des polymères (Fayolle & Verdu, 2005) :

- Le vieillissement physique : Ce type de vieillissement correspond à un processus qui modifie les propriétés de performance d'un matériau sans modifier sa structure chimique. Cela inclut les phénomènes de vieillissement sous contrainte mécanique, les phénomènes de relaxation, les phénomènes de transfert de masse (pénétration de solvant, migration d'additif) et les phénomènes de surface.

- Le vieillissement chimique : C'est une évolution de la structure chimique du polymère sous l'influence de l'environnement, les praticiens classifient les processus en fonction de la cause majeure de dégradation, nous pouvons en citer quelques-uns (Richaud & Verdu, 2011).
    - Le vieillissement thermique : causé par l'exposition à des températures élevées pendant de longues périodes. Cela peut provoquer une dégradation chimique du matériau, entraînant une perte de propriétés mécaniques.
    - Le vieillissement photochimique : causé par l'exposition aux rayons UV et à la lumière visible. Cela peut provoquer une dégradation du matériau, entraînant une perte de résistance mécanique, une décoloration, une fragilisation, etc.

o Le vieillissement hydrolytique : s'accompagnant d'une hydrolyse, entraîne des coupures statistiques des chaînes macromoléculaires du polymère, d'où une altération, à terme, des propriétés mécaniques. La réaction est généralement très lente à température ambiante, la vitesse de l'action chimique élémentaire étant elle-même faible et le processus étant le plus souvent contrôlé par la diffusion (également lente) de l'eau dans le matériau.

- <u>Le vieillissement mécanique</u> : causé par le stress mécanique, tel que la flexion, l'impact ou la friction. Cela peut provoquer des craquelures, des fissures ou une déformation permanente du matériau.

Il convient de noter que ces classes de vieillissement ne sont pas mutuellement exclusives, car les polymères peuvent être exposés simultanément à plusieurs facteurs de vieillissement.

En conclusion, le vieillissement des polymères est un phénomène complexe et irréversible qui peut survenir durant la phase de fabrication ou d'exploitation des matériaux. Les mécanismes de vieillissement des polymères peuvent être classés en trois grandes catégories : physique, chimique et mécanique. Chacune de ces classes peut causer des altérations des propriétés fonctionnelles du matériau, raccourcissant ainsi sa durée de vie. Les professionnels doivent donc prendre en compte ces mécanismes lors de la conception de produits en polymère et lors de leur utilisation, afin de prévoir et de minimiser l'impact du vieillissement sur la performance et la durabilité des matériaux.

1.6 La fabrication additive dans l'industrie de la chaussure

La création d'une chaussure entièrement réalisée par impression 3D constitue une entreprise qui n'est pas dépourvue de complexités. Les procédés d'impression tridimensionnelle, bien que porteurs d'un potentiel novateur, se caractérisent par leur cadence de production plus lente, leur moindre évolutivité et les coûts substantiels inhérents aux matériaux utilisés. Une problématique subséquente découle du processus de fabrication conventionnel des chaussures,

lequel implique la conception d'une matrice tridimensionnelle en bois ou en plastique servant de base à l'élaboration du modèle chaussant. Cependant, l'intégration totale de l'impression 3D pour la création de chaussures rendrait superflu le recours aux matrices traditionnelles, forçant ainsi les fabricants à repenser intégralement leur démarche de production. Cette transformation engendrerait, par voie de conséquence, des répercussions substantielles sur les parties prenantes et les fournisseurs tout au long de la chaîne de production préexistante.

Actuellement présentée comme l'uniques réalisations de chaussure entièrement imprimée en 3D sur le marché, la marque Fused Footwear et PEAK mettent en lumière les défis inhérents à ce domaine. Les ténors du marché de la chaussure de sport, au cours de la dernière décennie, ont déployé des efforts significatifs dans l'exploration des perspectives offertes par l'impression 3D et la fabrication avancée. Des acteurs tels que Nike, Adidas, New Balance, Reebok et Under Armor ont développé des chaussures de sport avec des semelles imprimées en 3D, ayant recours à diverses techniques d'impression, matériaux distincts et partenariats variés avec des entreprises spécialisées en impression tridimensionnelle. Cette dynamique est illustrée dans la Figure 1.6, extraite du site (Sher, 2020).
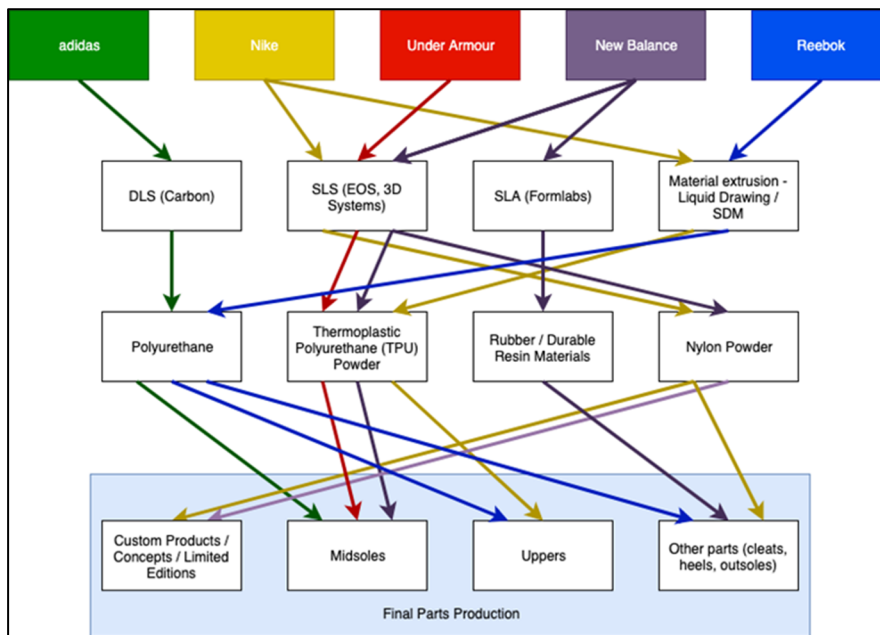
Figure 1.6 Vue d'ensemble des leaders des marques développant
des chaussures de sport avec des semelles fabriquées additivement

Tirée de Sher (2020)

L'étroite collaboration entre les maisons de renom dans l'univers de la chaussure et les fournisseurs de technologies s'avère être un catalyseur crucial dans le développement de nouveaux matériaux adaptés à l'impression 3D pour la conception de chaussures. À titre illustratif, Carbon a engagé une collaboration avec Adidas en vue de mettre au point un élastomère en polyuréthane utilisé pour les semelles intermédiaires des baskets "Futurecraft" d'Adidas. De manière similaire, New Balance s'est associée à Formlabs, une entreprise spécialisée dans les imprimantes 3D SLA, afin de concevoir des matériaux d'impression 3D hautement performants spécifiquement conçus pour les chaussures. Dans cette optique, une résine photopolymère exclusive baptisée "Rebound Resin" a été introduite, visant à la création de structures réticulées élastiques et robustes.

1.7 Conclusion

En résumé, la conception de produits durables joue un rôle essentiel dans la transition vers une économie circulaire. Les avancées technologiques telles que la fabrication additive et l'utilisation de matériaux architecturés offrent des opportunités pour réduire la quantité de matière utilisée, améliorer la performance et la durabilité des produits, et faciliter le processus de recyclage. Cependant, il est important de comprendre les mécanismes de vieillissement des polymères et de prendre en compte ces phénomènes lors de la conception et de l'utilisation de produits durables. En adoptant une approche d'ingénierie holistique, les professionnels peuvent concevoir des produits durables qui minimisent leur impact sur l'environnement et contribuent à la création d'une économie circulaire.

CHAPITRE 2

PROBLÉMATIQUE, OBJECTIFS ET MÉTHODOLOGIE DE RECHERCHE

2.1   Problématique et objectifs de recherche

La surconsommation de ressources naturelles et l'émission croissante de gaz à effet de serre sont des problèmes majeurs auxquels la planète fait face, et qui sont exacerbés par le modèle économique linéaire actuel. Dans ce contexte, l'économie circulaire est présentée comme une solution durable pour réduire la consommation de ressources naturelles et les émissions de gaz à effet de serre. Cependant, la mise en œuvre de la fabrication circulaire (FC) nécessite une conception réfléchie du produit, des matériaux et de la fabrication pour augmenter la recyclabilité du produit et faciliter sa réutilisation. Sachant le contexte actuel une **question de recherche** peut être posée :

Les technologies de fabrication additives et une conception pour assemblage et désassemblage peuvent-elles faciliter l'introduction de biens de consommation conçus dans une logique de fabrication circulaire?

L'objectif principal de ce travail consiste à proposer une approche innovante pour répondre à la question de recherche cité plus haut, en se concentrant sur le cas spécifique des chaussures à talons. Dans le cadre de cette étude, deux sous-objectifs de recherche seront poursuivis tel que présenté ci-après :

Sous objectif 1: Écoconception
Le premier sous-objectif consiste à explorer l'utilisation de nouvelles technologies de fabrication avancée, telles que la fabrication additive, pour proposer un prototype de chaussures à talons hauts imprimées en 3D, qui respectent les principes de l'écoconception et de l'EC.
Sous objectif 2: Allongement de la durée d'utilisation

Le deuxième sous-objectif de recherche vise à étudier le comportement des matériaux polymériques face aux facteurs environnementaux dans lesquels ils évoluent, afin de proposer un modèle de vieillissement des polymères imprimés en fonction du temps d'exposition et des conditions environnementales. Cette analyse contribuera à évaluer la durabilité des chaussures à talons imprimées en 3D et leur potentiel d'insertion dans une économie circulaire.

2.2 Méthodologie

Pour atteindre ces sous-objectifs et répondre à la problématique de recherche, nous adopterons une approche différente pour chaque sous objectif. Pour le premier sous objectif, il a été choisi d'utiliser une démarche de conception basée sur l'assemblage, le désassemblage et la fabrication additive (Design for Assembly « DfA », Design for Disassembly « DfD » and Design for Additive Manufacturing « DfAM »). Tandis que pour atteindre le second sous objectif, il a été choisi d'adopté une méthodologie empirique afin de de déterminer le comportement du polyamide 12 sous certaines conditions environnementales au fil du temps.
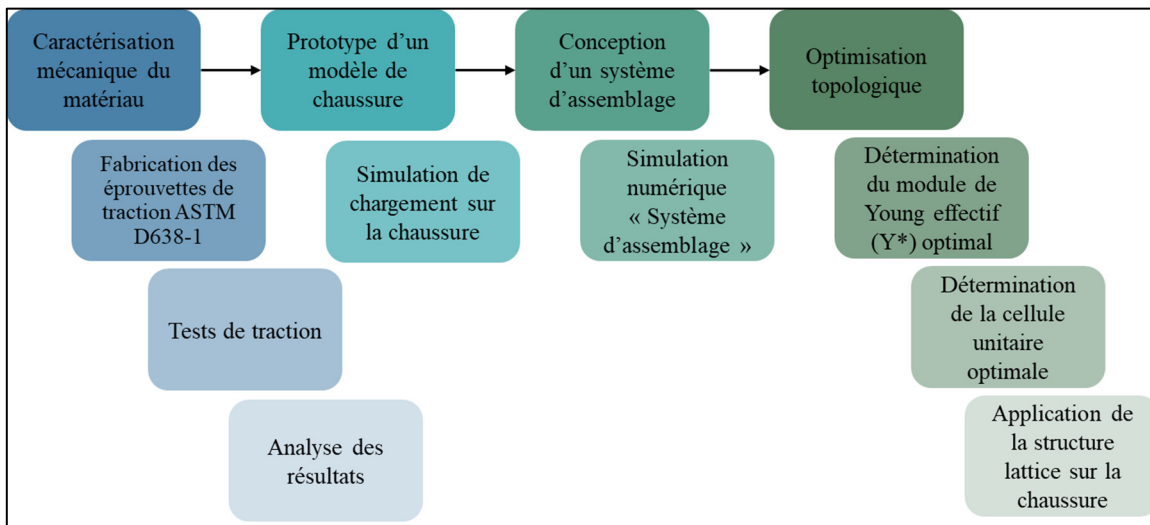
Figure 2.1 Méthodologie adoptée pour réaliser le sous objectif 1

(Présenté dans le Chapitre 3)

La Figure 2.1 montre une représentation schématique de la méthodologie adoptée pour réaliser le sous objectif 1 et qui se décompose en 4 phases principales tel que :

- La première étape est de caractériser le matériau qui sera utilisé.
- Proposer un prototype de chaussure monolithique, c'est-à-dire réduire au maximum le nombre de pièces utilisées. Tester le prototype obtenu numériquement afin de s'assurer qu'il respecte les normes en vigueur dans l'industrie des chaussures à talons.
- Concevoir un système d'assemblage mécanique qui permet de désassemblage aisé.
- Optimisation topologique afin d'augmenter le confort de la chaussure tout en réduisant la quantité de matière utilisée.
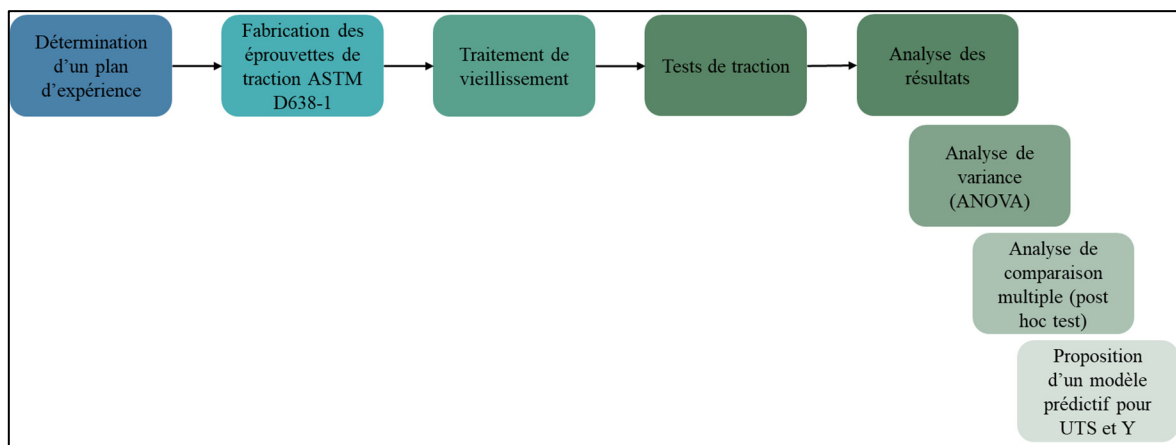
Figure 2.2 Méthodologie adoptée pour réaliser le sous objectif 2
(Présenté dans le Chapitre 4)

La Figure 2.2 présente schématiquement les étapes suivies pour la méthodologie empirique dans le but d'attendre le sous objectif 2 et cette méthodologie est subdivisée en plusieurs étapes comme suit :

- Détermination d'un plan d'expérience de traitement de vieillissement en chambre environnementale.
- Fabrication des éprouvettes de traction (ASTM D638 Type 1) (voir détails dans la section 2.2.1 et 4.3.1).

- Traitement de vieillissement appliqué sur le polyamide 12 fabriqué additivement et essais mécaniques afin de déterminer les propriétés mécaniques découlant du traitement subi (voir détails dans la section 2.2.2 et 4.3.2).
- Essais de traction sur les éprouvettes vieillies selon le plan d'expérience défini (voir détails dans la section 2.2.3 et 4.3.3).
- Analyse des résultats obtenu par analyse de la variance afin de déterminer les facteurs environnementaux influents et l'effet de leurs interactions sur la résistance mécanique et le module de Young. Puis une proposition de modèles mathématiques prédictifs pour la résistance mécanique et le module de Young en fonction des facteurs environnementaux déterminé dans le plan d'expérience (voir section 4.3.4).

2.2.1 Préparation des échantillons de PA12

Les échantillons sont basés sur la norme ASTM D638 Type 1 (ASTM, 2014) présentée dans la Figure 3.2.a. Tous les échantillons ont été imprimés à partir de poudre vierge de polyamide 12, également appelée PA 2200, provenant d'EOS sur une imprimante SLS EOS P110 avec une température de chambre de 168°C. La figure 3.2.b. présente une capture d'écran de la préparation de la chambre de construction ; on peut voir que les échantillons orientés XY et XZ sont répartis sur toute la hauteur de la chambre afin de réduire l'effet potentiel des variations de température sur un nombre maximum d'échantillons, et d'homogénéiser les échantillons en termes de propriétés mécaniques. Un traitement de polissage à la vapeur (Vp) a été appliqué à la moitié des échantillons (135), réalisé par le fournisseur AMTechnologies (AMTechnologies, 2022), afin d'estimer son effet protecteur sur le vieillissement de l'état de surface. Le tableau 3.I résume l'échantillonnage effectué.

2.2.2 Traitement de vieillissement des échantillons de PA12

Après fabrication des échantillons additivement, un plan d'expérience a été mis en place afin d'étudier les effets individuelles et combinés des facteurs environnementaux sur les propriétés mécaniques (Résistance mécanique ultime et le module de Young). Le vieillissement accéléré

des éprouvettes ASTM D638 de type 1 a été réalisé sur une chambre environnementale Q-Sun Xe-3 Xenon du fabricant (Q-LAB) (voir la Figure 2.3) avec une lampe UVA-340 ce qui reproduit au mieux la portion du spectre d'irradiation solaire pour chaque longueur d'onde entre 290 nm et 370 nm comme montré dans la Figure 2.4. Cet intervalle de longueur d'onde est celui qui cause le maximum de dégradation aux polymères. Deux niveaux d'irradiance ont été choisis pour induire une dégradation photochimique en se basant sur la variation saisonnière de l'irradiance entre les deux solstices d'hiver et d'été à savoir le 21 juin et le 21 décembre (voir la section 4.3.2). La Figure 2.5 présente un relevé de l'irradiance en fonction de la longueur d'onde pour trois différents moments de l'année afin de mettre en avant la variation saisonnière de l'irradiance.
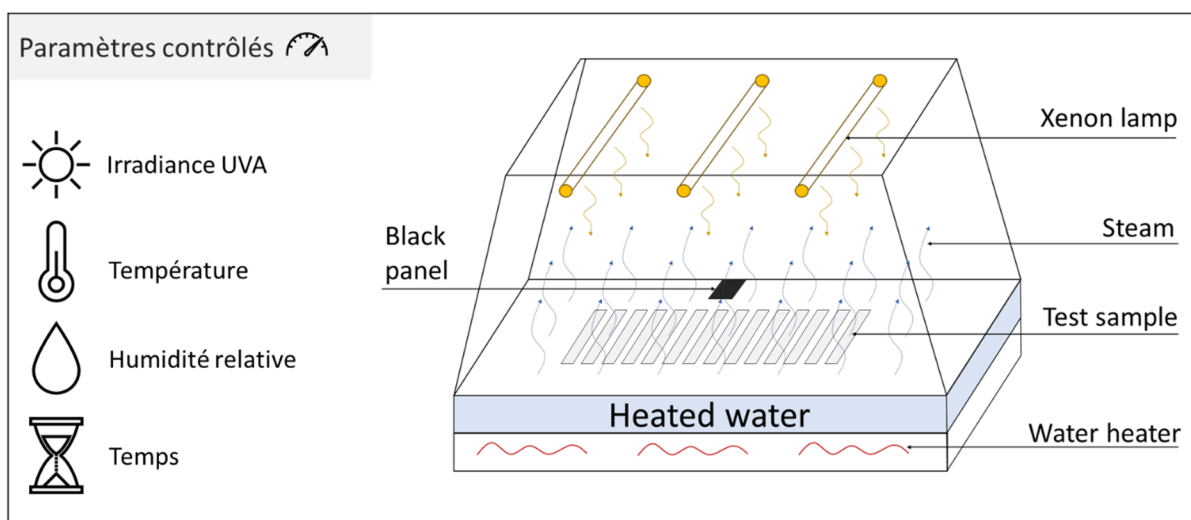
Figure 2.3 Schéma de fonctionnement de la chambre environnementale pour vieillissement accéléré Q-SUN XE-3 Xenon utilisé dans cette étude

26
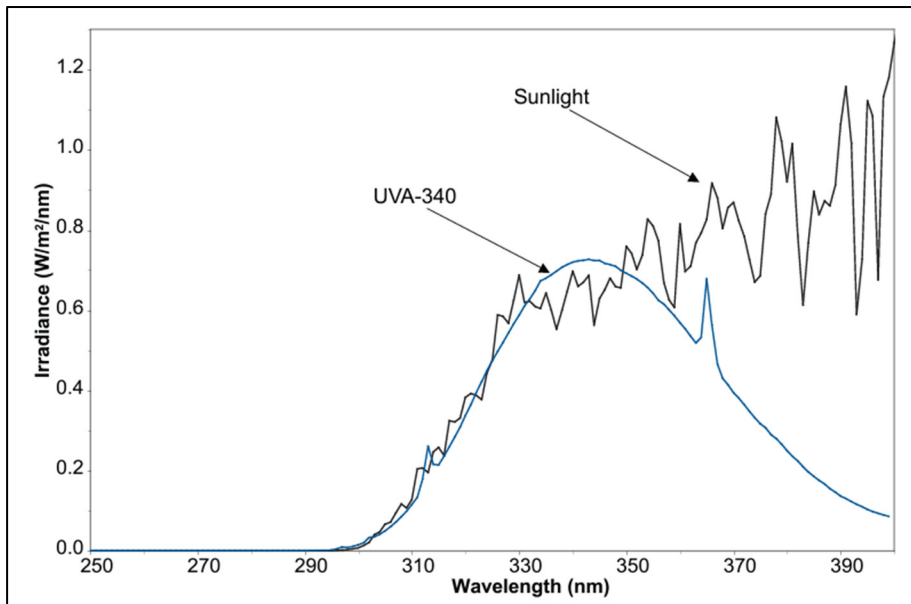
Figure 2.4 Superposition de l'irradiance solaire
et l'irradiance de la lampe UVA-340 de Q-LAB
Tirée de Q-LAB (2011)
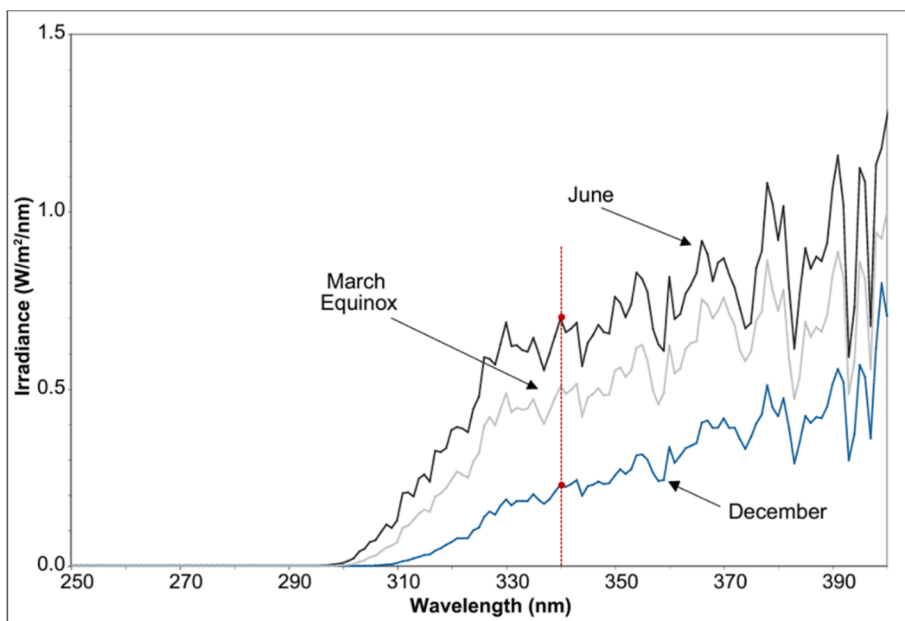
Figure 2.5 Variation saisonnière de l'irradiance solaire
pour les deux solstices (juin et décembre) et l'équinoxe de mars
Adapté de Q-Lab (2011)

2.2.3   Caractérisation mécanique des échantillons vieillis

Les essais de traction réalisés sur les éprouvettes ont été mis en œuvre selon la norme ASTM D638-22 Type 1 (ASTM, 2014) en utilisant une cellule de charge de 10kN sur une machine MTS Alliance RF/200 à 23°C et à 50% d'humidité (voir Figure 2.6). La vitesse de déplacement a été réglée à 5mm/min et la fréquence de capture des données de déplacement à 10Hz avec le même opérateur réalisant tous les essais présentés dans cette étude. Les dimensions exactes (largeur et épaisseur) des échantillons sont entrées dans le logiciel MTS pour chaque échantillon testé afin d'éviter les variations dimensionnelles dues au processus de fabrication et éventuellement aux traitements de vieillissement accéléré appliqués. Les échantillons sont directement placés dans des sacs scellés sous vide et stockés à 20°C dans un endroit sombre après avoir été retirés de la machine de vieillissement accéléré jusqu'à ce que les essais de traction soient effectués, afin d'éviter tout vieillissement incontrôlé des échantillons.
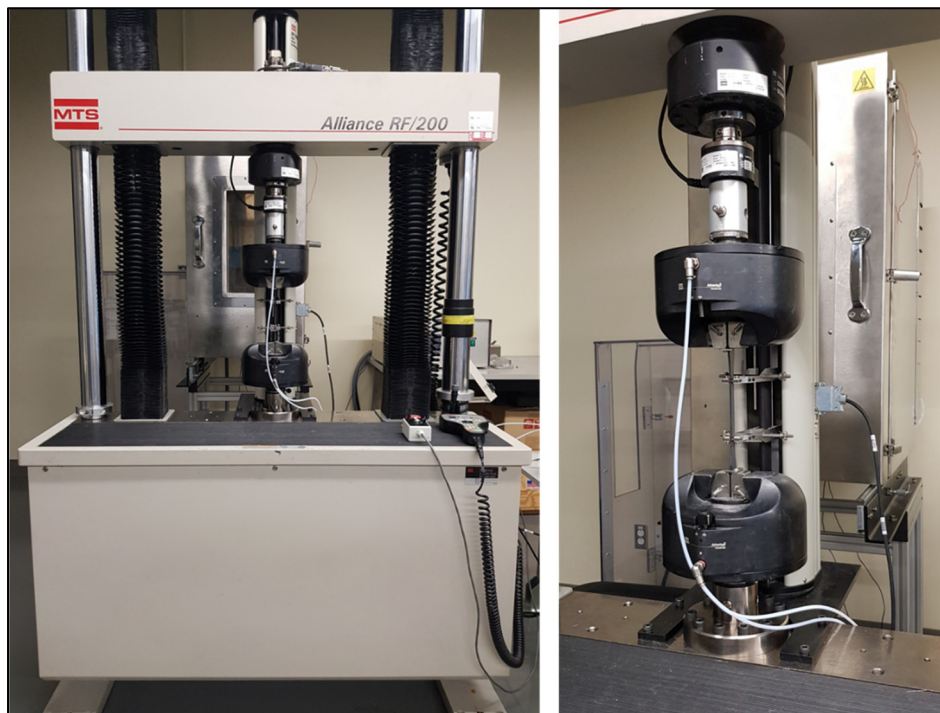
Figure 2.6 Machine de traction utilisée pour la caracrtérisation
des échantillons après traitement de vieillissement (MTS Alliance RF/200)

Le chapitre 2 traite des étapes décrite plus haut qui sont liées au sous-objectif 1 tout en les décrivant plus en détail sous forme d'un article publié dans « *Materials & Design* ». La partie empirique est quant à elle liées au sous-objectif 2 et est traitée et détaillée dans le chapitre 3 sous forme d'article soumis pour publication dans « *Additive Manufacturing* ».

CHAPITRE 3

ON SUSTAINABLE DESIGN AND MANUFACTURING FOR FOOTWEAR INDUSTRY – TOWARDS CIRCULAR MANUFACTURING

Chahine Ghimouz[a], Jean Pierre Kenné[a], Lucas A. Hof[a*]

[a] Mechanical Engineering Department, École de technologie supérieure, 1100, rue Notre-Dame Ouest, Montreal, Quebec, Canada H3C 1K3

3.1 Abstract

The global fashion industry is facing carbon footprint issues, but technological innovations are helping to improve its performance and environmental efficiency in terms of footwear manufacturing. This paper explores how technological innovations, specifically Design for Additive Manufacturing (DfAM), Design for Assembly (DfA), and Design for Disassembly (DfD) strategies, along with Additive Manufacturing's (AM) capability to produce intricate parts, can contribute to the fashion industry's shift towards a Circular Manufacturing model. The focus is on footwear manufacturing and its carbon footprint issues. The proposed additively manufactured shoe design utilizes Polyamide 12 and Thermoplastic polyurethane as feedstock, featuring a glueless mechanical assembly system based on a snapfit. Notably, the upper part of the shoe incorporates a variable lattice structure to ensure flexibility in different areas. Finite Element Analysis (FEA) demonstrates that the snapfit assembly exceeds the industry standard's minimum disassembly force requirement. Additionally, an optimization algorithm for the variable lattice structure results in a 34% mass reduction while maintaining the desired Young's modulus in each shoe zone. This design approach aligns with the footwear industry's sustainability goals, aiming to reduce environmental impact and enhance product durability. The study successfully develops a strategy to implement AM for sustainable shoe fabrication.

Keywords: Circular manufacturing; Additive manufacturing; Selective Laser Sintering; Snapfit design; Topology optimisation; Linear elasticity modeling

3.2   Introduction

The global consumption of natural resources is constantly increasing in this 21st century. Nowadays, the quantities of annually consumed natural resources worldwide are so excessive that their consumption occurs at a higher rate than required for their regeneration by the planet (WWF, 2012). In fact, it currently takes the planet earth 1.7 years to regenerate all the resources consumed in one year (Overshoot, 2021). In 2010, 72 billion tons of raw materials were extracted and consumed, twice the amount extracted in 1980, according to a 2015 report by the Organization for Economic Cooperation and Development (OCDE, 2015). With the current economical growth, annual consumption will reach the symbolic 100-billion-ton mark around 2030 (Bleischwitz et al., 2009). However, the corresponding human activity is progressively emitting anthropogenic greenhouse gases (GHG) each year, exceeding 48.9 giga tons of CO_2 equivalent (CO_2-eq) in 2018 as reported by Climate Watch Data (CLIMATEWATCH, 2019).

From these annual GHG emissions, an amount of 1.7 giga tons of CO_2-eq were emitted only by the textile and footwear industry in 2015 and if this trend continues, the BCG Retail value project predicts 2.7 giga tons of CO_2-eq emitted by this industry in 2030 (Eder-Hansen et al., 2017), representing an increase of 63%. As well, the waste generation from the clothing and footwear industry will increase from 92 mega tons in 2015 to 148 mega tons in 2030 (Eder-Hansen et al., 2017). In addition, only 5% of footwear is recycled globally (Lee & Rahimifard, 2012), which results in sustainability issues for this industry.

This acceleration of raw material consumption and GHG emissions in the manufacturing industry is partly due to the actual typical linear economic model (*Take*, *Make*, *Use* and *Throw*), also referred to as the "linear economy" (LE) (Ellen MacArthur Foundation, 2015). To address this issue of overconsumption and the environmental challenge that the planet is experiencing

(Mathieux et al., 2017), a more sustainable model has been proposed; the "circular economy" (CE). This approach, derived from initiatives dating back to the 1970s (Stahel, 2020), presents the economy as a business mindset that will enable a shift towards long-term sustainable development (McDowall et al., 2017) including a principle concept based on the 6Rs (*Reuse, Recycle, Redesign, Remanufacture, Reduce, and Recover*) (Jawahir & Bradley, 2016). Based on these developments, the "circular manufacturing" (CM) model is emerging as one of the engineering solutions to consider for sustainable production (Delpla, Kenné, & Hof, 2022). In such a CM model, the product design, used materials, and its manufacture play an essential role in the product's recyclability (Ellen MacArthur Foundation & IDEO, 2018). More specifically, a "circular design" process includes rethinking the product design not only for its end-use, but also for its user environment and process steps at its end-of-life (EOL) state to favor reuse, facilitating its reinsertion in a closed manufacturing loop and ultimately disassembly for improved recyclability (Ellen MacArthur Foundation, 2017).

In such circular manufacturing systems, design for assembly (DfA) and design for disassembly (DfD) strategies are key methodological elements for product and process development aimed at reducing costs and improving reliability without changing product function (Geoffrey Boothroyd, 1994). These DfA and DfD approaches are based on some specific design principles including: *Reduce the number of parts*; *Simplify the design*; *Design for easy assembly and disassembly*; *Design for efficient joining and fastening*; *Minimize flexible parts and interconnections*; *Standardize parts and materials*; and *Design modular products*.

Additive manufacturing (AM), or 3D printing, which is a relatively new technology (Su & Al'Aref, 2018), has an interesting potential for circular manufacturing, by reducing waste, energy consumption and manufacturing costs at small production scales (Hegab, Khanna, Monib, & Salem, 2023). It also facilitates reuse by creating parts in modular designs that facilitates their reuse and repair (Marita Sauerwein, Doubrovski, Balkenende, & Bakker, 2019). In addition, AM enables the development of sustainable products by considering sustainable and circular development principles from the beginning of the design process. This can result in products that are more sustainable and easily recyclable or reusable at the end of their life (M Sauerwein, Bakker, & Balkenende, 2017; Marita Sauerwein et al., 2019).

In 2019, a record-year regarding the volume of produced footwear, 24.3 billion pairs were produced and sold or more than 65 million pairs of shoes per day (WorldFootwear.com, 2020). However, footwear manufacturing is a labor-intensive process, as typical footwear products consist of 65 individual parts including around 360, mostly manual, manufacturing steps (Cheah et al., 2013). This traditional manufacturing approach is still highly labor and machine intensive for footwear part production and final product assembly. Consequently, footwear manufacturers are looking for new ways to optimize their manufacturing process (Commitment, 2020). AM offers a promising alternative allowing footwear manufacturers to streamline the production of certain shoe components (Beiderbeck, Krüger, & Minshall, 2020; Manoharan, Chou, Forrester, Chai, & Kong, 2013; Spahiu, Almeida, Manavis, Kyratsis, & Jimeno-Morenilla, 2021).

However, these developments are still in their infancy, and it is difficult to produce fully 3D printed footwear due to the high rejection rate caused by manufacturing defects (Kreutz, Böttjer, Trapp, Lütjen, & Freitag, 2022). To date, 3D printing is primarily only used to manufacture specific footwear parts, such as the midsole, which is the shock-absorbing layer between the insole and the outsole. The mechanical performances of the used materials are different from one to another and have very distinct applications. However, the steps involved in the AM process are critical to increase the capabilities of functional prototypes. Hence, a good understanding of key process parameters, such as build orientation, print speed, and layer thickness, affect mechanical properties (Pugalendhi, Ranganathan, & Chandrasekaran, 2020), and research is just emerging in this field (Rouf et al., 2022).

3.2.1   Additive Manufacturing

Compared to conventional polymer manufacturing processes, such as injection moulding, thermoforming, or extrusion (Osswald, 2017), additive manufacturing (AM), or 3D printing, is a relatively new manufacturing process, debuting from the 1980s, that has not yet reached its full maturity (Lezama-Nicolás, Rodríguez-Salvador, Río-Belver, & Bildosola, 2018). Among the seven AM technologies defined in the ISO/ASTM 52900:21 standard (ISO/ASTM,

2022), powder bed fusion (PBF) of polyamide 12 (Nylon 12 or PA12) is considered as the most mature technology for industrial product applications (Tan et al., 2020). The most widely used AM technologies for PBF are Multi Jet Fusion (MJF) (Wu, Lu, Zhao, Bosiakov, & Li, 2022) and Selective Laser Sintering (SLS) (Wu et al., 2022). SLS uses a laser to melt and fuse the feedstock powder, while MJF uses a bonding agent, heat and infrared light to fuse the powder to create the final object. Both technologies involve heating of feedstock powder particles, with typical size between 45 and 90 μm (Schmidt et al., 2019), to sinter and consolidate the particles layer by layer to form a three-dimensional (3D) object. Compared to conventional manufacturing, AM provides high geometric freedom in design and fabrication (Gibson et al., 2014). In addition, PBF AM processes facilitate product manufacturing for mass customization, weight reduction, surface texturing and dimensional accuracy (Attaran, 2017), which opens up new manufacturing opportunities for biomimicry based designs, e.g. by replicating natural cellular materials to achieve heterogenic mechanical behaviour of monolithic material. Reducing the number of different types of material is interesting for circular design and manufacturing strategies, as it facilities the product disassembly and recycling processes at a product's EOL (Giurco et al., 2014; Santander et al., 2020).

To date, polymer AM is emerging for functional applications in different domains, such as the medical industry (Salmi, 2021), the automotive industry (Gibson et al., 2014), the aerospace industry, and as spare parts for maintenance (Khajavi et al., 2014). Nevertheless, a remaining challenge of these layer-based manufacturing methods is the generation of anisotropic mechanical properties, i.e. the parts' properties are directly dependent on its orientation during printing and the layer thickness (Ligon, Liska, Stampfl, Gurr, & Mülhaupt, 2017). In addition to low manufacturing speeds, post-processing is also required to ensure a satisfying surface finish for functional parts in industrial applications (Kumbhar & Mulay, 2018). However, the anisotropic nature of the properties can be exploited for specific applications by studying this property in depth and controlling factors influencing it. The creation of architectured material is an excellent way to achieve this.

3.2.2   Architectured materials

Natural cellular materials such as wood, cork or bone have been well used for centuries, and their structure is imitated in modern engineering materials such as honeycombs and foams to take advantage of their specific mechanical properties due to their porosity. This bio-inspired engineering field opens up many new possibilities, resulting in the creation of architectured materials such as lattice structures (Maconachie et al., 2019). AM and more specifically SLS is very well suited for the fabrication of such structures, hence the relatively large number of studies on this topic (Helou & Kara, 2018). Lattice structures are three-dimensional periodic arrangements of a unit cell resulting in a coherent and homogeneous material with specific mechanical and thermal properties. The type of unit cell can be divided into three main classes, which are 1) *strut-based lattices*, 2) *planar lattices*, and 3) *surface-based lattices*, where each category demonstrates different mechanical behavior (Maconachie et al., 2019).

The control of the lattice structures' mechanical properties depends strongly on its class as well as on its type, such as diamond, gyroid or other (Al-Ketan et al., 2018). Recent literature revealed that depending on the nature of the macroscopic loading, the structure deforms with a combination of bending, torsion or stretching of the lattice struts (Khaderi, Deshpande, & Fleck, 2014). The mechanical properties' dependence on the structure's density is impacted by the loading mode it is exposed to (Deshpande, Ashby, & Fleck, 2001). In fact, the sheet type *Triply Periodic Minimal Surface (TPMS)*, belonging to the *surface-based lattices* class, depends the least on its relative density and it has the highest modulus of elasticity and mechanical strength for the same density compared to the other classes (Al-Ketan et al., 2018). Hence, this sheet TPMS surface-based lattice type provides a large design space to control the mechanical properties of the architected material. Therefore, this lattice type and class have been chosen for the present study.

Current architecture materials applications are mainly in the biomedical and aerospace field. The main use of lattice structures in the biomedical field is focused on implant designs to control their mechanical properties (e.g. Young's modulus) in order to approach bone behavior

and optimal osseointegration capability. The aerospace industry appreciates the high thermal capabilities of lattice structures and the potential to reduce the number of parts while keeping a similar mechanical strength. Nevertheless, one of the limitations of cellular structures is their behavior under cyclic loading; the fatigue behavior is directly related to the density of the material and, therefore, fractures occur in fewer cycles for lattice structures compared to bulk materials (Maconachie et al., 2019).

3.2.3   Objectives and contributions of the present study

The main objective of this study is to develop a CM approach for footwear manufacturing using AM techniques to increase their remanufacturability and recyclability by focusing on a design for disassembly. The novelty of the presented approach includes the development of an entirely AM-based footwear manufacturing process to achieve footwear (high heels) that are easy to disassemble and offer an adaptable design approach to optimize user comfort by topological optimization. AM offers new design possibilities that are exploited in the developed production strategy to reduce the number of footwear parts and to achieve glue-less component assembly, which favors disassembly for remanufacturing and recycling when reaching the end-of-life stage of the shoes.

This paper is organized as illustrated in Figure 2.1 and started by introducing the background and current state-of-the-art of AM and its use as production method for polymer parts in section 1. Section 2.1 presents the used materials, and design methodology, e.g. for the assembly system and the topological optimization, followed by the presentation of the developed footwear prototype including both analytical and numerical finite element analysis (FEA) validations for critical shoe elements, such as the heel and outsole (section 2.2) and a discussion on the design workflow for the high-heel upper part development (section 2.3). The obtained results are presented and discussed in section 3. Finally, the conclusions of the developed work on CM for footwear and an outlook towards future studies are outlined in section 4.
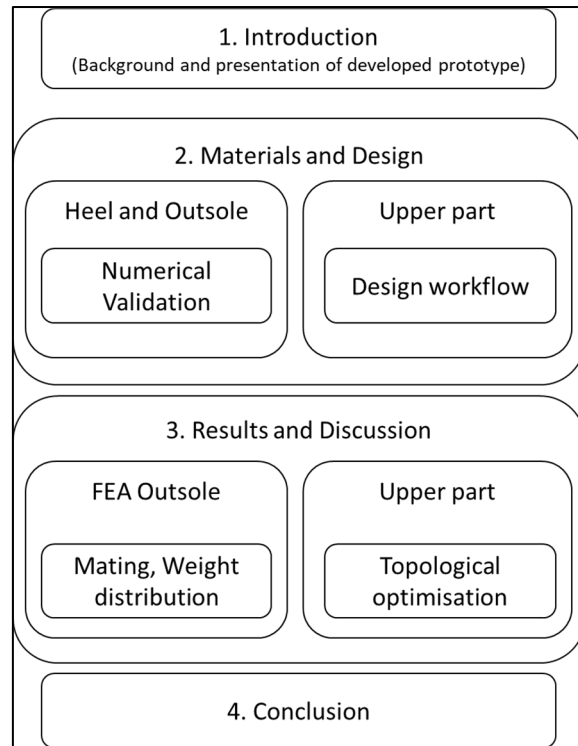
Figure 3.1 Schematic illustration representing the structure of the present study

3.3   Materials, Design and Methods

The overarching methodology of the present study includes: 1) design of a 3D printable footwear prototype (high-heel), 2) material and AM technology selection and characterization, 3) design of a glue-less mechanical assembly system, and finally 4) topological optimization and weight reduction to improve footwear user's comfort and to reduce the quantity of used material. Section 2.1 discusses the developed high-heel prototype, which was designed using a Design for Additive Manufacturing (DfAM) approach (Kumke, Watschke, & Vietor, 2016). Fusion 360 (AUTODESK) and CATIA V5 3D modeling software (Dassault Systemes) were adopted in this design step. Section 2.2 details the selected materials and its mechanical characteristics, as well as the sample preparation by the selected AM technology and post-processing method to validate and compare the material's properties net-printed and post-treated. Section 2.3 outlines the glue-less assembly system for the different printed footwear parts and its adopted Design for Assembly (DfA) (G. Boothroyd & Alting, 1992) and Design

for Disassembly (DfD) (G. Boothroyd & Alting, 1992) strategies based on snap-fit part connections. A concept for the high-heel reinforcement integration is analysed and presented as well. Section 2.4 discusses the topological optimization for the selected sheet type TPMS surface-based lattice structure, which was performed using the *nTop platform* and *nTopcl* from the nTopology software (nTopology_Inc).

Figure 2.2 illustrates the different steps of the adopted methodology to achieve sustainable and additive manufacturing of footwear (here: a high-heel). In a first step, typical AM suitable polymeric material is selected and characterized on mechanical performance. Secondly, a footwear prototype model is proposed including the simulation of the load distribution (foot) during usage. In a third step, the assembly system to integrate the individual footwear components into a product (high-heel) is developed including numerical simulations for functional and strength validation. Finally, a topological optimization of the developed high-heel has been performed to determine the most appropriate lattice structure for upper part of the final footwear product. Details and preliminary design results for each step are presented in section 3.3.1, 3.3.2, 3.3.3, and 3.3.4 respectively.
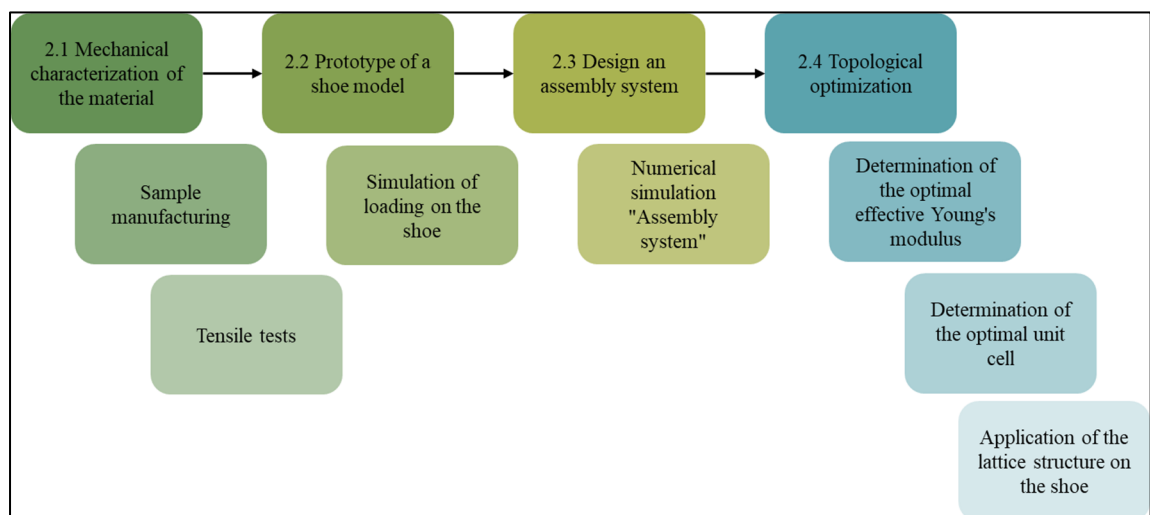
Figure 3.2 The adopted methodology to achieve this study's objectives on sustainable footwear development

3.3.1   Prototype design

A high-heeled shoe is traditionally composed of more than 60 pieces per pair. However, new production possibilities are appearing with the arrival of new manufacturing technologies, notably 3D printing. This enables the design of more complex parts and the capacity to merge different footwear assemblies into one monolithic part, thereby reducing the risks of defects due to the assembly, as well as accommodating shoe disassembly followed by repurposing (remanufacturing or recycling) at its EOL state.

The prototype design considered to the integration of key footwear parts to maintain three (3) functional parts that will be used in the assembly; the *outsole*, *insole* and *upper part* as shown in Figure 3.3 The outsole will be subjected to the load distribution applied to the shoe due to a user's weight and therefore it must be able to withstand this load with a specified safety factor. The insole must have a certain amount of flexibility (low stiffness) to ensure the users' comfort when wearing the shoe. Similarly, the upper part - being in direct contact with the skin and having the role of containing the foot – needs to have a specific stiffness to ensure the comfort of the shoe while keeping a certain resistance to tearing.
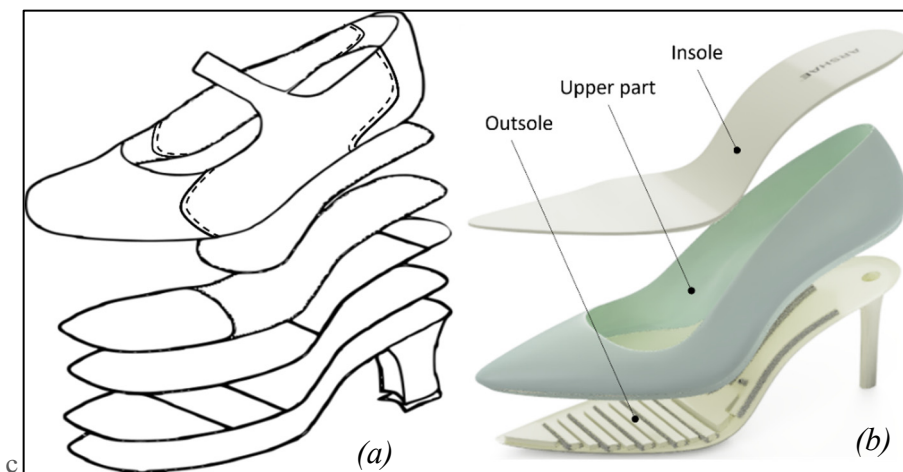
Figure 3.3 Illustration of the assembled high-heeled shoe after reduction of the number of parts, (a) simplified traditional shoe, (b) developed prototype

3.3.2 Printing material and technology

Based on their mechanical properties (see Tableau 3.1), two materials were selected in the developed novel footwear concept: polyamide 12 (also called nylon 12 or PA12) and a thermoplastic polyurethane (TPU). The nylon 12 material *PA2200* from EOS (EOS) was selected for the *outsole* and the thermoplastic polyurethane LUVOSINT TPU X92A-1 NT from LEHVOSS Group (LehVossGroup, 2019) for the *upper part* and the *insole*.

Tableau 3.1 Mechanical properties provided by the manufacturer

Materials	Tensile Strength (MPa)	Young modulus (MPa)	Elongation at break (%)
PA2200	48	1650	18
LUVOSINT TPU X92A-1 NT	20	92*	520

* Shore hardness A

Both materials were used for the fabrication of ASTM D638-14 (ASTM, 2014) standardized tensile test samples by selective laser sintering (SLS) (see Figure 3.4). The EOS FORMIGA P110 Velocis machine and the FARSOON 252P HT machine were used as SLS machines for the PA12 and TPU based materials, respectively.

The orientation of the SLS printing was done in the lateral XY plane as shown in Figure 3.4 and 100% virgin powder was used as feedstock. In order to assess the influence of postprocessing on the SLS printed samples' mechanical properties (e.g. Young's modulus, Tensile Strength, Elongation at break), half of the printed polyamide specimen batch (lot size: $n = 16$) did undergo a chemical surface treatment by Vapor Polishing (AMTechnologies, 2022) on a POSTPRO SF100 machine (AMTechnologies) and the other half of the batch was left untreated.
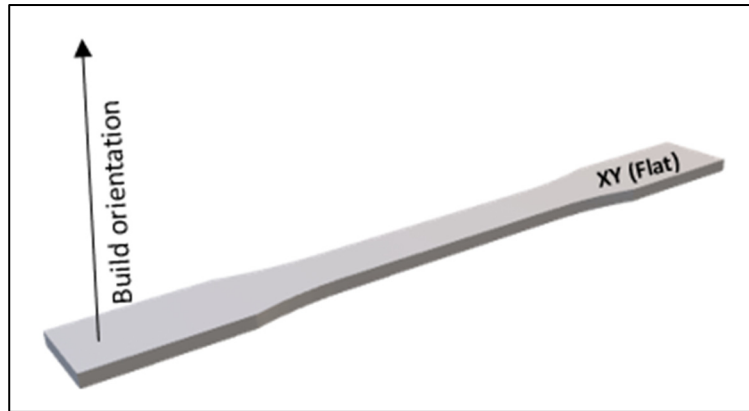
Figure 3.4 Specimen orientation during printing

Hence, to compare the mechanical properties of the PA2200 material as printed and vapor polished, for further use in this work, tensile tests were performed with a 10kN load cell on an MTS Alliance RF/200 machine at 23°C and 50% humidity.

3.3.3   Design of the mechanical assembly system

To achieve footwear disassembly for complete repurposing (remanufacturing or recycling) at its end-of-life, it is essential to eliminate the use of chemical glue during the shoe assembly process. Avoiding the use of glue facilitates footwear parts disassembly for their individual recycling. Therefore, in this study, we have developed an exclusively mechanical assembly system instead of using chemical connections. The proposed assembly system has been divided into two parts, the first part consists of designing an assembly system for the front part of the shoe, which is beyond the scope of this work, the second part consists of developing a mechanical system for the rear part of the shoe (at the heel). A snapfit system is proposed to assemble the upper and the outsole as shown in Figure 3.5 An aluminum pin (cross-section shown in yellow in Figure 3.5(a), and a 3D image presented in Figure 3.5(b)) has been inserted into the heel to increase the lateral impact resistance.
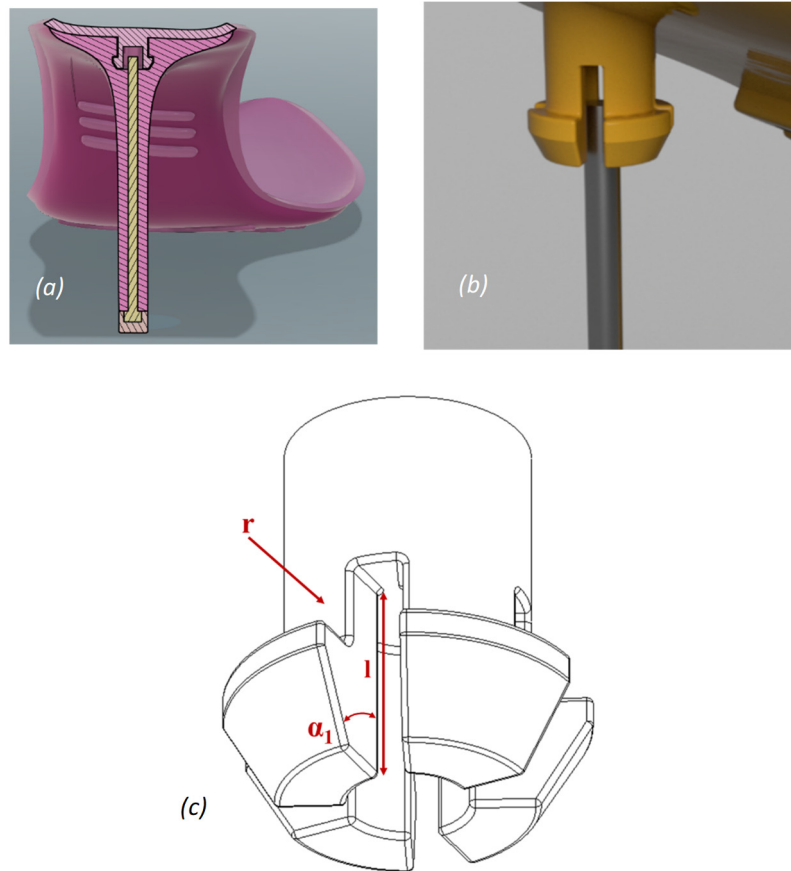
Figure 3.5 Cross section (a) illustrating the integration of the snapfit in the shoe, and (b) integration of the male part of the snapfit to the upper part, and (c) illustration of snapfit dimensional parameters

The snap-fit connection was designed according to the guidelines proposed by Bonenberger (Bonenberger, 2016). Analytical calculations of snap-fit parameters, such as assembly and disassembly forces and maximum rod deflections, were performed to dimension and validate the preliminary design.

The equations used in this section are based on the work of Ticona (Ticona, 2009) on snap-fit connections of plastic parts. The maximum deflection of each rod in the snap connection is calculated as follows by Eq. (3.1):

$$H_{max} = 0.555 \frac{l^2}{r} \frac{\varepsilon_{max}}{100} \tag{3.1}$$

Where H_{max} is the maximum deflection in mm, l is the length of the snapfit legs in mm, r is the outer radius of the circular legs in mm, and ε_{max} is the maximum allowable strain (recommended as 1/3 of the ultimate strain).

Using a snapfit legs' (see Fig. 5.(c)) length of 3.5 mm and a outer radius of 2 mm in Eq.1 results in a maximum deflection H_{max} of 5.9 mm to reach the allowable limits with a strain of 1/3 of 520% according to our design (maximum elongation provided by the manufacturer of the selected TPU X92A-1 NT) (LehVossGroup, 2019).

To calculate the joining force, $F1$, the following equations (3.2) and (3.3) were deployed:

$$F1 = \frac{3H\,E_s\,J}{l^3}\,\frac{\mu + \tan\alpha1}{1 - \mu\,\tan\alpha1} \qquad (3.2)$$

$$J = 0.0508\,r^4 \qquad (3.3)$$

Note that H is the bending of the snapfit legs (designed as $H = 2.5$ mm for proper mating), E_s is the secant modulus of elasticity calculated from the data obtained by performing tensile tests according to ASTM D638 on the selected LUVOSINT TPU X92A-1 NT material (resulting in $Es = 37$ MPa), J is the moment of inertia based on the study of Ticona (Ticona, 2009), l is the length of the legs, μ is the coefficient of friction, and $\alpha1$ is the assembly angle of the legs (here $\alpha1 = 30°$). The coefficient of friction was estimated to be $\mu = 0.329$ after consulting the work on "Surface quality improvement of selective laser sintered polyamide 12" by Guo, Bai, Liu, and Wei (J. Guo, Bai, Liu, & Wei, 2018) and the previously cited design guide (Bonenberger, 2016), which prescribes a coefficient of friction μ between 0.3 and 0.4 for polyamide 12 material.

Equations (3.1), (3.2) and (3.3) give us a force per rod equal to 5.9N which must be multiplied by the number of snapfit legs, which is 4 in our case, giving us the mounting force of 23.6N. The disassembly force, $F2$, for a 90° angle can be calculated with the equation (3.4)

$$F2 = A\,\tau_b \qquad (3.4)$$

With *A* being the shear area (Figure 3.6) of the rod and τ_b being 60% of the ultimate stress of the material used (0.6 x 20 MPa). This results in a disassembly force of *F2* = 156 N per rod, which we multiply by 4 to obtain the total force, or 624 N (63.63 kgf) for the TPU X92A-1 NT material, which is significantly higher than the normal force resistance applied for high heel pull-off as recommended by the SATRA TM113:1996 footwear standard (40kgf).
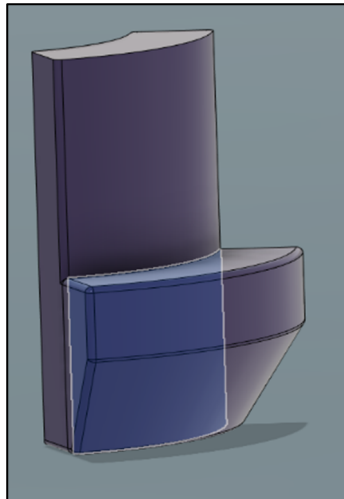
Figure 3.6 Illustration of a quarter of the designed circular snapfit legs, including the surface A (highlighted in blue) that is used in equation (4) to calculate the disassembly force

3.3.4   Topology optimisation and weight reduction

Additive manufacturing is emerging in the fashion sector, and especially the footwear industry. Specific interest has been reported on the exploitation of the full design potential provided by AM technology, i.e. the creation of parts with complex geometries, for example witnessed by the use of lattice structures for shoe soles (Thomasson & Michalska, 2017). There is abundant literature on this subject, which focuses mainly on the sole design to improve users' comfort (Teixeira et al., 2021; Z. Wang, Srinivasa, Reddy, & Dubrowski, 2022) by absorbing the energy transmitted to the sole during walking or running.

The present study proposes to address the comfort issue for the one-piece printed high-heel shoe by topological optimization of the monolithic material based upper part to approach the

comfort offered by conventionally manufactured heterogenic material-based footwear. It should be noted, that in the current footwear market the approach chosen by manufacturers is to use different materials with different density and mechanical properties to optimize the absorption of energy due to walking.

Figure 3.7 illustrates the Shore A hardness gradient for high-heeled shoes as recommended by industrial shoe designers. A conversion of the Shore A hardness is therefore necessary towards a mechanical property that can be manipulated by architectural materials. This study proposes to use the Young's modulus which has several methods of conversion to Shore A hardness (Larson, 2017; Meththananda, Parker, Patel, & Braden, 2009; A. W. Mix & A. J. Giacomin, 2011).
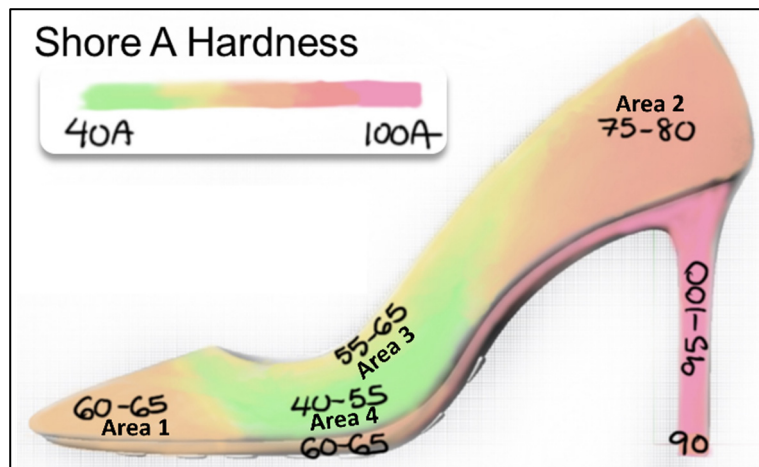
Figure 3.7 Illustration of the Shore A hardness in different areas of the shoe

Tableau 3.2 presents the conversion results according to different developed Shore A hardness – Young's modulus conversion methods, i.e. the Gent Function, the Error Function, the Ruess Function, and Mix & Giacomin's method. The conversion relations for each method are presented below by equations (3.5), (3.6), (3.7) and (3.8) from literature studies, respectively (Larson, 2017; Meththananda et al., 2009; A. W. Mix & A. J. Giacomin, 2011).

[Gent Function]

$$Y = (0.0981(56 + 7.62336\, S_A))/(0.137505(254 - 2.54\, S_A)) \qquad (3.5)$$

[Error Function]

$$S_A = 100 \text{ erf } (3.186 \ 10^{-4}\sqrt{Y}) \tag{3.6}$$

[Ruess Function]

$$Y = 10^{0.0235 \ S_A - 0.6403} \tag{3.7}$$

[Mix & Giacomin]

$$Y = (3 \ F_0 \ (1 + Mi \ S_A)/(1 - S_A \ ))/8 \ p_0 \ r \tag{3.8}$$

In these relations Y represents the Young's modulus and S_A the value indicated by the durometer according to ASTM D2240-05 (ASTM-International, 2021). For equation (3.8), Mi is the Mechanical indentability, which can be calculated using the relations presented in literature (A. W. Mix & A. J. Giacomin, 2011), and the constants F_0, p_0 et r are the characteristics of the durometer for Scale A (A. W. Mix & A. J. Giacomin, 2011). In equation (3.8), Mi is the mechanical indentability, which can be calculated using equation (3.9) (A. W. Mix & A. J. Giacomin, 2011)

$$Mi = kp_0/\sigma F_0 \tag{3.9}$$

where k is the stiffness constant of the spring mounted inside the durometer, and the constants F_0, p_0 and r equal the values of 0.55 N, 0.25 cm, and 0.0395 cm respectively (A. W. Mix & A. J. Giacomin, 2011). These constants are the characteristics of the durometer used for the Shore A scale (A. W. Mix & A. J. Giacomin, 2011).

Tableau 3.2 Conversion of Shore A hardness to Young's modulus using different methods

Areas	Shore A	Gent function (MPa)	Ruess function (MPa)	Error function (MPa)	Mix & Giacomin Method (MPa)
1	60 - 65	3,6 - 4,42	5,88 - 7,71	3,48 - 4,3	4,79 - 5,88
2	75 - 80	7,05 - 9,35	13,24 - 17,36	6,5 - 8,09	9,38 - 12,43
3	55 - 65	2,96 - 4,42	4,48 - 7,71	2,81 - 4,3	3,94 - 5,88
4	40- 55	1,68 - 2,98	1,99 - 4,48	1,35 - 2,81	2,24 - 3,94

Since not all the methods presented above give the same result, the method of Mix and Giacomin (A. Mix & A. Giacomin, 2011) was chosen for this study as their method is suggested by the ASTM standard D2240-15(2021) (ASTM-International, 2021; A. W. Mix & A. J. Giacomin, 2011), as typically adopted by industry.

To create an appropriate lattice structure for the upper part of the shoe, an optimization algorithm was developed using Python and the nTop platform via nTopcl (nTopology Inc (nTopology_Inc)), as a tool for creating lattice structures. The design was based on the TPMS type, which is considered as the most appropriate lattice type for small thickness structures. The material properties were determined using the numerical homogenization method (George. Papanicolau, Alain. Bensoussan, & Lions, 1978; Strömberg, 2022), which involved applying boundary conditions (Khan & Al-Rub, 2018; Khan, Al Hajeri, & Khan, 2021) on a finite element model representing a unit cell in a periodic structure. The homogenized elastic properties of the material are calculated from the displacement fields associated with six-unit strain loads in the X, Y, Z, XY, YZ, ZX directions under periodic boundary conditions. The nTop platform allows to test the elastic response of each created unit cell and it enables to determine the stiffness tensor of the structure according to the different directions in the form of a 6x6 sized matrix, using the generalized Hooke's law $\sigma_{ij} = C_{ijkl}\varepsilon_{kl}$, where σ_{ij}, ε_{kl}, and

C_{ijkl} are the components of the Stress, strain and stiffness tensor respectively, which we can be represented as follows (Eq. (3.10)) using Voigt's notation:

$$\begin{pmatrix} \sigma_1 \\ \sigma_2 \\ \sigma_3 \\ \sigma_4 \\ \sigma_5 \\ \sigma_6 \end{pmatrix} = \begin{bmatrix} C_{11} & C_{12} & C_{13} & C_{14} & C_{15} & C_{16} \\ C_{21} & C_{22} & C_{23} & C_{24} & C_{25} & C_{26} \\ C_{31} & C_{32} & C_{33} & C_{34} & C_{35} & C_{36} \\ C_{41} & C_{42} & C_{43} & C_{44} & C_{45} & C_{46} \\ C_{51} & C_{52} & C_{53} & C_{54} & C_{55} & C_{56} \\ C_{61} & C_{62} & C_{63} & C_{64} & C_{65} & C_{66} \end{bmatrix} \begin{pmatrix} \varepsilon_1 \\ \varepsilon_2 \\ \varepsilon_3 \\ \varepsilon_4 \\ \varepsilon_5 \\ \varepsilon_6 \end{pmatrix} \tag{3.10}$$

In the case of cubic elasticity, the stress is written as shown in equation (3.11). Then, the following relations for the stiffness tensor components are deployed: $C_{11} = C_{22} = C_{33}$, $C_{12} = C_{21} = C_{13} = C_{31} = C_{23} = C_{32}$, $C_{44} = C_{55} = C_{66}$, and the rest of the components are equal to zero:

$$\begin{pmatrix} \sigma_1 \\ \sigma_2 \\ \sigma_3 \\ \sigma_4 \\ \sigma_5 \\ \sigma_6 \end{pmatrix} = \begin{bmatrix} C_{11} & C_{12} & C_{12} & 0 & 0 & 0 \\ C_{12} & C_{11} & C_{12} & 0 & 0 & 0 \\ C_{12} & C_{12} & C_{11} & 0 & 0 & 0 \\ 0 & 0 & 0 & C_{44} & 0 & 0 \\ 0 & 0 & 0 & 0 & C_{44} & 0 \\ 0 & 0 & 0 & 0 & 0 & C_{44} \end{bmatrix} \begin{pmatrix} \varepsilon_1 \\ \varepsilon_2 \\ \varepsilon_3 \\ \varepsilon_4 \\ \varepsilon_5 \\ \varepsilon_6 \end{pmatrix} \tag{3.11}$$

To obtain the shear coefficient G and the Poisson ratio v from the compliance tensor S, it is necessary to invert the stiffness tensor using $\varepsilon = C^{-1}\sigma$ and $C^{-1} = S$. The compliance tensor can then be presented by:

$$S = \begin{bmatrix} 1/Y & -v/Y & -v/Y & 0 & 0 & 0 \\ -v/Y & 1/Y & -v/Y & 0 & 0 & 0 \\ -v/Y & -v/Y & 1/Y & 0 & 0 & 0 \\ 0 & 0 & 0 & 1/G & 0 & 0 \\ 0 & 0 & 0 & 0 & 1/G & 0 \\ 0 & 0 & 0 & 0 & 0 & 1/G \end{bmatrix} \tag{3.12}$$
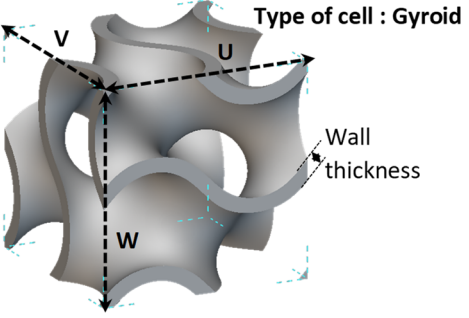
With
$$G = \frac{Y}{2(1 + v)}$$
(3.13)

Here, Y is the Young's modulus, v is the Poisson's ratio and G is one of the shear coefficients. The full mathematical homogenization model, that was used in this study, will not be developed here, since it is not the focus of this work. More details on this adopted model can be found in literature (Khan & Al-Rub, 2018; Khan et al., 2021).

The chosen independent variables are the type of unit cell, the thickness of the cell walls, and the dimensions of the box containing the cell as presented in Tableau 3.3. The algorithm implemented for the creation of the optimized model of the lattice structure that meets the given constraints (Young modulus) at each point of the shoe. Figure 3.8 illustrates the implemented workflow to achieve this design optimization goal, which consist of two phases.

The automatic phase includes an optimization program that has the coordinates of a point cloud and the associated target as input, and the output of this program consists of the values of the independent variables that allowed us to reach the targeted effective Young's module (Y*). The manual phase consists in creating a mesh of the model with the requested mesh quality (noting that the gradual transition of unit cell geometric parameters between the zones depends greatly on the size of the chosen mesh) and subsequently extracting the point cloud that corresponds to the nodes of the mesh. After the automatic phase, it is necessary to implement the results of the topological optimization to the point cloud using the "*Ramp bloc*" function on the nTop platform to ensure a gradual evolution of the dimensions of the unit cells in order to obtain a more refined and aesthetical final model and product.

Tableau 3.3 Description of the used independent variables

Designation	Range	Type of cell : Gyroid
Wall thickness (mm)	[0.06 to 0.1]	
Size UVW (mm) $U = V = W$	[2 to 5]	
Lattice cell type (TPMS)	Gyroid, Shwarz, Diamond, Lidinoid, SplitP, Neovius	
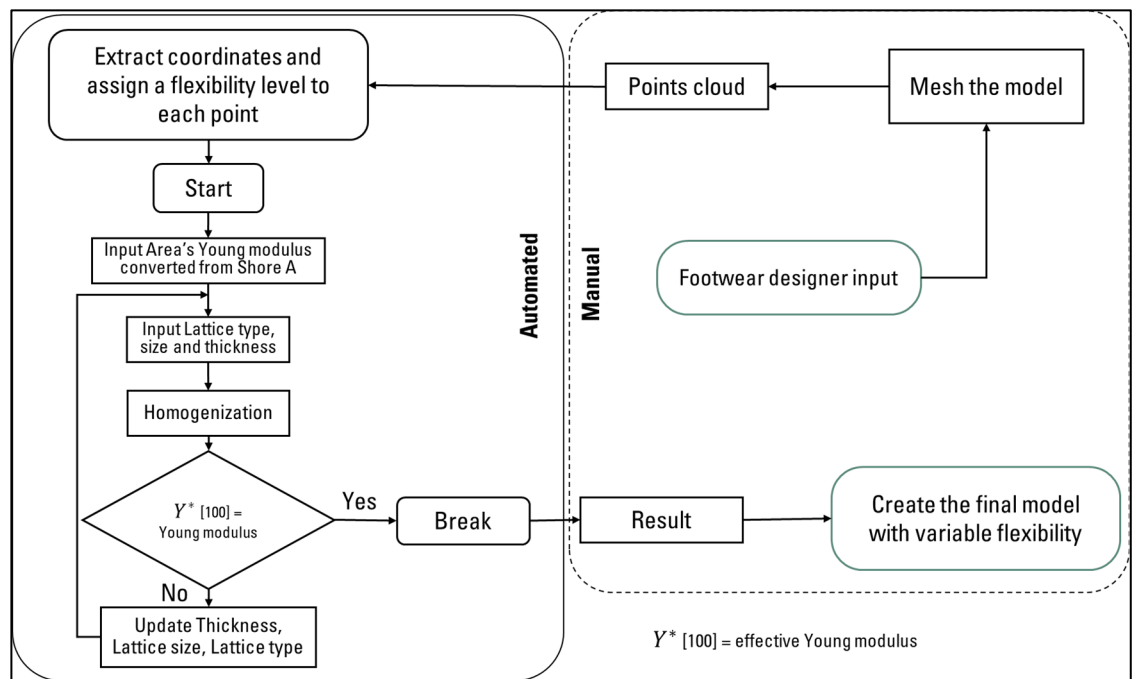
Figure 3.8 Algorithm for optimizing the unit cell parameters to achieve the targeted flexibility at any point

3.4   Results and Discussion

This section presents the obtained results on the development of the proposed high-heel shoe. It starts by presenting the results of the tensile tests performed on the used material (section 3.1), followed by a numerical FEA simulation of the snapfit assembly to validate the realized

geometry and dimensions (section 3.2). The results of a static study on the weight distribution on the Outsole will be presented in section 3.3, and the results of the topological optimization algorithm performed on the upper part are discussed in section 3.4.

3.4.1 Tensile strength tests

Tensile tests were performed to determine the main mechanical characteristics of each material (modulus of elasticity, ultimate strength, and ultimate elongation) for their implementation in the numerical simulation software to validate the proposed designs. Tensile tests were performed according to the ASTM D638-14 protocol (ASTM, 2014) at a strain rate of 50 mm/minute on 8 specimens per type at an ambient temperature of $21° \pm 0.5$. The average results of the tensile strength tests are presented in Tableau 4. These results show the differences on the mechanical properties for the surface treated samples and the as-printed samples. It can be clearly observed that there is a statistically significant increase (p-value < 0.0001) in the ultimate strength (UTS) of the vapor polished samples, however the elongation at break (E) and the Young's modulus (Y) do only very slightly differ between the treated and as-printed parts. This small difference may be due to the manufacturing variability of the SLS printed specimens. As well, it should be noted that this difference in the average Y between the as-printed and vapor polished samples is 2.04%, which is within the normal variability of the PA2200 AM feedstock, which is about 5.8% for the SLS printing technology (Faes, Wang, Lava, & Moens, 2015).

Tableau 3.4 Average uniaxial tensile tests results

Material	Mean UTS [MPa] (SD)	CoV [%]	Mean E [%] (SD)	CoV [%]	Mean Y [MPa] (SD)	CoV [%]
EOS PA2200 As printed	52.0 (0.42)	0.80	18.8 (2.60)	13.79	2135.8 (142.64)	6.68
EOS PA2200 Vapor Polished	54.1 (0.71)	1.31	18.9 (2.04)	10.77	2093.0 (48.94)	2.34

UTS = Ultimate Tensile Strength; E = Elongation at break; Y = Young Modulus; (SD) = standard deviation; CoV = Coefficient of Variance

Figure 3.9 presents a typical stress-strain curve of an as-printed and vapor polished Nylon 12 specimen. The higher tensile strength for vapor polished samples compared to the as-printed specimens can be clearly witnessed in this figure, as well as the similarity in Young's modulus for both samples.
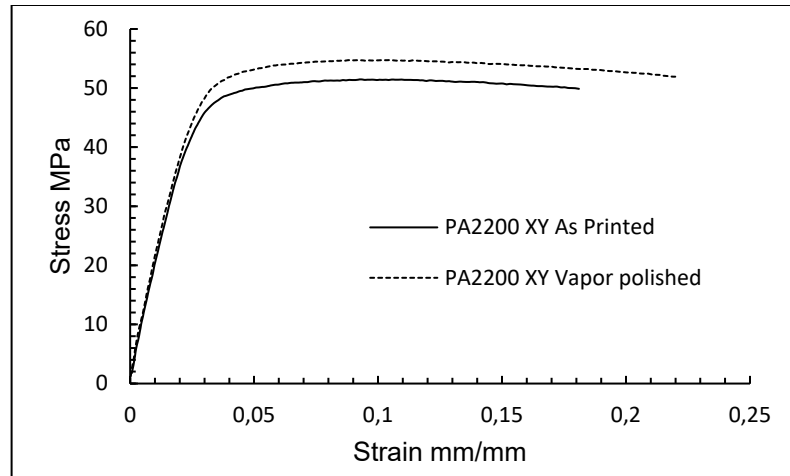
Figure 3.9 Difference in stress-strain behaviour between the as-printed and vapor polished SLS fabricated PA2200 samples

3.4.2   Simulation of snapfit mate

The NASTRAN solver version 17.0.0.21 (AUTODESK) through the Fusion 360 software (AUTODESK) was used to perform a dynamic FEA to analyze occuring stresses and strains of the snapfit legs during mating of the circular snapfit. Concerning the boundary conditions, the female part (PA12) was fixed in all degrees of freedom, and a vertical movement with velocity of 4 mm/s was induced to the male part (TPU). A global coefficient of friction between all faces was set at 0.329 (J. Guo et al., 2018).

Figure 3.10 shows a mapping of the equivalent Von Mises stress in MPa and the equivalent strain on the male part of the TPU snapfit. It can be clearly identified that the Von Mises stress reaches a maximum of 11.7 MPa and does not exceed the tensile strength of the TPU X92A-1, which is equal to 20 MPa according to the supplier. Note that a very small strain is applied for the snapfit assembly.
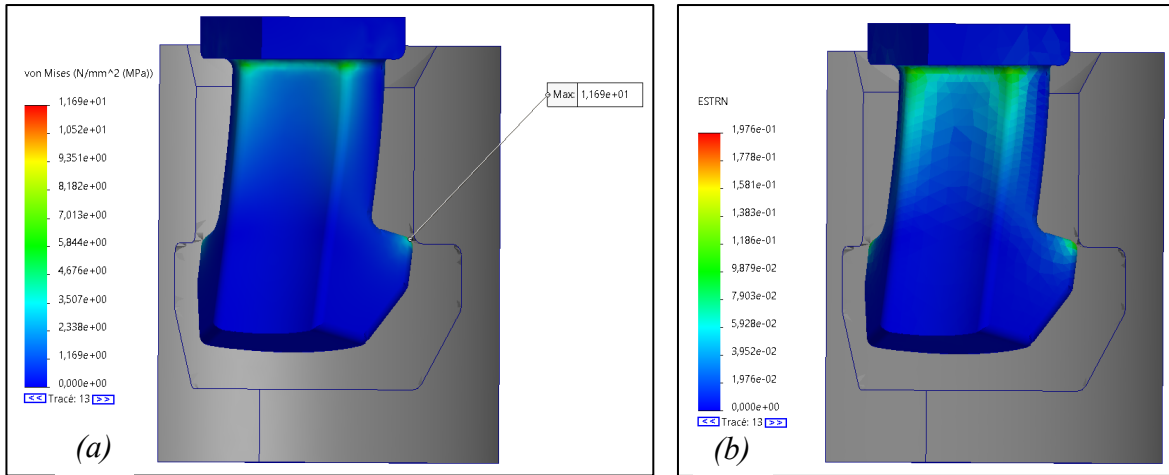
Figure 3.10 Distribution of (a) Von Mises stress and (b) equivalent strain in the designed snapfit model

Figure 3.11 shows the evolution of the von Mises stress as a function of time during assembly at the critical point of the snapfit (the radius at the base of the cylindrical snapfit legs). It can seen that the highest stress reached here is 6 MPa knowing that the TPU X92A-1 used for this part has a tensile strength of 20 MPa according to the data sheet provided by the manufacturer (LehVossGroup, 2019). Hence, the simulation validates the design of the developed snapfit printed in TPU X92A-1.
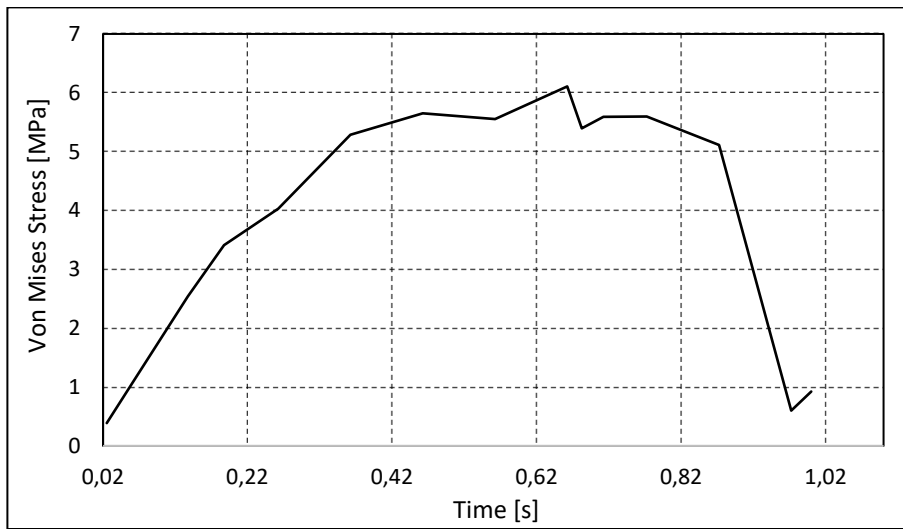
Figure 3.11 Nonlinear Von Mises stress in function of time at the base of each leg

3.4.3   Static study

This section will focus on a static study (no evolution of the load as a function of time) and will be divided into 3 subsections, which will cover respectively plantar division useful for mapping the load on the shoe, the weight distribution, and the stresses of the shoe with the integration of snapfit.

3.4.3.1   Plantar division

The sole of the feet is divided into eight (8) anatomical zones based on the work of Shang et al. [43], these zones are referred to as (T1): big toe, (T2-5): small toe, (M1): first metatarsal, (M23): central forefoot, (M45): lateral forefoot, (MF): midfoot, (MH): medial heel, (LH): lateral heel. These plantar areas are shown in Tableau 3.5.

3.4.3.2   Weight distribution

The calculation of the weight distribution is based on the experimental work of Shang et al (Shang et al., 2020), which was carried out on twenty adult female volunteers with a weight of (53.56 ± 5.75 kg) and an age of (20.89 ± 3.04 years) and which consists of measuring (using an F-Scan® measuring device from the manufacturer Tekscan® (Teskan)) the distribution of forces applied to different types of footwear during their use. A static study was carried out by simulating the application of pressure on the different plantar zones described above according to Tableau 2.5.

Tableau 3.5 Distribution of pressure on the assembled shoe
Tirée de Shang et al. (2020)

Contact Area	Surface [mm²]	Pressure [kPa]
T1	537	13,79
T2-5	796	10,6
M1	721	17,27
M23	662	18,09
M45	639	9,59
MF	626	6,09
MH	1285	10,42
ML	943	8,79

For simplification and reduction of computational time, the upper part was cut at the height of the outer sole and a FEA was performed, simulating the application of pressure on the different plantar zones described above, which is discussed in the previous section.

3.4.3.3   Snapfit integration performance

The FEA simulation was performed on the NASTRAN solver version 17.0.0.21 (AUTODESK) through the Fusion 360 software (AUTODESK). A quadratic tetrahedral mesh size based on the 1% model and an adaptive mesh size refinement based on the accuracy of the Von Mises constraint with a convergence rate tolerance of 5% were configured. Since the objective of this part of the study is to analyze the behavior of the shoe under gait loading, a bonded type of contact was implemented between the upper part and Outsole surfaces. This setting results in a total of 370897 mesh elements for the two parts with the worst aspect ratio of 9 out of 4% of the elements located at non-critical locations of the analyzed parts. After 9 iterations of adaptive refinement, a convergence rate of 0% is recorded for the total

displacement, validating the satisfying quality of the FEA simulation. Figure 3.12 illustrates the results of the FEA of the shoe loading with the weight distribution described above. Figure 3.12-a presents the mapping of the resulting displacement (mm) on the upper part; the maximum displacement is less than 1mm and is located at the rear end of the shoe (MH and ML). Figure 3.12-b represents the resulting displacement (mm) on the Nylon 12 (PA12) printed Outsole and indicates that the maximum displacement is 0.43mm under 6.09 kPa and is located at the Midfoot (MF). The bending at the MF can be limited by integrating a metal part (shank) to prevent material fatigue due to repeated loading on it. The integration of the snapfit does not create a weak zone, despite the hollow space provided for its assembly, due to the steel pin A36 inside the high heel, which plays a central role in the absorption of loads applied to the shoe. It should be noted that all the calculations presented in the results section have been carried out with the characteristics of materials not treated on the surface (i.e. non Vapor Polished).
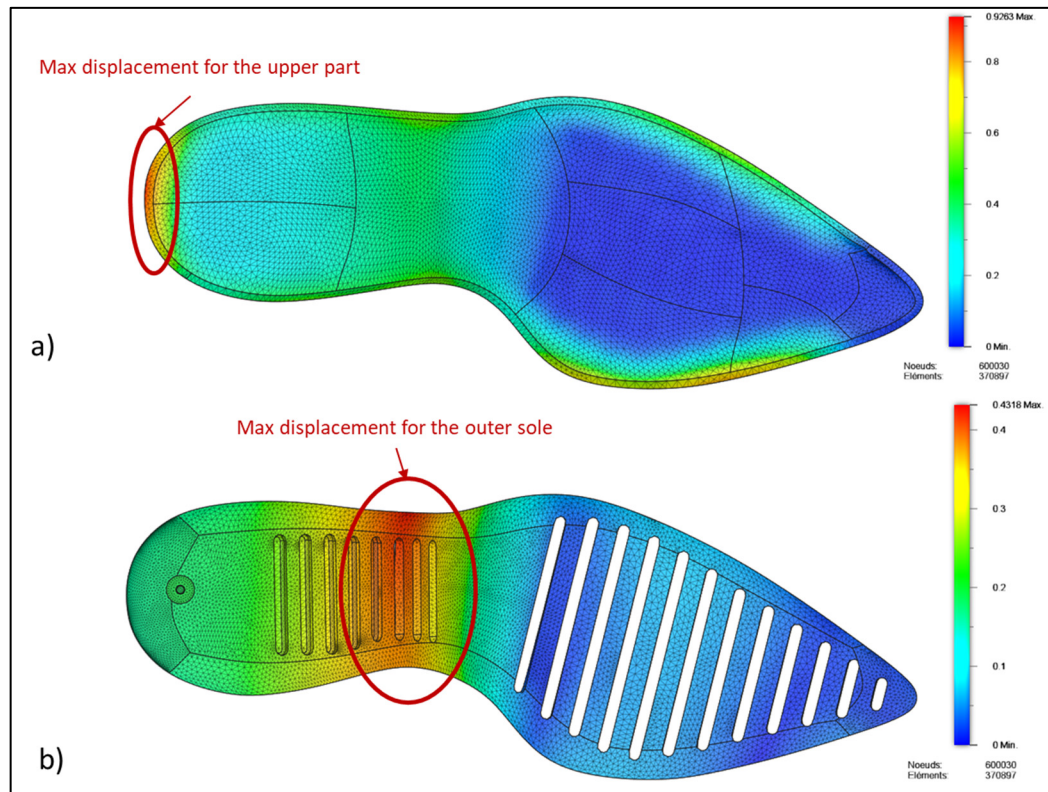
Figure 3.12 Total displacement mapping in millimeter (mm) of the developed shoe components, presenting (a) the bottom part of upper part, and (b) the outer sole

3.4.4   Topology optimisation and weight reduction

A topological optimization was performed having as objective function a minimum difference between the calculated effective Young's modulus (Y*) and the Y converted from Shore A hardness data shown in Figure 3.7 for each shoe area. Using the Block "Homogenize Unit Cell", the nTop platform allows us to obtain the elasticity tensor for each cell configured as mentioned above, we must therefore calculate Y* in all directions as well as the shear modulus and the Poisson ration, and for that we use the characteristic parameters of the fourth order elasticity tensor (Bohlke & Bruggemann, 2001; Nordmann, Aßmus, & Altenbach, 2018). We will use a modified and adapted version of MATLAB program published by Nordmann et al. (Nordmann et al., 2018) to perform the calculations and the spatial representation of Y* as well as the shear modulus and the Poisson ratio (Nordmann et al., 2018).

The results of the optimization lead to the selection of the Diamond type unit cell for its large spread of values of the Y* as a function of the geometrical parameters, which provides more possibilities to vary the flexibility of the architected material.
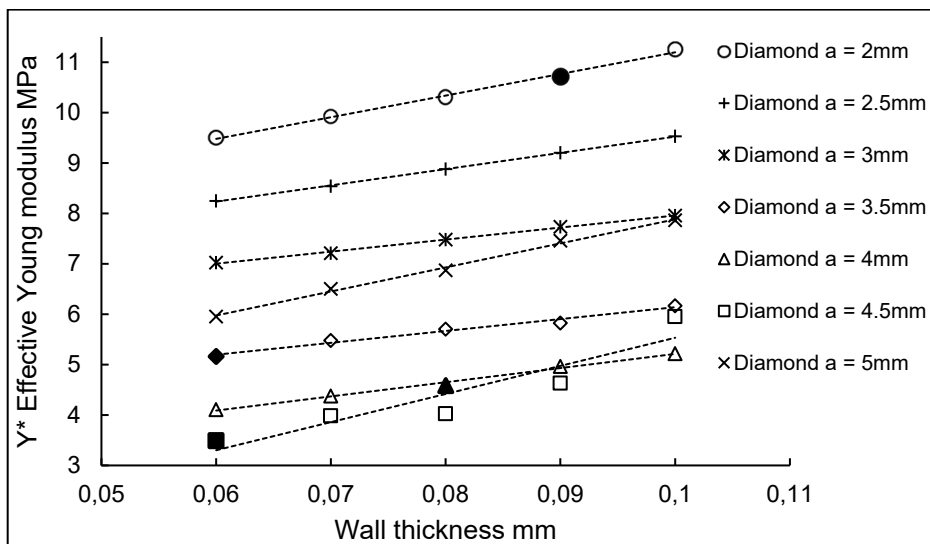
Figure 3.13 Evolution of effective Young's moduli as a function of wall thickness for the Dimond cell and different cell sizes. The highlighted points represent the parameters chosen for the different shoe areas

Figure 3.13 shows the linear evolution of the Y* as a function of wall thickness for different sizes of Diamond unit cells after homogenization. The effective Young's modulus (Y*) evolves positively with increasing wall thickness and decreases with increasing nominal unit cell size *a*. The filled markers in Figure 3.13 denote the cell parameters chosen for the different regions to obtain the targeted effective Young's modulus. Having an interval for each region of the shoe (see Fig. 7), a rule has been applied to select the points closest to the mid-ranges of Y given in Table 2, as expressed by equation (3.14)

$$Y^*(n) = \ \min\left(Y^* - \left(\frac{Y_2 + Y_1}{2}\right)\right) \qquad (3.14)$$

Where Y1 and Y2 are the boundaries of the Young's modulus range calculated using Mix and Giacomin's method (A. Mix & A. Giacomin, 2011). The following values were selected for the regions n=1, 2, 3, 4; Y*(1) = 5.16 MPa, Y*(2) = 10.71 MPa, Y*(3) = 4.58 Mpa, Y*(4) = 3.48 MPa.

Having an interval for each region of the shoe (see Figure 2.7), it was chosen to take for the first region Y*(1) = 5.16 MPa, for the second Y*(2) = 10.71 MPa, the third Y*(3) = 4.58 MPa and finally for the fourth Y*(4) = 3.48 MPa.

Figure 2.14 represents the spatial (direction dependent) visualization of the calculated effective parameters such as Y*, G* and V* for each area 1 to 4 (see Figure 3.7). In this case study, the architected material's elastic characteristics can be manipulated to control the flexibility by reorienting the unit cell, although this feature will not be utilized. Instead, all cells will be oriented such that the maximum Y*max aligns with the direction normal to the upper part of the shoe at all points. Since it is assumed that the material is cubic elastic, the Zener ratio (Li & Bradt, 1987) is also calculated to evaluate the degree of elastic anisotropy of the created structures. $Z = \ 2C_{44}/(C_{11} - C_{22})$ where $C_{11}, C_{22} \ and, C_{44}$ are component of the stiffness tensor presented in equation (3.11). A Zener ratio of 1 represents an isotopically elastic structure and the larger the deviation the more anisotropic the cellular material.

58
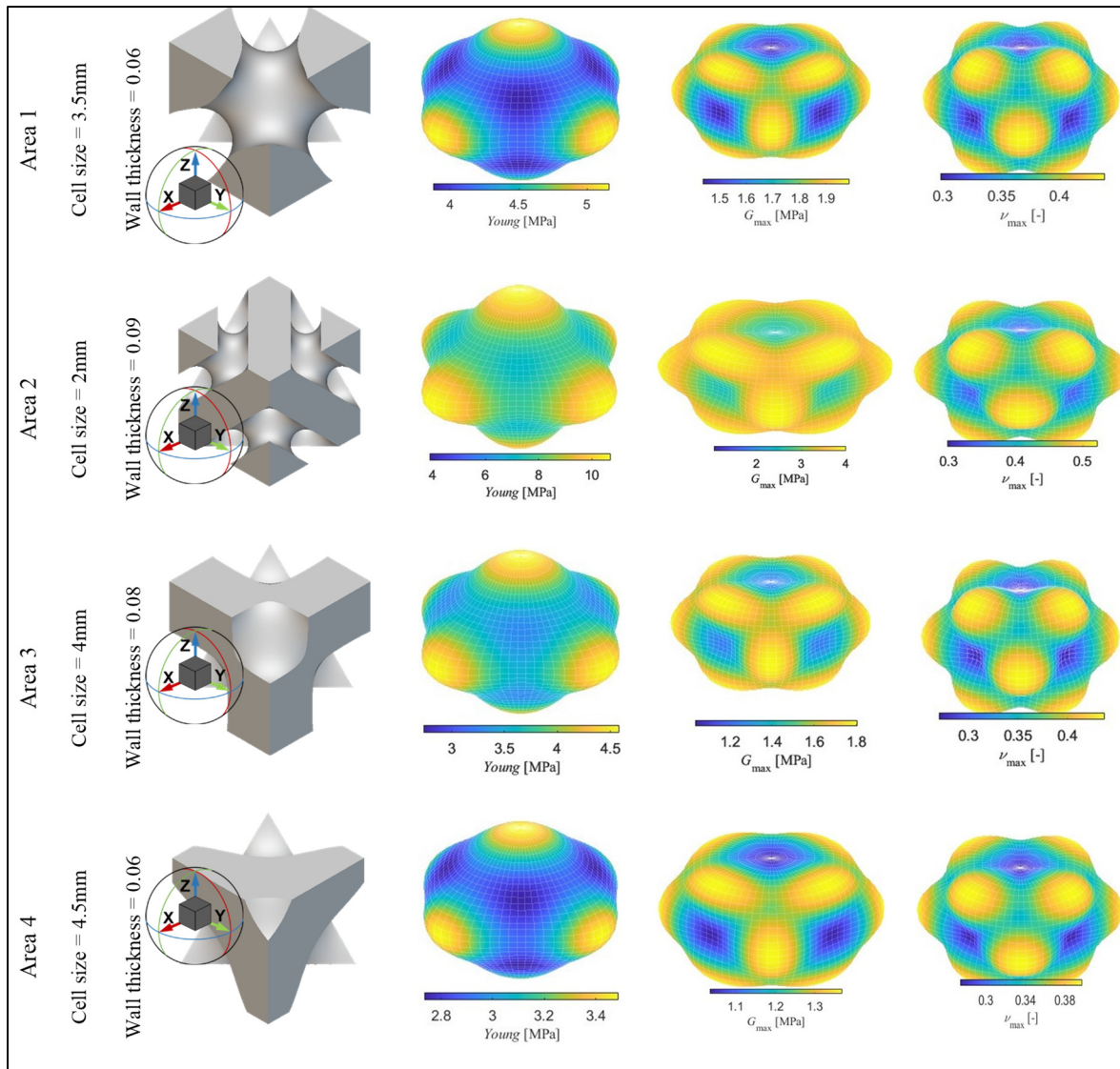
Figure 3.14 Spatial visualisation of effective Young's moduli (Y*), Shear moduli (G*) and
Poisson Ratio (V*) for the selected unit cells
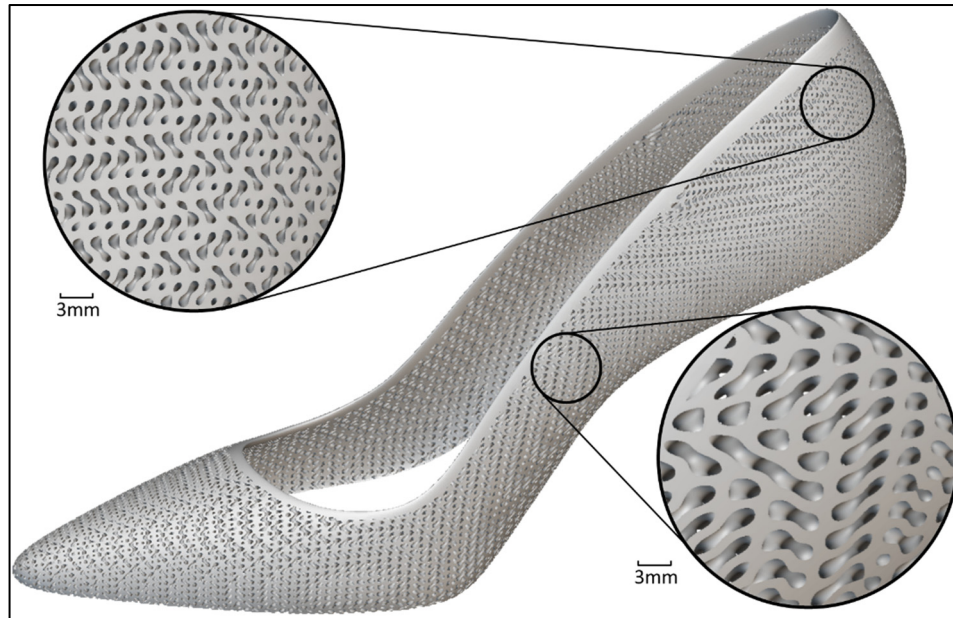
Figure 3.15 Applied lattice structure on the developed high-heel shoe according to the optimisation results

A variable flexibility has been implemented for the high-heel shoe to ensure the required user comfort (flexibility/stiffness), following footwear industry recommendations (see Figure 3.7), with a monolithic (upper) part as shown. Figure 3.15 presents this stiffness variation, which was realized by the unit cell variation in the targeted zones, including a transition gradient between each zone to ensure proper fabrication by AM and avoiding stress concentrators. A significant mass reduction of this essential high-heel component (upper part) was realized, i.e. the mass was reduced from 55.6g for the original part to 36.5g for the new design with the lattice structure. Hence, a 34% mass reduction is achieved, which contributes to the main objective of the present study aiming to minimize the use of raw materials towards a more sustainable and circular manufacturing approach for the footwear industry.

3.5   Conclusion

In summary, this study has successfully demonstrated the development of a comprehensive approach for footwear manufacturing focused on design for disassembly using AM techniques, enabling the realization of a fully 3D printed footwear product for the first time. By taking

advantage of the benefits of AM as fabrication method, including new design possibilities and glueless assembly by snapfit systems, the proposed approach reduces the number of parts used for footwear production and improves the re-manufacturability and recyclability of (high-heeled) shoes. The footwear design was validated by finite element analysis, based on the use of PA2200 and TPU polymeric materials as AM feedstock, and an assembly and disassembly system compliant with industrial standards, such as SATRA TM113:1996, was developed. As well, the selected polymer material was tested on mechanical performance (tensile strength) with and without a vapor polishing treatment after AM sample fabrication.

In addition, a topological optimization algorithm was implemented to reduce the mass of the shoe by 34% while achieving variable flexibility in a monolithic product, following footwear industrial standards for required comfort and durability. Overall, the developed approach is consistent with the footwear industry's goal of reducing the environmental impact and increasing the durability of its products. Future work includes physical testing of the designed parts and the multi-material snapfit system to further validate their mechanical characteristics (e.g. on elasticity and on wear and tear) and performance for consumer's usage.

Declaration of Competing Interest

The authors declare that they have no known competing financial interests or personal relationships that could have appeared to influence the work reported in this paper.

Data availability

The raw and processed data, including developed codes for the topology optimization, required to reproduce the findings reported in the present study are available to download from https://github.com/ChahGhim/Topo-Optimisation_Footwear

CHAPITRE 4

INFLUENCE OF ENVIRONMENTAL AGING FACTORS ON THE MECHANICAL PROPERTIES OF POWDER BED FUSION FABRICATED PA12 PARTS

Chahine Ghimouz[a], Jean Pierre Kenné[a], Lucas A. Hof[a*]

[a] Mechanical Engineering Department, École de technologie supérieure, 1100, rue Notre-Dame Ouest, Montreal, Quebec, Canada H3C 1K3

Les ingénieurs et concepteurs jouent un rôle clé dans la transition vers un système en boucle fermée. En effet un des piliers de l'EC est d'allonger la durée d'utilisation des biens, et ceci peut être atteint par une conception bien réfléchie de ces derniers. La compréhension du comportement des matériaux au fil du temps est primordiale pour une conception adaptée à chaque utilisation et ainsi allonger la durée de vie des pièces imaginées par les ingénieurs. Le vieillissement des polymères est un phénomène omniprésent d'où l'importance de comprendre les facteurs qui joue un rôle à son accélération pour une conception durable des pièces en polymère.

La fabrication additive de polymères engendre des résultats hétérogènes d'un point de vue des propriétés mécanique, il est donc plus juste d'aborder la question de ces propriétés avec une approche statistique pour tenir compte de la variabilité de celles-ci.

4.1 Abstract

This paper presents an experimental study to increase understanding of the influence of environmental factors and printing orientation on the aging of 3D printed polyamide 12. A multifactorial experimental design was developed to age specimens under different controlled environments. The results of analysis of variance showed that temperature, irradiance, relative humidity, and time have a significant effect on the ultimate mechanical strength (UTS) and Young's modulus (Y) of the material. Using multiple linear regression, two predictive models

were proposed to explain the evolution of the UTS and Y as a function of environmental factors. The obtained results demonstrate that the UTS-related predictive model has a coefficient of determination (R^2) equal to .9075, which means that the model explains 90.75% of the variability, while the Y-related predictive model has an R^2 value of .5226, which explains 52.26% of the variability. These developed predictive models can help to better understand the aging of 3D printed polyamide 12, hence contributing to the design of more sustainable mechanical parts.

Keywords: Additive manufacturing, Powder bed fusion, Accelerated weathering, Polymer degradation, Mechanical properties, Nylon 12

4.2   Introduction

Polymers, often referred to as plastics, are a class of materials that have been intensively developed and studied since the beginning of the 20th century and have been mass produced for almost a hundred years now (Gewert et al., 2015). Their low masses, high flexibility and ease of shaping, give them a wide range of applications in the field of engineering. Compared to the long history of polymer engineering processes, additive manufacturing (AM) is still an emerging manufacturing process that has not yet reached its maturity, having made its beginning in the 1980s (Kodama, 1981; Su & Al'Aref, 2018). Among the seven principle AM technologies defined in the ISO/ASTM 52900:15 standard (ISO/ASTM, 2022), powder bed fusion (PBF) of polyamide 12 (Nylon 12 or PA12) is considered as the most mature category for industrial product uses (Sillani et al., 2019; Tan et al., 2020). The most widely deployed polymer AM technologies for PBF in industry are Multi Jet Fusion (MJF) (Rosso et al., 2020; Wu et al., 2022) and Selective Laser Sintering (SLS) (Rosso et al., 2020; Wu et al., 2022). SLS uses a laser to melt and fuse the feedstock powder, while MJF uses a bonding agent, heat, and infrared light to fuse the powder to create the final object. Both technologies involve heating of feedstock powder particles, with typical size between 45 and 90 μm (Schmidt et al., 2019), to sinter and consolidate the particles layer by layer to form a three-dimensional (3D) object.

When comparing to conventional manufacturing techniques, AM provides a high degree of geometric freedom in design and fabrication (Gibson et al., 2014). The advantages of PBF AM processes are numerous, such as mass customization, mass reduction, surface texturing and dimensional accuracy. To date, polymer AM is used in many applications, for example in the medical industry (Salmi, 2021), in the automotive industry (Gibson et al., 2014), in aerospace applications, and as spare parts for maintenance and repair (Khajavi et al., 2014). However, this layer-based manufacturing method results in anisotropic mechanical properties, i.e. the fabricated part's properties are directly dependent on the orientation of the part during printing and on the layer thickness (Ligon et al., 2017). In addition to low manufacturing speeds, post-processing is required in most industrial cases to ensure a satisfactory surface finish.

The composition of feedstock polymer powders used in additive manufacturing can vary significantly depending on the manufacturer, resulting in particles with different morphologies such as spherical, flaky, rounded, or irregular (G. Wang, Wang, Zhen, Zhang, & Ji, 2015). Moreover, these particles also exhibit heterogeneous sizes, leading to variations in packing density and, consequently, the final density of the additively manufactured parts. This variability in density has a direct impact on the mechanical properties of the part. Furthermore, the degradation of the material is an important factor to consider, especially when reusing powder over multiple cycles (Khajavi et al., 2014). One notable vulnerability of polymers is their susceptibility to degradation caused by environmental factors, commonly known as weathering (Ligon et al., 2017).

Polymers are formed through the polymerization process; wherein short monomers are chemically bonded to create long molecular chains comprising tens of thousands of monomers. However, prolonged exposure to environmental factors, including heat, humidity, and ultraviolet (UV) radiation, can induce structural degradation within these polymer chains. The degradation mechanisms encompass various types such as photo-oxidative degradation, thermal degradation, ozone-induced degradation, mechanochemical degradation, catalytic degradation, and biodegradation among others (G. Wang et al., 2015). It is important to note that all these degradation mechanisms can adversely affect the mechanical properties of the

polymer, which is discussed in detail in literature (Shackleford, Williams, Brown, Wingham, & Majewski, 2021). The impact of weathering on polymers has been a subject of investigation since the 1950s (Ligon et al., 2017). In order to simulate the environmental stresses that polymers experience, specialized equipment for accelerated weathering has been developed, enabling laboratories to replicate and study the effects of these stresses on polymers. The literature offers abundant studies on the aging of injection molded polymers, however, aging studies for parts additively manufactured by PBF are quite limited. Aging studies were most often carried out during the manufacturing process in order to understand the degradation of the powder and the impact of mixing recycled with virgin powder on the mechanical properties of the final part. Literature reports several studies that have contributed to the study of the aging of materials manufactured by PBF, e.g. the degradation of SLS fabricated PA12 parts after accelerated Ultraviolet B (UVB) exposure (Shackleford et al., 2021), the effect of water conditioning on the fracture behavior of composite PA12 parts (Seltzer, de la Escalera, & Segurado, 2011), and the comparison of heat conditioning on SLS and injected molded parts (Wörz, Wudy, Drummer, Wegner, & Witt, 2018). A recently published comprehensive study evaluates the effect of accelerated weathering of different materials on their mechanical properties based on method A of the ISO-4982-3 standard (ISO, 2016), which involves an Ultraviolet A (UVA)-340 radiation at 0.76 W/m^2 under an exposure at 60°C during 8 hours, followed by a 4 hours condensation phase at 50°C and repeating this 12 hours cycle for a total duration of 1500 hours (Puttonen, Salmi, & Partanen, 2021). However, the protocol provided by this standard does not allow the evaluation of the direct effect of each factor independently of the others (e.g., temperature, relative humidity, and ultraviolet light irradiance) or the combined effect on polymer degradation due to the different environmental factors.

In the context of sustainable manufacturing, improved understanding of the effect of aging on additively manufactured (polymer) materials is needed to design parts that consider their mechanical properties over time, hence their durability. A major current knowledge gap in this research field is the study of the individual and combined effect of environmental factors on polymer AM part performance. Therefore, this study aims to address this research gap by establishing an experimental design to assess the independent effect of each environmental

factor contributing to material degradation, as well as to evaluate the combined binary effect of the different independent environmental variables.

In addition, vapor polishing is evaluated as post-process for the PA12 AM parts to compare mechanical properties and weathering resistance between vapor polished and as-build samples.

4.3 Materials and Methods

The developed methodology for this study consists of four (4) stages that are presented in Figure 4.1 and discussed in the following sections 4.2.1, 4.2.2, 4.2.3 and 4.2.4. In a first step (section 4.2.1), the specimens for material degradation tests are prepared, while a second step (section 4.2.2) involves the development of the experimental design for the weathering tests, detailing both the dependent and independent variables. The third step (section 4.2.3) includes the tensile tests to determine the mechanical properties after each weathering test. Finally, in step four (section 4.2.4), the results are thoroughly analyzed by statistical methods.
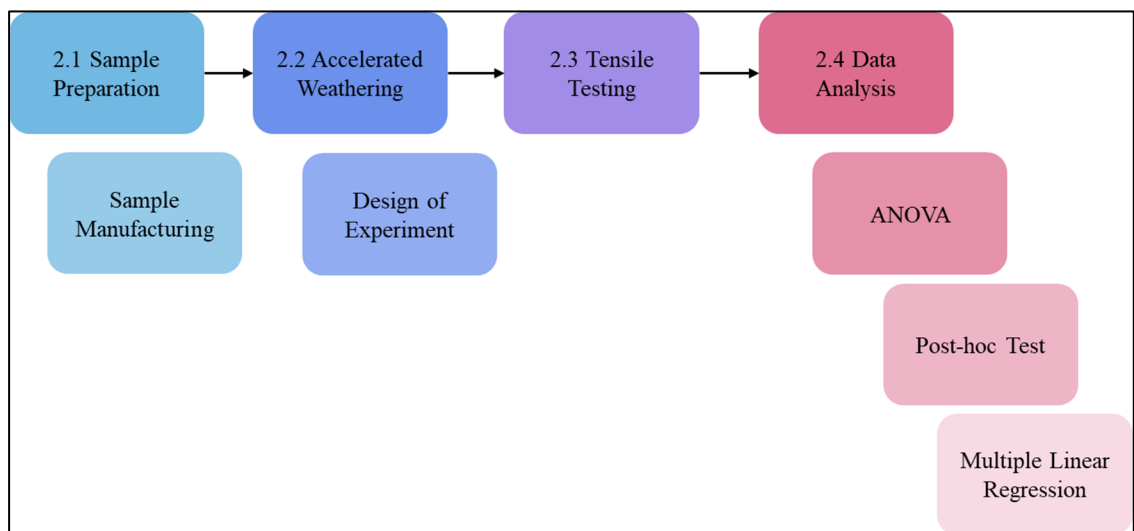
Figure 4.1 Schematic overview of the methodology adopted in this study

4.3.1 Sample preparation

Tensile tests are required to estimate the mechanical properties of interest in this work. Therefore, several suppliers were contacted to print the ordered specimens, the specimens are based on ASTM D638 Type 1 (ASTM, 2014) presented in Figure 4.2.a. All specimens were printed from virgin Polyamide 12, also referred to as PA 2200, powder from EOS on an EOS P110 SLS printer with a chamber temperature of 168°C. Figure 3.2.b. presents a screenshot of the build chamber preparation; It can be seen that the XY and XZ oriented specimens are distributed over the entire height of the chamber in order to reduce the potential effect of temperature variations on a maximum number of specimens, and to homogenize the specimens in terms of their mechanical properties.. A vapor polishing (Vp) treatment was applied to half of the specimens (135), performed by the supplier AMTechnologies (AMTechnologies, 2022), in order to estimate its protective effect on the aging of the surface condition. Tableau 4.1 summarizes the performed sampling.
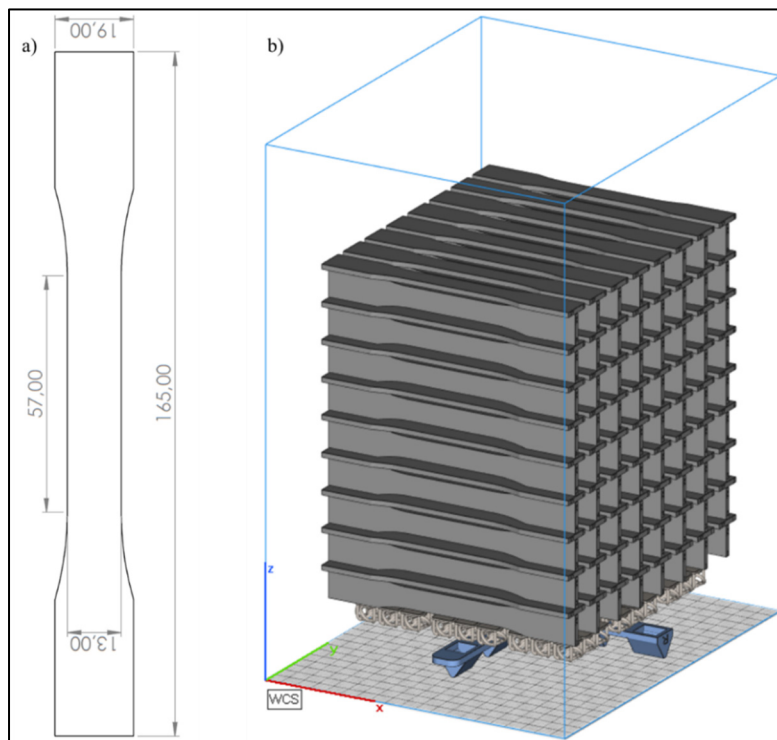
Figure 4.2 a) ASTM D638-Type 1 Specimen dimensions,
b) Build orientation XY and XZ

Tableau 4.1 Samples presentation

Materials	Supplier	Process	Orientation	Machine	Dimensions	Surface	Color
PA 2200	EOS GmbH	SLS	XY	EOS P110	ASTM D638-1	As printed	White
PA 2200	EOS GmbH	SLS	XZ	EOS P110	ASTM D638-1	As printed	White
PA 2200	EOS GmbH + AMT	SLS	XY	EOS P110	ASTM D638-1	Vapor smoothed	White
PA 2200	EOS GmbH + AMT	SLS	XZ	EOS P110	ASTM D638-1	Vapor smoothed	White

4.3.2   Accelerated weathering

An experimental design was developed including six two-level factors applied on 276 samples. The factors used in this study for accelerated aging are Temperature, Relative Humidity, Irradiance at 340nm, Time, Vapor Polishing and Layer Orientation during printing. The dependent variables under study are Ultimate Tensile Strength (UTS) and Young's modulus (Y). The details of the two-level fractional factorial experimental design are presented in Tableau 4.2 and Figure 4.3. The choice to select only particular configurations was made on the basis of the ability of the used machine. The weathering was performed on a Q-Sun Xe-3 Xenon Test Chamber (Q-LAB) using UVA lamps with a wavelength of 340 nm. A single cycle is performed on the specimens in each configuration, and the machine is recalibrated every 500 hours. The specimens are flipped to the other side in the middle of each cycle to have a homogeneous aging on both sides of each sample. Due to the seasonality of irradiance, the choice of irradiance levels is based on average values measured according to the summer and winter season (in June and December). Details of such the measurements are presented in detail in literature (Q-LAB). Regarding the temperature, humidity and time levels were chosen to have a measurable effect of each factor and that exceeds the variability of mechanical properties due to the manufacturing process (SLS) (Faes et al., 2015). The choice of the used (typical) values is based on complementary studies found in the literature (Goodridge, Hague, & Tuck, 2010; Pilipović, Ilinčić, Bakić, & Kodvanj, 2022).

Tableau 4.2. Levels for each factor

Factor		Temperature °C	Humidity % (%)	Irradiance W/m^2 .nm	Time hours	Vapor Polishing	Build Orientation
Levels	1	30	50	0,23	250	No	XY
	2	70	80	0,68	500	Yes	XZ

Figure 4.3 shows the fractional multifactorial experimental design that was developed, including the total number of specimens (276) of which 32 (11.6%) served as reference (without aging treatment). Regarding the aging treatment, 8 different configurations were tested, which is also illustrated in Figure 4.3. Tableau 3.2 presents the different levels of each independent variable for the eight (8) configurations with the corresponding number of aged specimens specified in Figure 4.3.

276 Samples

136 XZ orientation

140 XY orientation

66 With Vapor polishing

70 Without Vapor polishing

69 With Vapor polishing

71 Without Vapor polishing

8 58 8 62 8 61 8 63

No aging treatment (n=32)

Configuration (number of specimen)	Temperature	Relative Humidity	Irradiance	Time
C1 (n=31)	1	1	1	1
C2 (n=31)	1	1	1	2
C3 (n=29)	2	1	2	1
C4 (n=30)	2	1	2	2
C5 (n=32)	1	2	2	1
C6 (n=32)	1	2	2	2
C7 (n=29)	2	2	1	1
C8 (n=30)	2	2	1	2

Figure 4.3 Presentation of the fractional multifactorial experimental design

4.3.3   Tensile testing

The tensile tests conducted on the specimens were implemented according to the ASTM D638-14 Type 1 standard (ASTM, 2014) using a 10kN load cell on an MTS Alliance RF/200 machine at 23°C and at 50% humidity. The displacement speed was set to 5mm/min and the displacement data capture frequency was 10Hz with the same operator performing all the tests presented in this study. The exact dimensions (width and thickness) of the specimens are entered into the MTS software for each tested specimen to avoid dimensional variations due to the manufacturing process and possibly to the applied weathering treatments. The specimens are directly placed in vacuum sealed bags and stored at 20°C in a dark storage place after being removed from the accelerated weathering machine until the tensile tests are performed, to avoid any uncontrolled aging of the specimens.

4.3.4   Data analysis

For each factor level configuration, the number of specimens tested (n) is presented in the first column of Tableau-A I-1 in Appendix I with a total of 244 specimens tested in addition to the 32 reference specimens.

A description is presented in Tableau 3.5, which summarizes the UTS and Y results for the two levels of each factor including absolute frequencies. The collected data of the tensile results (UTS and Y) are then analyzed by analysis of variance (ANOVA) to determine the significance of the individual and combined effects of the independent variables (temperature, irradiance, relative humidity, time, presence of surface treatment by vapor polishing and build orientation) with a 95% confidence level. A post-hoc pairwise multiple comparison (Tukey test (Abdi & Williams, 2010)) for each interaction is also performed to study them include the combined binary factor effect presented in Tableau 4.2.

A multiple linear regression (MLR) model for the prediction of UTS and Y is proposed, composed of the independent variables and their possible interactions, based on the ANOVA results. If there is a need to compare multiple models, the Akaike criterion (AIC) (Cavanaugh & Neath, 2019) will be used to estimate the relative quality of each proposed model. It should be noted that the health of the models presented will be diagnosed by checking the assumptions

of linearity, absence of autocorrelation, homoscedasticity, normality of the error term, absence of multicollinear values as well as the absence of influential values using the Cook distance (Cook, 2011; Liu & Welsh, 2011). The coefficients of each independent and interaction variable will be presented and interpreted along with their associated p-values.

The explanation of the variability of the dependent variables (UTS and Y) by the independent variables (Temperature, Irradiance, Relative Humidity, Time, Vapor polishing and Build direction) is evaluated for the proposed MLR models using the coefficient of determination R^2 and adjusted R^2 metrics. R^2 adjustment is used to penalize the number of predictors used in MLR models, and the R^2 and adjusted R^2 values are calculated by Eq. (4.1) and (4.2), where n is the number of observations, and k is the number of predictors.

$$R^2 = 1 - SS_{res}/SS_{total} \qquad (4.1)$$

$$R^2{}_{Adjusted} = 1 - (n-1)\frac{(SS_{res}/SS_{total})}{(n-k)} \qquad (4.2)$$

Here, SS_{res} is the sum of squared residuals, and SS_{total} is the total sum of the squares, as denoted in Eq. (3.3) and (3.4), respectively.

$$SS_{res} = \sum_{1}^{n}(y - y^*)^2 \qquad (4.3)$$

$$SS_{total} = \sum_{1}^{n}(y - \bar{y})^2 \qquad (4.4)$$

Here, y is the individual observed value, y^* is the individual predicted value, and $\bar{y}$ is the overall mean.

4.4   Results and discussion

Reference tests were carried out on 8 specimens per category that had not received any ageing treatment, the results are summarized in Tableau 4.3. As discussed in the introduction, additive manufacturing implies a greater or lesser variability of mechanical properties depending on the control of manufacturing parameters (Caulfield, McHugh, & Lohfeld, 2007; Y. Guo, Jiang, & Bourell, 2015) and the properties of the powder used (Goodridge, Tuck, & Hague, 2012).

Tableau 4.3 Mechanical properties of PA2200 printed in orientations flat (XY)
and on edge (XZ) with and without Vp

Mechanical properties		XY as printed	XY *Vp*	XZ as printed	XZ *Vp*
UTS **MPa**	*Mean (SD)*	52,01 (0,41)	54,10 (0,70)	48,95 (0,62)	51,73 (0,39)
	CoV	0,79	1,31	1,27	0,77
	Min / max	51,30 / 52,40	52,80 / 55,00	48,10 / 50,10	51,20 / 52,30
Y **MPa**	*Mean (SD)*	2135,82 (142,64)	2093.04 (48.93)	2179,88 (208,59)	2011,02 (154,95)
	CoV	6,67	2.33	9,56	7,70
	Min / max	1933,42 / 2323,84	2031.78 / 2164.71	1811,45 / 2467,05	1856,23 / 2283,04
Elongation **at break** **%**	*Mean (SD)*	18,82 (2,59)	18.90 (2.03)	21,68 (3,42)	20,91 (2,14)
	CoV	13,79	10.76	15,80	10,25
	Min / max	15,30 / 23,20	16.10 / 21.90	15,90 / 26,90	18,50 / 23,90

The coefficient of variation (CoV) is quite low for the UTS which indicates a good repeatability as well as for the Young's modulus which has a CoV between 6.67% and 9.56 % which corresponds to the coefficient determined by Faes et al. between 5.61% and 6.5% *(Faes et al., 2015)*.

After the ANOVA of the reference results presented in Tableau 4.3, in Tableau 4.4 we can observe that the surface treatment by Vp significantly increases the mechanical strength (UTS) for any printing orientation with a p-value < 0.0001. Regarding the elongation only the orientation of the part during printing influences it with a p-value = 0.0133. Young's modulus

is not significantly affected by either Vp or part orientation during printing. No interaction between Vp and part orientation is observed for the three dependent variables.

Tableau 4.4 ANOVA for mechanical properties of PA2200 printed in orientations flat (XY) and on edge (XZ) with and without Vp

UTS		Young's modulus		Elongation at break	
Factors	*P-value*	**Factors**	*P-value*	**Factors**	*P-value*
A: Vapor polishing	<0,0001	A: Vapor polishing	0,0562	A: Vapor polishing	0,7072
B: Build direction	<0,0001	B: Build direction	0,7235	B: Build direction	0,0133
Interactions		**Interactions**		**Interactions**	
AB	0,0843	AB	0,2452	AB	0,6486

Tableau 4.5 presents a description of the data that provided by the tensile tests for both levels of the different factors by presenting the minimum (*Min*), maximum (*Max*), mean (*Mean*), standard deviation (*SD*) and absolute frequencies (*n*). It should be noted that the averages in Tableau 4.5 are not representative for the individual effect of each factor, here the effect of other factors is not considered to describe the dependent variables UTS and Y. However, the evolution of the average values is in good agreement with the literature (Puttonen et al., 2021).

Tableau 4.5 Data description: Ultimate Tensile Strength
and Young's modulus for each level of factors

	Levels	UTS (*Mpa*)			Y (*Mpa*)		
		Min	*Max*	*Mean (SD)*	*Min*	*Max*	*Mean (SD)*
Temperature (*°C*)	*30 (n=126)*	35,80	53,60	48,77 (2,97)	1745,80	2604,53	2073,92 (172,87)
	70 (n=118)	10,80	47,90	31,82 (9,21)	1640,25	4846,26	2262,75 (428,08)
Relative Humidity (*%*)	*50 (n=137)*	10,80	53,60	39,35 (12,16)	1745,80	4846,26	2269,29 (373,71)
	80 (n=107)	22,70	50,80	42,14 (8,65)	1640,25	2674,55	2032,02 (216,60)
Irradiance (W/m^2 . *nm*)	*0,23 (n=121)*	22,70	53,60	44,26 (9,13)	1640,25	2674,55	2037,32 (217,60)
	0,68 (n=123)	10,80	50,80	36,95 (11,18)	1828,54	4846,26	2291,10 (381,31)
Time (*hours*)	*250 (n=121)*	22,70	53,40	41,27 (10,50)	1640,25	3315,56	2149,18 (278,04)
	500 (n=123)	10,80	53,60	39,89 (11,16)	1723,05	4846,26	2181,04 (384,22)
Vapor polishing *No / Yes*	*No (n=125)*	18.00	51,70	41,93 (10,19)	1640,25	3193,13	2076,70 (284,81)
	Yes (n=119)	10,80	53,60	39,15 (11,34)	1805,03	4846,26	2258,24 (359,86)
Build orientation *XY / XZ*	*XY (n=124)*	18.00	53,60	41,18 (11,14)	1693,96	3315,56	2185,26 (308,48)
	XZ (n=120)	10,80	52,10	39,95 (10,51)	1640,25	4846,26	2144,56 (361,40)
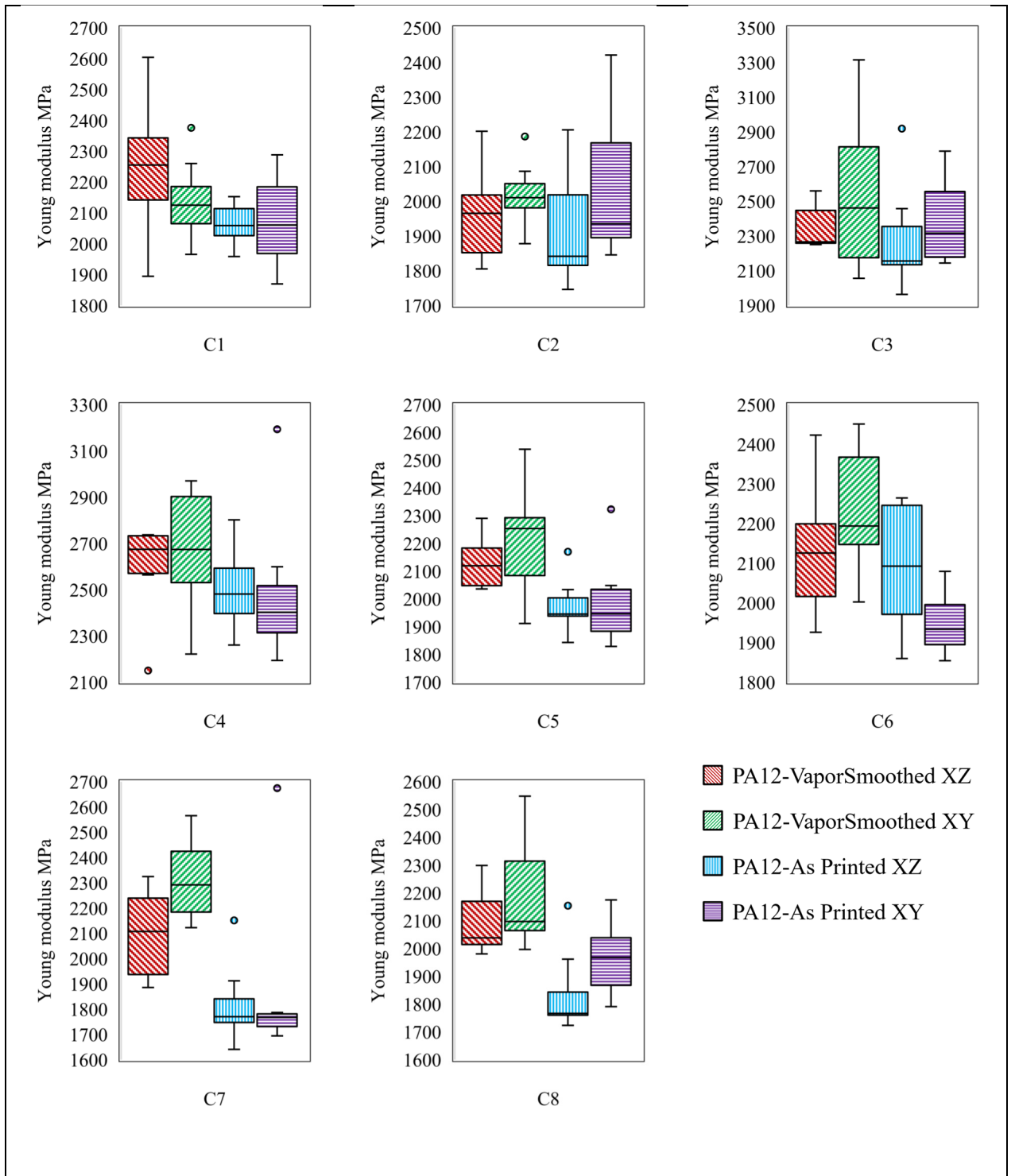
Figure 4.4 Variation of Young's modulus (Y) as a function of treatment for samples with/without Vapor polishing and according to the construction orientation
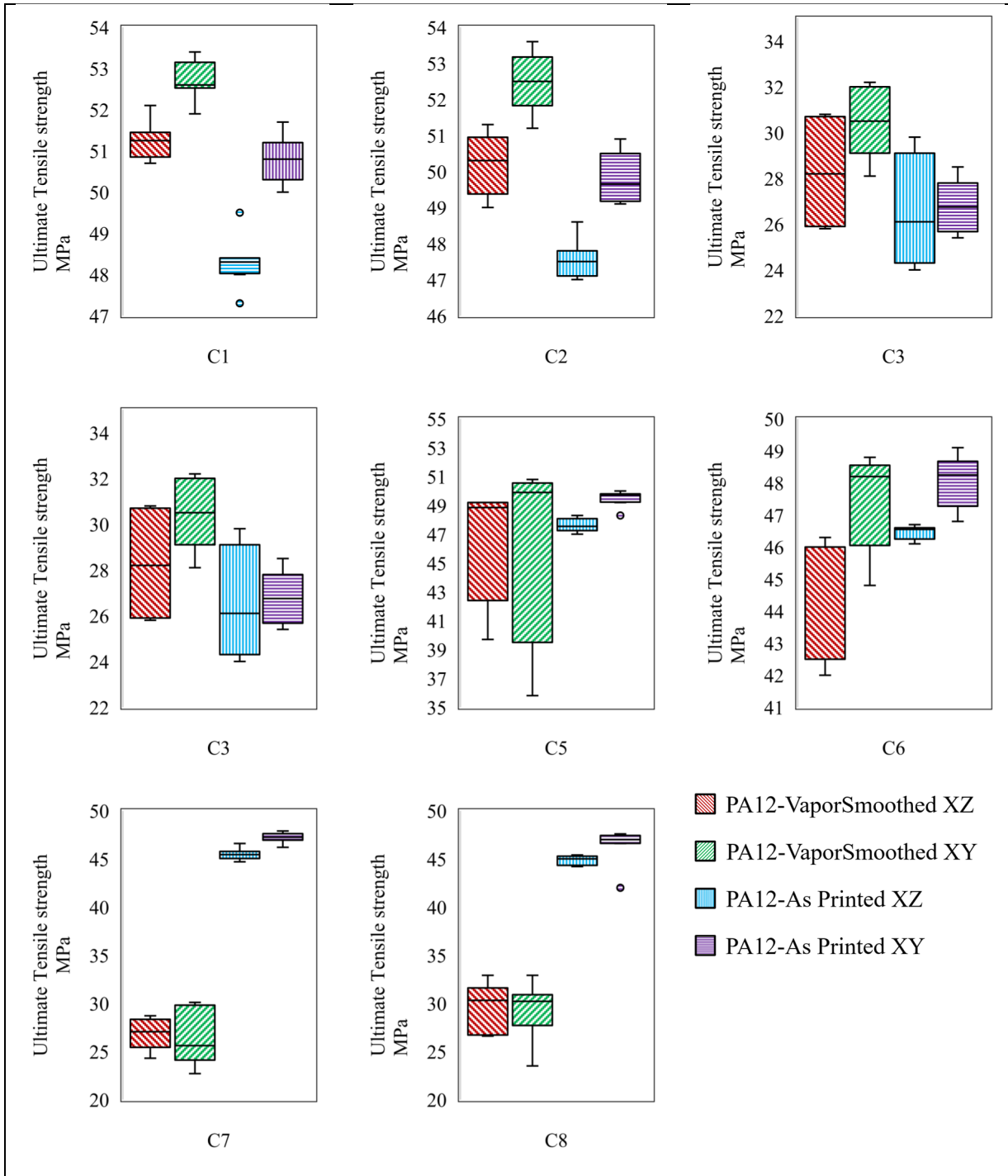
Figure 4.5 Variation of Ultimate tensile strength (UTS) as a function of treatment for samples with/without Vapor polishing and according to the construction orientation

Figure 4.4 shows the variation of the Young's modulus according to the eight configurations (C1 - C8) presented in section 2.2 for the studied four (4) cases including Vapor polished (Vp) and as-built samples, as well as different printing orientations. It can be noticed that for all the configurations the Vp treatment increases the stiffness for PA12 for the XY and XZ construction orientation. It can also be observed that for PA12 with Vp and as printed in the XY orientation results in a higher median of Y compared to the XZ orientation printed samples. The ANOVA (section 4.1) suggests that it is required to evaluate the direct influence of the independent variables as well as their interactions, thus it is not necessary to look at the levels of dependant variable Y at this time.

The variation of the UTS values according to the different aging treatment configurations is presented in Figure 4.5, which demonstrates that for some configurations the effect of Vp increases the value of UTS while for other configurations leaving the specimens as-printed results in a higher mechanical resistance. This is caused by the interaction effect of the independent variables (Temperature, Relative Humidity, Irradiance, Vapor polishing, Build orientation, and Time) which justifies to investigate further by conducting an analysis of variance. Furthermore, it was noticed that the XY printing orientation systematically gives a higher UTS than the XZ orientation and this for any configuration, with or without Vp.

4.4.1   Analysis of variance (ANOVA)

In view of the limited number of performed configurations, three different models (model 1, model 2, and model 3) are analyzed to determine the effect of the factors on the dependent variables UTS and Y. These models include five (5) factors each, indeed, the time, Vp treatment, and different build orientations (XY and XZ) are treated in each model. Tableau 4.6 and 4.8 present the ANOVA results indicating the significance of the effect of the independent factors as well as the significant interactions whose p-values are lower than 0.05 (highlighted in red).

For the three developed models, the p-values of the ANOVA indicate a significant effect of the factors used in the models on the mechanical strength of the tested specimens (Tableau 4.7). Regarding the Young's modulus (Tableau 4.11), it is noticed that in the three models the

two (2) factors (time and part orientation during printing) do not have a direct significant effect on Y (p-value >0.05).

Tableau 4.6 Results of the ANOVA of the three models for UTS

	UTS							
	Factors	***p-value***		**Factors**	***p-value***		**Factors**	***p-value***
Model 1	A: Temperature	<0,0001	**Model 2**	A: Temperature	<0,0001	**Model 3**	A: Irradiance	<0,0001
	B: Relative Humidity	<0,0001		B: Irradiance	<0,0001		B: Relative Humidity	0,0010
	C: Time	<0,0001		C: Time	0,0172		C: Time	0,8717
	D: Vapor polishing	<0,0001		D: Vapor polishing	<0,0001		D: Vapor polishing	0,0011
	E: Build direction	0,0034		E: Build direction	0,0114		E: Build direction	0,0122
	Interactions			**Interactions**			**Interactions**	
	AB	<0,0001		AB	<0,0001		AB	<0,0001
	AD	<0,0001		AD	<0,0001		AD	<0,0001
	BD	<0,0001		BD	<0,0001		BD	<0,0001
				BC	0,0103			

In Tableau 4.6 it can be clearly concluded that beyond the individual effects of the factors, there is also the effect of the binary interactions between the different factors which is statistically significant. In the purpose of studying and understanding the interactions multiple pairwise comparisons (post hoc tests) are proposed.

Tableau 4.7 Post hoc test for interactions that affect UTS

	UTS *(MPa)*								
Temperature °C	**Relative Humidity %.**				**Relative Humidity %.**	**Temperature °C**			
	50 *(i)*	80 *(j)*	*(i-j)*	*p-value*		30 *(i)*	70 *(j)*	*(i-j)*	*p-value*
30	49,56	47,48	2,08	0,0001	50	49,56	25,86	23,7	<0,0001
70	25,86	37,79	-11,93	<0,0001	80	47,48	37,79	9,69	<0,0001
Temperature °C	**Vapor polishing**				**Vapor polishing**	**Temperature °C**			
	No *(i)*	Yes *(j)*	*(i-j)*	*p-value*		30 *(i)*	70 *(j)*	*(i-j)*	*p-value*
30	48,49	49,03	-0,54	0,3074	No	48,49	35,47	13,02	<0,0001
70	35,74	27,64	8,10	<0,0001	Yes	49,03	27,64	21,39	<0,0001
Relative Humidity %.	**Vapor polishing**				**Vapor polishing**	**Relative Humidity %.**			
	No *(i)*	Yes *(j)*	*(i-j)*	*p-value*		50 *(i)*	80 *(j)*	*(i-j)*	*p-value*
50	36,66	41,51	-4,85	0,0199	No	36,66	46,95	-10,29	<0,0001
80	46,95	34,97	11,98	<0,0001	Yes	41,51	34,97	6,54	0,0022

UTS (MPa)											
Irradiance *W/m2.nm*	**Temperature** *°C*				**Temperature** *°C*	**Irradiance** *W/m2.nm*					
	30 *(i)*	70 (j)	*(i-j)*	*p-value*		0,23 *(i)*	0,68 (j)	*(i-j)*	*p-value*		
0,23	50,42	37,79	12,63	<0,0001	30	50,42	47,16	3,26	<0,0001		
0,68	47,16	25,86	21,3	<0,0001	70	37,79	25,86	11,93	<0,0001		
Irradiance *W/m2.nm*	**Vapor polishing**				**Vapor polishing**	**Irradiance** *W/m2.nm*					
	No *(i)*	Yes (j)	*(i-j)*	*p-value*		0,23 *(i)*	0,68 (j)	*(i-j)*	*p-value*		
0,23	47,5	40,86	6,64	<0,0001	No	47,5	36,45	11,05	<0,0001		
0,68	36,45	37,46	-1,01	0,6171	Yes	40,86	37,46	3,40	0,1025		
Irradiance *W/m2.nm*	**Time** *hours*				**Time** *hours*	**Irradiance** *W/m2.nm*					
	250 *(i)*	500 (j)	*(i-j)*	*p-value*		0,23 *(i)*	0,68 (j)	*(i-j)*	*p-value*		
0,23	44,32	44,21	0,11	0,9490	250	44,32	38,27	6,05	0,0013		
0,68	38,27	35,63	2,64	0,1925	500	44,21	35,63	8,58	<0,0001		
Irradiance *W/m2.nm*	**Relative Humidity** *%.*				**Relative Humidity** *%.*	**Irradiance** *W/m2.nm*					
	50 *(i)*	80 (j)	*(i-j)*	*p-value*		0,23 *(i)*	0,68 (j)	*(i-j)*	*p-value*		
0,23	50,42	37,79	12,63	<0,0001	50	50,42	30,2	20,22	<0,0001		
0,68	30,2	47,48	-17,28	<0,0001	80	37,79	47,48	-9,69	<0,0001		

Tableau 4.7 demonstrates that the interaction effect of the pair of factors (Temperature/Relative Humidity) affect the UTS significantly in both directions, i.e., when the temperature is set at any level the effect of relative humidity differs, which is supported by a p-value less than 5%. In the case where we fix the relative humidity at any level the effect of temperature on UTS is also significantly different.

The interaction between temperature and Vp is shown in Tableau 4.7. However, this interaction is only one-directional. The effect of Vp is not significant at a temperature of 30°C, but it is significant at 70°C. In the opposed direction, by applying the Vp treatment or not, the temperature has a significant effect on the mechanical strength of the studied material. This finding is valid for the first and second model presented in Tableau 4.6. Hence, this may suggest that Vp protects the material from thermal degradation (i.e., here defined as not affecting its UTS) at low temperatures (e.g., 30 °C), however, at higher temperatures (e.g., 70 °C) the protection from the Vp treatment is lost. Further research could be conducted to study more precisely the temperature limits for PA2200 protection by the Vp process against thermal degradation. It should be noted that the present work entails a pairwise comparison and the effect of other factors is not considered, However, other factors and their interactions may help to explain the average values obtained when switching from the first temperature level to the second.

Another interaction (RH/Vp) is significantly bidirectional (note that the interaction is present in the first and third models), for any level of humidity the Vp to a different effect and vice versa. Same for the couple (Irradiance/Temperature) that is present in model 2, for any level of either, the other factor will have a different effect on the UTS.

For a non-vapor polished material, irradiance has a significant effect while for samples that have received the Vp treatment well the effect of irradiance becomes non-significant which implies a line of thought on the protection of Nylon 12 by Vp treatment against photo degradation. A significant decrease in the average UTS with a p-value <0.0001 indicates that at 0.23 W/m^2.nm, Vp has a significant effect contrary to a level of 0.68 W/m^2.nm where there is no effect on the mechanical strength.

For both levels of irradiance, the time has no effect, however for both levels of time the effect of irradiance is well present significantly and with a different effect depending on the time of exposure. It should be noted that this interaction is present only in model 2, in the third proposed model the interaction between irradiance and time does not seem to be significant with a p-value equal to 0.8868.

For the interaction of the pair (Irradiance/Relative Humidity) found in model 3, there seems to be an effect of both factors for any level of the other. Hence, a bidirectional interaction is observed.

Tableau 4.8 Results of the ANOVA of the three models for Young's modulus

	Factors	p-value		Factors	p-value		Factors	p-value
Model 1	A: Temperature	<0,0001	**Model 2**	A: Temperature	<0,0001	**Model 3**	A: Irradiance	<0,0001
	B: Relative Humidity	<0,0001		B: Irradiance	<0,0001		B: Relative Humidity	<0,0001
	C: Time	0,3419		C: Time	0,3102		C: Time	0,9475
	D: Vapor polishing	<0,0001		D: Vapor polishing	<0,0001		D: Vapor polishing	<0,0001
	E: Build direction	0,1978		E: Build direction	0,1906		E: Build direction	0,3222
	Interactions			**Interactions**			**Interactions**	
	AB	<0,0001		AB	<0,0001		AB	0,0001
	AC	0,0047		AC	0,0035		AC	0,0330
	AD	0,0391		AD	0,0342		BD	0,0022
				BC	0,0012			

Tableau 4.8 shows the presence of significant binary interactions between the different factors for each model. As for the mechanical strength (UTS) a post-hoc test was performed on the collected data of the Young's modulus (Y) and shown in Tableau 4.9.

Tableau 4.9 Post hoc test for interactions that affect the Young's modulus (Y)

Y *(MPa)*									
Temperature *°C*	**Relative Humidity** *%.*				**Relative Humidity** *%.*	**Temperature** *°C*			
	50 *(i)*	80 (j)	*(i-j)*	*p-value*		30 *(i)*	70 (j)	*(i-j)*	*p-value*
30	2085.26	2055.50	29.76	0.3501	50	2085,26	2512,58	-427,32	<0,0001
70	2512.52	2012.93	499.65	<0,0001	80	2055,5	2012,93	42,57	0,3143
Temperature *°C*	**Vapor polishing**				**Vapor polishing**	**Temperature** *°C*			
	No *(i)*	Yes (j)	*(i-j)*	*p-value*		30 *(i)*	70 (j)	*(i-j)*	*p-value*
30	2012,05	2133,85	-121,8	<0,0001	No	2012,05	2140,33	-128,28	0,0112
70	2140,33	2402,99	-262,66	0,0007	Yes	2133,85	2402,99	-269,14	<0,0001
Temperature *°C*	**Time** *hours*				**Time** *hours*	**Temperature** *°C*			
	250 *(i)*	500 (j)	*(i-j)*	*p-value*		30 *(i)*	70 (j)	*(i-j)*	*p-value*
30	2102,82	2045,02	57,8	0,0603	250	2102,82	2199,54	96,72	0,0556
70	2199,54	2323,86	-124,32	0,1151	500	2045,02	2323,86	-278,84	<0,0001
Irradiance *W/m² .nm*	**Temperature** *°C*				**Temperature** *°C*	**Irradiance** *W/m² .nm*			
	30 *(i)*	70 (j)	*(i-j)*	*p-value*		0,23 *(i)*	0,68 (j)	*(i-j)*	*p-value*
0,23	2060,53	2012,93	47,6	0,2306	30	2060,53	2086,89	-26,36	0,3942
0,68	2086,89	2512,58	-425,69	<0,0001	70	2012,93	2512,58	-499,65	<0,0001
Irradiance *W/m² .nm*	**Time** *hours*				**Time** *hours*	**Irradiance** *W/m² .nm*			
	250 *(i)*	500 (j)	*(i-j)*	*p-value*		0,23 *(i)*	0,68 (j)	*(i-j)*	*p-value*
0,23	2073,37	2001,85	71,52	0,0705	250	2073,37	2223,75	-150,38	0,0026
0,68	2223,75	2357,33	-133,58	0,0517	500	2001,85	2357,33	-355,48	<0,0001
Irradiance *W/m² .nm*	**Relative Humidity** *%.*				**Relative Humidity** *%.*	**Irradiance** *W/m² .nm*			
	50 *(i)*	80 (j)	*(i-j)*	*p-value*		0,23 *(i)*	0,68 (j)	*(i-j)*	*p-value*
0,23	2060,53	2012,93	47,6	0,2306	50	2060,53	2441,86	-381,33	<0,0001
0,68	2441,86	2055,5	386,36	<0,0001	80	2012,93	2055,5	-42,57	0,3143
Relative Humidity *%.*	**Vapor polishing**				**Vapor polishing**	**Relative Humidity** *%.*			
	No *(i)*	Yes (j)	*(i-j)*	*p-value*		50 *(i)*	80 (j)	*(i-j)*	*p-value*
50	2225,51	2304,42	-78,91	0,2206	No	2225,51	1934,87	290,64	<0,0001
80	1934,87	2176,62	-241,75	<0,0001	Yes	2304,42	2176,62	127,8	0,0625

As can be observed in Tableau 4.9 the effect of the interaction between temperature and relative humidity is not significantly manifested for all configurations, for a temperature of 70° C, the increase in the level of relative humidity lowers the Young's modulus of Nylon 12. However,

for a relative humidity of 50% the increase in temperature makes the material stiffen increasing the Young's modulus in this model.

Regarding the interaction of temperature and Vp treatment, the results show that Vp protects the material from thermal degradation for both temperature levels tested. Time seems to have an effect only for long exposure times, we observe a difference of (Y) between the two temperature levels.

PA12 responds significantly to the effect of temperature for irradiance at 0.68 W/m^2.nm by increasing the average (Y) for higher temperatures. However, the irradiance has a significant effect only for a temperature of 70° C. In addition, the results show that there is an interaction between time and irradiance, the latter has a significant effect at a confidence level greater than 99% whatever the level of time used.

The interaction of irradiance with relative humidity (RH) is present in the third model with a p-value less than 0.0001, the effect of RH is manifested only for an irradiance set to 0.68 W/m^2.nm, as well as the effect of irradiance is manifested only for an RH of 50%.

The protective effect of the surface treatment Vp seems to be present significantly only for RH = 80%, moreover RH to a significant effect when the treatment Vp is not applied with a decrease in the mean of Y.

4.4.2   Prediction model development

Based on the results of the analysis of variance presented earlier in this paper, regression models were constructed and compared with each other using the Akaike criterion (AIC) in order to determine which, one performs best while penalizing the models with the largest number of independent variables. The same work was done for the explained variable UTS as well as for Y. For the construction of the MLR models all the variables are numerical except for the variable Vp and Building Orientation (BO), for an application of the steam polishing treatment the variable takes the level 1 otherwise 0, and for the orientation on the printer buildplate (XY) BO= 0 and for (XZ) BO= 1. As mentioned in the methodology section, the models has been diagnosed is responds favorably to the assumptions of the MLR (see Appendix II).

The proposed MLR model to predict the variation of UTS as a function of the independent variables follows the results of the analysis of variance and is expressed by Eq. (4.5):

$$UTS = \beta_0 + \beta_1 Temp + \beta_2 RH + \beta_3 Time + \beta_4 Vp + \beta_5 BO + \beta_6 Temp\ RH \qquad (4.5)$$
$$+ \beta_7 Temp\ Vp + \beta_8 RH\ Vp$$

Tableau 4.10 presents the coefficients, significance (p-value), standard error and 95% confidence interval of the independent variables used in the model explaining UTS (Eq. (4.5)).

Tableau 4.10 The values of the p-value, coefficients, standard errors and 95% confidence intervals of independent variables for the model explaining UTS

Predicted variable	Independent variable	Coefficient	Std. Error	p-value	95% Confidence interval	
					Lower bound	Upper bound
Ultimate tensile strength (UTS)	Constant	$\beta_0 = 81{,}2404$	3,0653	<0,0001	75,2013	87,2796
	A: Temperature	$\beta_1 = -1{,}1380$	0,0512	<0,0001	-1,2388	-1,0371
	B: Relative Humidity	$\beta_2 = -0{,}2863$	0,0426	<0,0001	-0,3702	-0,2025
	C: Time	$\beta_3 = -0{,}0099$	0,0018	<0,0001	-0,0134	-0,0064
	D: Vapor polishing	$\beta_4 = 29{,}3482$	2,1008	<0,0001	25,2093	33,4871
	E: Build orientation	$\beta_5 = -1{,}2689$	0,4292	0,0034	-2,1145	-0,4232
	AB	$\beta_6 = 0{,}0125$	0,0007	<0,0001	0,0110	0,0139
	AD	$\beta_7 = -0{,}1441$	0,0222	<0,0001	-0,1878	-0,1005
	BD	$\beta_8 = -0{,}4139$	0,0301	<0,0001	-0,4732	-0,3547

The effects of the independent variables can be estimated by considering the effect of the interactions as follows, for example for a Relative Humidity of 50% by increasing the temperature of 1°C, the UTS will vary from $\beta_1 + \beta_6(50) = -1.1379 + (0.0125 * 50) = -0.5145\ MPa$. Thus, when a Vp treatment is applied Vp = 1, and for an increase in temperature of 1°C, the UTS will vary from $\beta_1 + \beta_7(1) = -1.1379 + (-0.1441 * 1) = -1.282\ MPa$. This reasoning can be applied to all independent variables if they interact with each other, resulting in a model with a value of the coefficient of determination $R^2 = 0.9075$ and a R^2 adjusted = 0.9043, which is satisfactory to validate this model.

The proposed MLR model uses the results of the analysis of variance to predict the variation of Y as a function of the independent variables and is expressed as follows

$$\log(Y) = \beta_0 + \beta_1 Temp + \beta_2 Irr + \beta_3 Time + + \beta_4 Temp\, Vp + \beta_5 Temp\, Irr \qquad (4.6)$$
$$+ \beta_6 Temp\, Time + \beta_7 Irr\, Time$$

Tableau 4.11 The values of the p-value, coefficients, standard errors and 95% confidence intervals of independent variables for the model explaining and Y

Predicted variable	Independent variable	Coefficient	Std. Error	p-value	95% Confidence interval	
					Lower bound	Upper bound
Log(Y)	Constant	$\beta_0 = 7,9730$	0,0073	<0,0001	7,8297	8,1170
	A: Temperature	$\beta_1 = -0,0069$	0,0012	<0,0001	-0,0092	-0,0046
	B: Irradiance	$\beta_2 = -0,5886$	0,1104	<0,0001	-0,8062	-0,3710
	C: Time	$\beta_3 = -0,0007$	0,0002	<0,0001	-0,0010	-0,0004
	A*Vp	$\beta_4 = 0,0017$	0,0002	<0,0001	0,0012	0,0021
	AB	$\beta_5 = 0,0112$	0,0014	<0,0001	0,0085	0,0139
	AC	$\beta_6 = 0,0000$	0,0000	0,0018	0,0000	0,0000
	BC	$\beta_7 = 0,0008$	0,0002	0,0007	0,0003	0,0012

Tableau 3.11 presents the independent variables used in the MLR explaining Y, their coefficients, the standard error, the associated p-value, and the upper and lower bounds of the 95% confidence interval.

The rationale for interpretation is the same as for UTS, with one exception: the variation in Y is calculated in percentage (%) rather than MPa, as the explanatory variable underwent a logarithmic transformation during model development. This was done to stabilize the variance of the variable Y and reduce the effect of extreme values.

To estimate the variation of Y for an irradiance fixed at 0.23 W/m.nm for each 1°C temperature increase, Y will vary by $\beta_1 + \beta_5(0.23) = 100(-0,0069 + (0,0112 * 0.23)) = -0.4324\%$. The model has an $R^2 = 0.5226$ and a R^2 adjusted $= 0.5084$.

These models were built to predict the UTS and Y values using values of the independent variables between level 1 and level 2 presented in Tableau 4.2.

4.5   Conclusion

An experimental design was developed in this work to age 3D printed Polyamide 12 specimens with SLS technology, to evaluate the impact of six (6) independent variables (Temperature, Relative Humidity, UV Irradiance, Time, Vapor Polishing and Construction Orientation) on the ultimate mechanical strength (UTS) as well as Young's modulus (Y). An analysis of variance was performed to determine the significance of individual effects and binary interactions between the independent variables, followed by a post hoc analysis to investigate the interactions. A multiple linear regression model was proposed to predict the UTS and the Y using the Akaike criterion (AIC) as a model selection criterion. The result allowed to develop a model that explains the relationship between UTS and Y, exhibiting an R^2 value of .9075 for UTS and .5226 for Y.

In summary, this research work not only fills an apparent gap in current knowledge, but also has substantial implications for practical applications. The results of the study enable a more informed approach to the design of 3D printed parts with enhanced longevity and durability. Manufacturers can now take advantage of the predictive model to optimize the fabrication process by adjusting environmental parameters to achieve the desired mechanical properties. Consequently, this study not only improves the fundamental knowledge base, but it also translates directly into tangible benefits for the additive manufacturing industry. In practical terms, the outcomes of this research hold promising implications for the application of 3D printed Polyamide 12 components in real-world scenarios. Industries ranging from automotive to medical devices could leverage these findings to optimize part fabrication processes and enhance product performance. By tailoring the manufacturing parameters based on the identified optimal conditions, manufacturers can achieve parts that maintain their structural integrity and functional properties over prolonged periods, thus minimizing the risk of premature failure and so adding to the development of more sustainable manufacturing practices.

As a next step of the present study, it is suggested to test the predictive performance of the two developed models, for UTS and Y, experimentally and thus be able to explore larger time

scales to better understand the aging of the 3D printed material in the long term and design the parts accordingly.

Data availability

The raw and processed data, required to reproduce the findings reported in the present study are available to download from https://github.com/ChahGhim/SLS_PA2200_Degradation

CONCLUSION ET RECOMMANDATIONS

Il est indiscutable que l'économie circulaire se révèle être une réponse cruciale aux défis environnementaux pressants engendrés par la surconsommation de ressources naturelles et les émissions grandissantes de gaz à effet de serre. Le modèle économique linéaire actuel montre ses limites, tandis que l'économie circulaire émerge comme une voie prometteuse pour réduire notre empreinte écologique. Cependant, l'adoption réussie de la fabrication circulaire (FC) nécessite une transformation complète des pratiques industrielles, avec une focalisation accrue sur la conception éclairée des produits, l'utilisation de matériaux durables et la mise en œuvre de technologies de fabrication avancées.

En réponse à la question de recherche posée, cette étude a réussi à démontrer de manière convaincante que l'intégration de technologies de fabrication avancées et d'une conception réfléchie peut effectivement faciliter l'introduction de biens de consommation, en l'occurrence les chaussures à talons hauts, dans une approche de fabrication circulaire. Grâce à l'exploration approfondie de technologies telles que la fabrication additive, l'élaboration d'un prototype de chaussures imprimées en 3D a été réalisée, incarnant les principes d'écoconception et d'économie circulaire. Cette recherche a ainsi apporté des éclaircissements substantiels sur la faisabilité et les avantages de l'application de ces concepts novateurs, contribuant ainsi de manière significative à la transformation potentielle du modèle de production linéaire vers un modèle circulaire, tout en offrant des perspectives tangibles pour la durabilité environnementale et économique dans le domaine des biens de consommation.

L'étude adressant le premier sous-objectif a démontré comment l'intégration de la fabrication additive dans le processus de conception de chaussures peut apporter des avantages significatifs en termes de réduction du nombre de composants, de personnalisation des designs et de possibilités d'assemblage sans colle. Cela a ouvert la voie à une nouvelle ère de conception de produits, où l'efficacité environnementale est placée au cœur du processus créatif.

En ce qui concerne le deuxième sous-objectif, l'étude approfondie du comportement des matériaux polymériques dans des conditions environnementales variables a permis de modéliser avec succès le vieillissement de ces polymères imprimés en 3D. Cette démarche fournit une base solide pour évaluer la durabilité de ces chaussures dans le contexte d'une économie circulaire, où l'allongement de la durée d'utilisation des produits est un objectif essentiel.

Les résultats de cette étude ont des implications significatives pour l'industrie de la mode et de la fabrication, offrant des pistes tangibles pour la création de produits respectueux de l'environnement tout en répondant aux normes de qualité et de confort attendues.

Pour poursuivre cette recherche passionnante, il serait recommandé de réaliser des essais pratiques plus étendus pour valider les modèles de vieillissement des polymères et pour évaluer la performance mécanique à long terme des chaussures imprimées en 3D. Une collaboration continue entre les domaines de la technologie des matériaux, de la conception et de la fabrication sera cruciale pour traduire ce pas en avant en applications pratiques et durables à grande échelle.

En prolongement, Une analyse du cycle de vie (ACV) serait nécessaire pour évaluer la valeur ajoutée environnementale de cette approche. Il serait pertinent par la suite d'envisager l'expansion de cette approche à d'autres produits de consommation, afin de saisir pleinement l'étendue de son influence potentielle. De plus, une collaboration accrue entre les domaines de la conception, de la technologie des matériaux et de l'ingénierie est essentielle pour créer une convergence fructueuse, en permettant une innovation véritablement holistique.

ANNEXE I

DÉTAIL DU PLAN D'EXPÉRIENCE ADOPTÉ AFIN D'ÉTUDIER LE VIEILLISSEMENT DU POLYAMIDE 12

Tableau-A I-1. Presentation of all configurations used in the design of the experiment

Configuration (number of specimen)	Temperature	Relative Humidity	Irradiance	Time	Vapor polishing	Build orientation
C1 (n= 7)	1	1	1	1	1	1
C2 (n=8)	1	1	1	2	1	1
C3 (n=8)	2	1	2	1	1	1
C4 (n=8)	2	1	2	2	1	1
C5 (n=8)	1	2	2	1	1	1
C6 (n=8)	1	2	2	2	1	1
C7 (n=8)	2	2	1	1	1	1
C8 (n=8)	2	2	1	2	1	1
C9 (n=8)	1	1	1	1	2	1
C10 (n=8)	1	1	1	2	2	1
C11 (n=7)	2	1	2	1	2	1
C12 (n=7)	2	1	2	2	2	1
C13 (n=8)	1	2	2	1	2	1
C14 (n=9)	1	2	2	2	2	1
C15 (n=7)	2	2	1	1	2	1
C16 (n=7)	2	2	1	2	2	1
C17 (n=8)	1	1	1	1	2	2
C18 (n=8)	1	1	1	2	2	2
C19 (n=7)	2	1	2	1	2	2
C20 (n=7)	2	1	2	2	2	2
C21 (n=8)	1	2	2	1	2	2
C22 (n=7)	1	2	2	2	2	2

Configuration (number of specimen)	Temperature	Relative Humidity	Irradiance	Time	Vapor polishing	Build orientation
C23 (n=6)	2	2	1	1	2	2
C24 (n=7)	2	2	1	2	2	2
C25 (n=8)	1	1	1	1	1	2
C26 (n=8)	1	1	1	2	1	2
C27 (n=7)	2	1	2	1	1	2
C28 (n=7)	2	1	2	2	1	2
C29 (n=8)	1	2	2	1	1	2
C30 (n=9)	1	2	2	2	1	2
C31 (n=7)	2	2	1	1	1	2
C32 (n=7)	2	2	1	2	1	2

Tableau-A I-1 in Appendix I represents all configurations including the 6 independent variables (Temperature, Irradiance, Relative Humidity, Time, Vapor polishing, Build orientation).

DIAGNOSIS OF THE LINEAR MULTIPLE REGRESSION MODEL EXPLAINING UTS AND Y

1-   Diagnosis of the linear multiple regression model explaining UTS

The *R language* (Team, 2022) was used for the diagnosis of the developed UTS linear multiple regression model under the *RStudio development* environment.

$$UTS = \beta_0 + \beta_1 Temp + \beta_2 RH + \beta_3 Time + \beta_4 Vp + \beta_5 BO + \beta_6 Temp\ RH$$
$$+ \beta_7 Temp\ Vp + \beta_8 RH\ Vp$$

A summary of the developed code is presented below:

```
Call:
lm(formula = UTS ~ Temp + RH + Time + Vp + BO + Temp:RH + Temp:Vp +
    RH:Vp, data = dataset)

Residuals:
    Min 1Q Median 3Q Max
-12.4431 -1.9074 0.2175 2.2012 7.2512

Coefficients:
              Estimate Std. Error t value Pr(>|t|)
(Intercept) 81.2404847 3.0653826 26.503 < 2e-16 ***
Temp -1.1379513 0.0511906 -22.230 < 2e-16 ***
RH -0.2863444 0.0425817 -6.725 1.33e-10 ***
Time -0.0099023 0.0017699 -5.595 6.12e-08 ***
Vp 29.3482466 2.1008457 13.970 < 2e-16 ***
BO -1.2688879 0.4292435 -2.956 0.00343 **
Temp:RH 0.0124672 0.0007491 16.644 < 2e-16 ***
Temp:Vp -0.1441404 0.0221520 -6.507 4.58e-10 ***
RH:Vp -0.4139403 0.0300844 -13.759 < 2e-16 ***
---
Signif. codes: 0 '***' 0.001 '**' 0.01 '*' 0.05 '.' 0.1 ' ' 1

Residual standard error: 3.352 on 235 degrees of freedom
Multiple R-squared: 0.9075,    Adjusted R-squared: 0  .9043
F-statistic: 288.2 on 8 and 235 DF, p-value: < 2.2e-16
```

Hypothesis testing to validate the model:
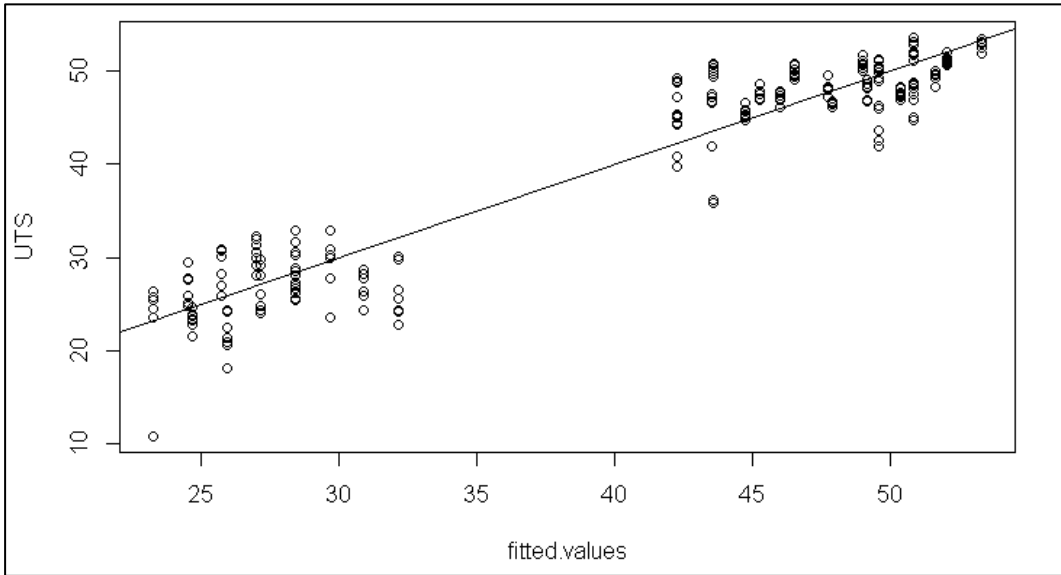
   a- Linearity assumption

Figure A-II.1 Plot of UTS vs. fitted values

Figure A-II.1 shows UTS as a function of the fitted values. The points seem to be clustered around the line $y = x$ which confirms the linearity of the model.
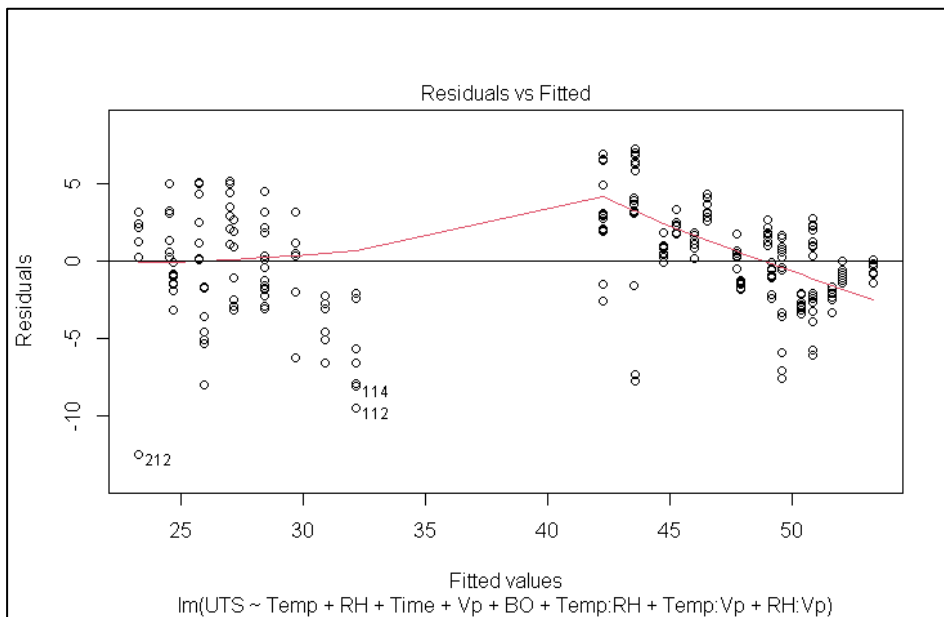

Figure A-II.2 Residuals vs. adjusted values

The residuals do have a mean (red line) that is close to zero and appear to be evenly distributed along the X axis. This indicates that there are no non-linear relationships between the independent variables and the dependent variable, and a good fit between the model and the data.
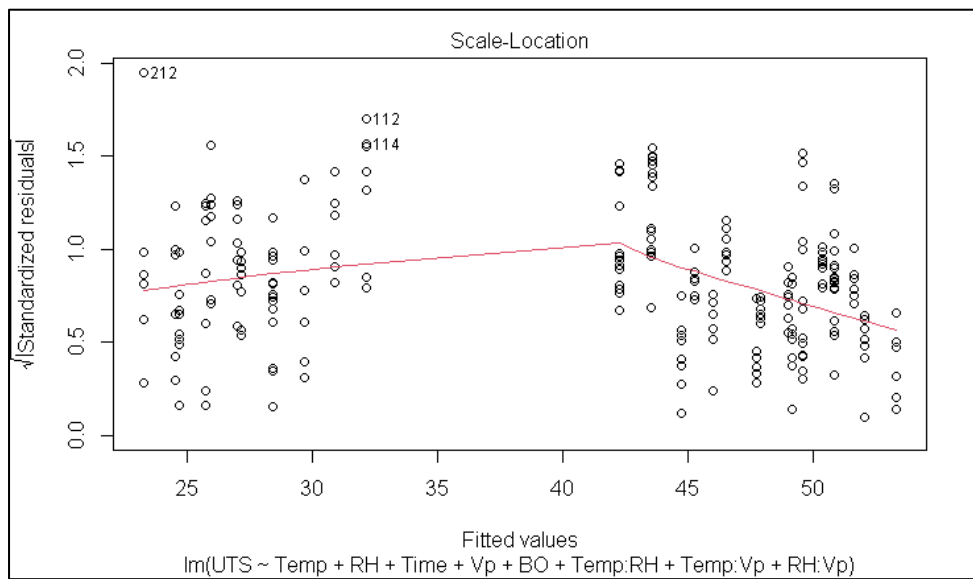
b- Assumption of homoscedasticity

Figure A-II.3 Square root of standardized residuals vs. adjusted values

We notice in Figure A-II.3 that the LOESS-fitted regression line does not seem to indicate an increasing or decreasing trend in the scatterplot (it grows and then starts to decrease) and thus a satisfaction of the homoscedasticity assumption.

c- Assumption of normality of the error term
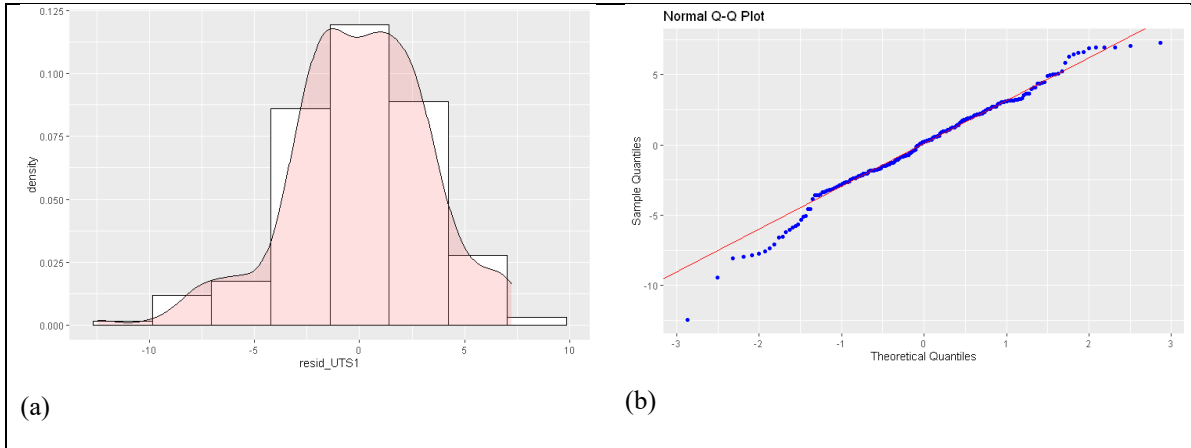

(a)

(b)

Figure A-II.4 Bell curve of residuals (a), Q-Q plot (b)

The bell shape is well present in Figure A-II.4 (a) and the residuals are well clumped on the right in the Q-Q plot in (b) which shows that the assumption is well verified, the residuals do follow a normal distribution.

d- Assumption of no influential values
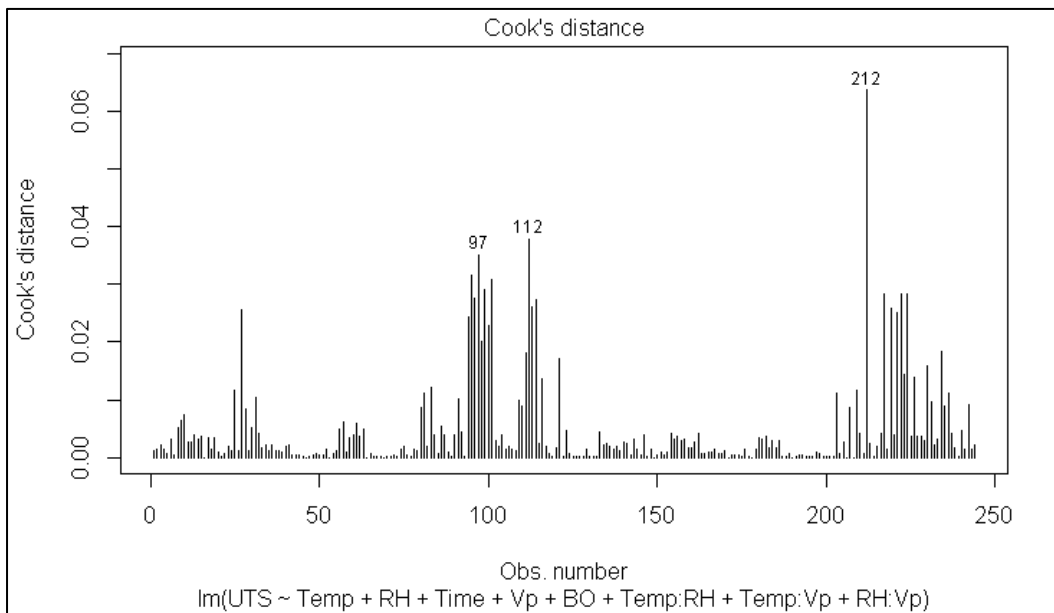
Figure A-II.5 Cook's distance for the 244 observations (UTS)
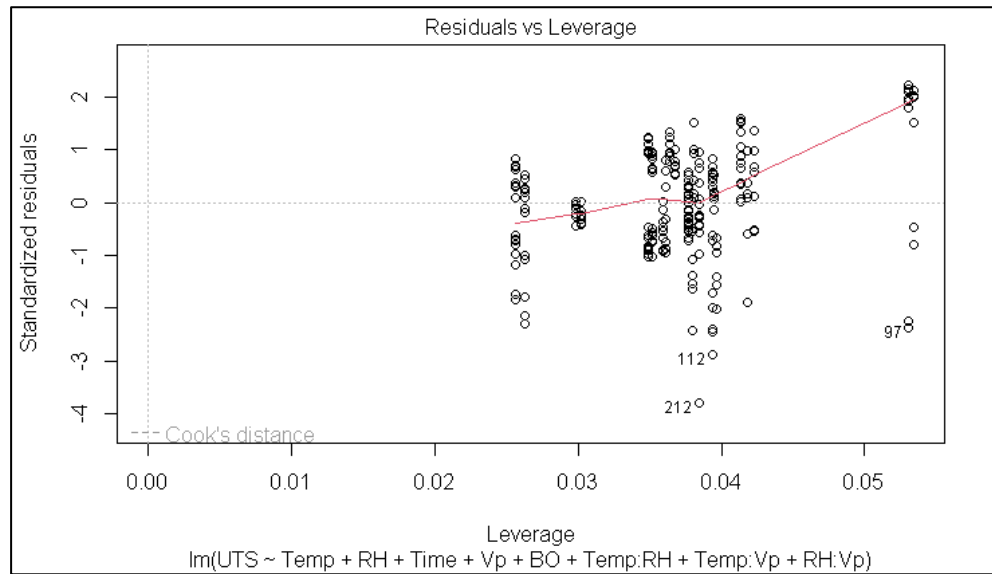
Figure A-II.6. Standardized residuals vs. leverage

We observe in Figure A-II.5 that the Cook distance of each observation is below the threshold of 0.5. And that in Figure A-II.6 the Cook distance that is supposed to be represented with a dotted line is so far away that it is not represented in the graph. This indicates that there are no influential values and that the conclusions will be the same even if we decide to delete an observation.
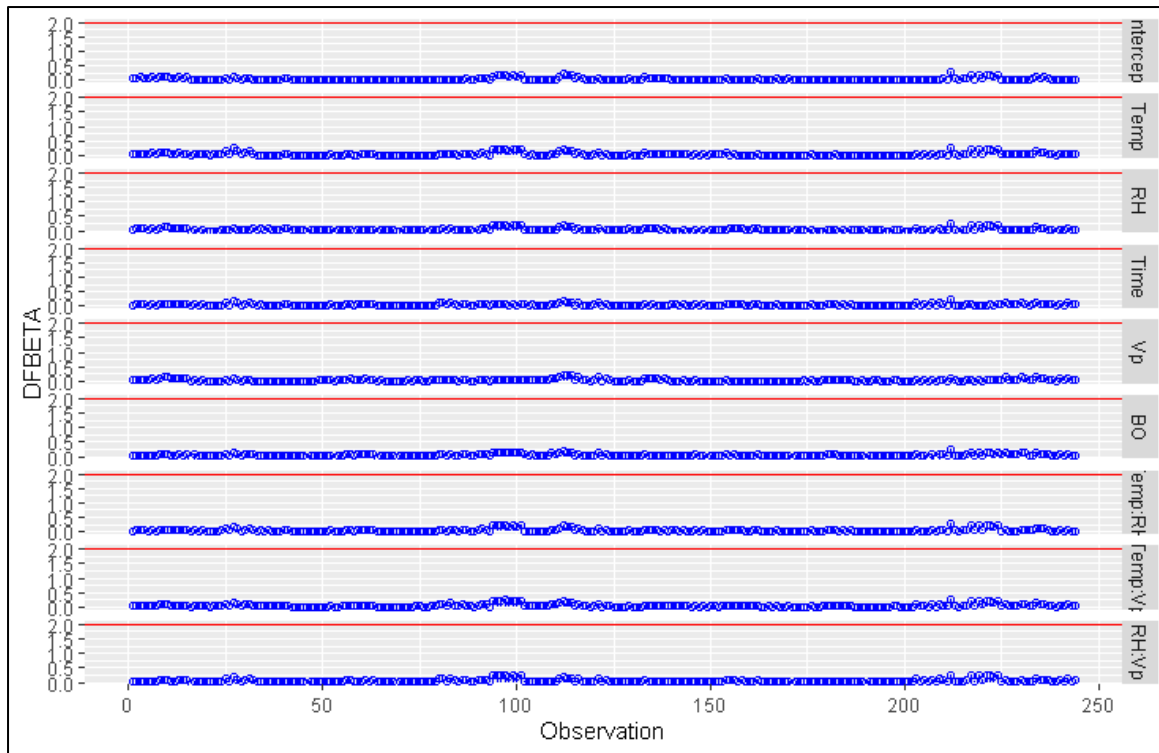
Figure A-II.7 DFBETAS for all observations as a function of each
variable in the MLR model explaining UTS.

Figure A-II.7 shows the DFBETAS that measure the impact of each observation on the regression coefficients in terms of the number of standard errors. It can be observed that no values exceed the threshold value of 2 for any of the variables in the model which again justifies the absence of influential values.

2-   Diagnosis of the linear multiple regression model explaining Y

The *R language* (Team, 2022) was used for the diagnosis of the developed Y linear multiple regression model under the *RStudio development* environment.

$$\log(Y) = \beta_0 + \beta_1 Temp + \beta_2 Irr + \beta_3 Time + + \beta_4 Temp\,Vp + \beta_5 Temp\,Irr$$
$$+ \beta_6 Temp\,Time + \beta_7 Irr\,Time$$

A Summary of developed code is presented below

Call:

lm(formula = log(Y) ~ Temp + Irr + Time + Temp:Irr + Temp:Time +
   Temp:Vp + Irr:Time, data = dataset)

Residuals:
   Min   1Q   Median   3Q   Max
-0.25117 -0.06197 -0.01342 0.05341 0.56161

Coefficients:
         Estimate Std. Error t value Pr(>|t|)
(Intercept) 7.973e+00 7.292e-02 109.345 < 2e-16 ***
Temp   -6.888e-03 1.173e-03 -5.873 1.44e-08 ***
Irr   -5.886e-01 1.104e-01 -5.330 2.30e-07 ***
Time   -6.954e-04 1.669e-04 -4.166 4.35e-05 ***
Temp:Irr   1.118e-02 1.381e-03   8.101 2.92e-14 ***
Temp:Time   7.854e-06 2.485e-06   3.161 0.001779 **
Temp:Vp   1.662e-03 2.337e-04   7.112 1.36e-11 ***
Irr:Time   7.572e-04 2.208e-04   3.430 0.000712 ***

Signif. codes: 0 '***' 0.001 '**' 0.01 '*' 0.05 '.' 0.1 ' ' 1

Residual standard error: 0.09697 on 236 degrees of freedom
Multiple R-squared: 0.5226,   Adjusted R-squared: 0.5084
F-statistic: 36.91 on 7 and 236 DF, p-value: < 2.2e-16

Hypothesis testing to validate the model:

   a- Linearity assumption
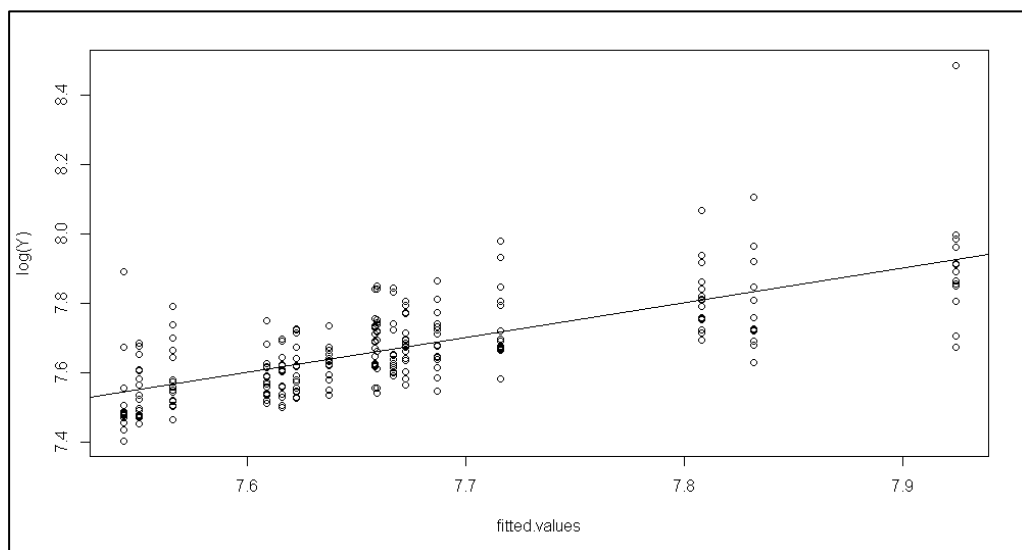
Figure A-II.8 Plot of Y vs. fitted values

The relationship between Y and the fitted values is depicted in Figure A-II.8. The data points exhibit clustering around the y = x line, affirming the model's linearity.
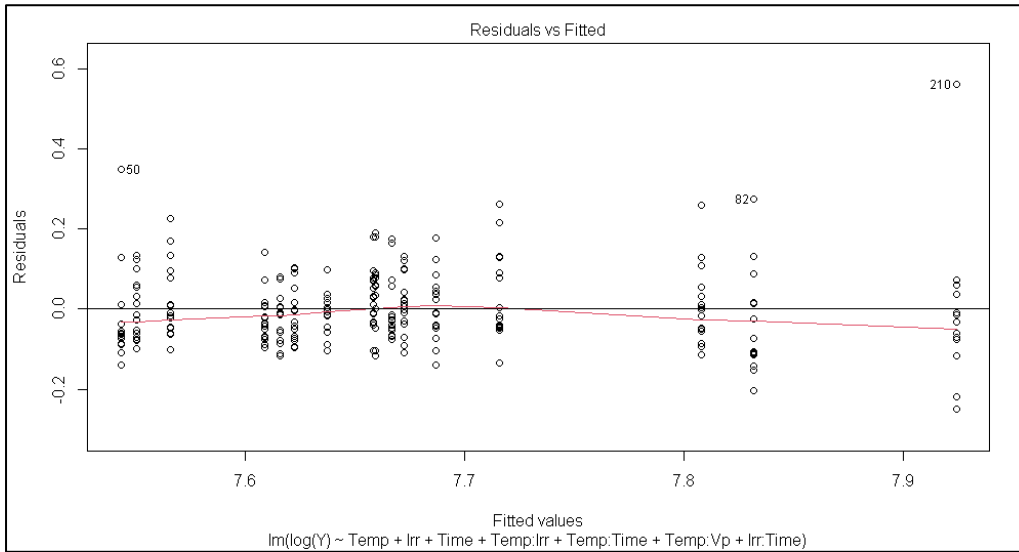
Figure A-II.9 Residuals vs. adjusted values

Examining the residuals, it's apparent in Figure A-II.9 that their mean (red line) hovers close to zero. Additionally, their distribution along the X axis appears even. These findings suggest the absence of nonlinear relationships between the independent and dependent variables, establishing a robust fit between the model and the data.

b- Assumption of homoscedasticity
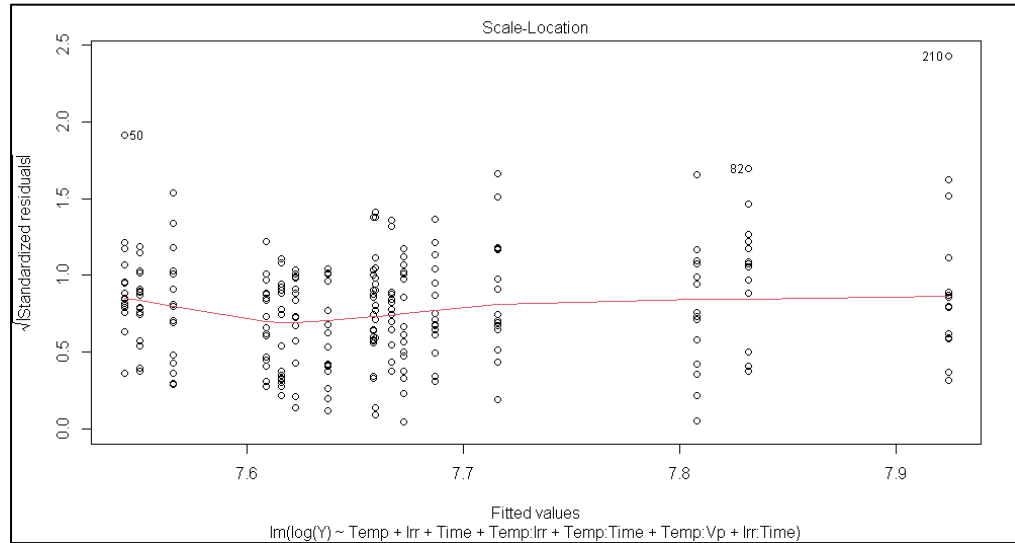
Figure A-II.10 Square root of standardized residuals vs. adjusted values

In Figure A-II.10, the LOESS-fitted regression line doesn't indicate a consistent upward or downward trend within the scatterplot; it shows a growth followed by a decline. This observation indicates the fulfillment of the homoscedasticity assumption.

c- Assumption of normality of the error term
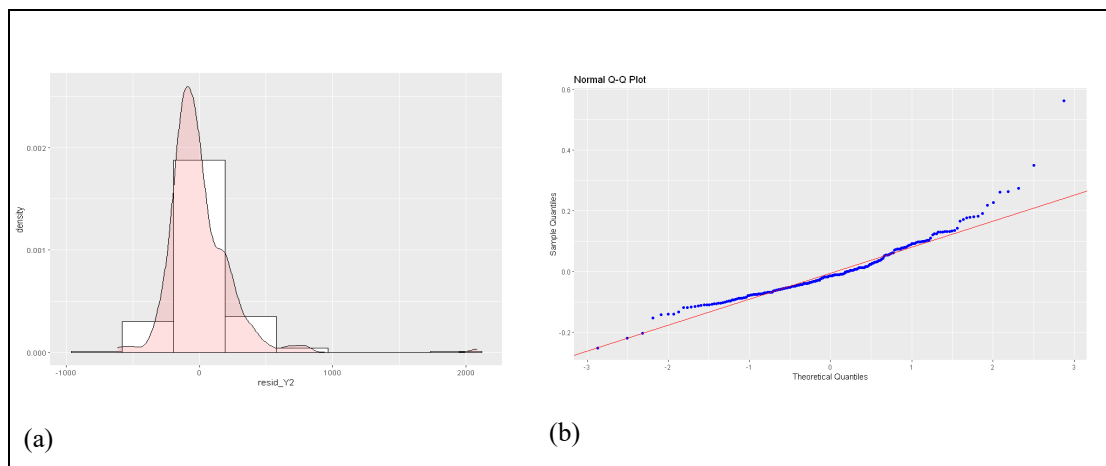
Figure A-II.11 Bell curve of residuals (a), Q-Q plot (b)

102

The bell-shaped pattern is clearly visible in figure A-II.11 (a), and the residuals in the Q-Q plot (b) are tightly clustered on the right-hand side. This alignment means that the hypothesis of normal residual distribution is validated.

d- Assumption of no influential values
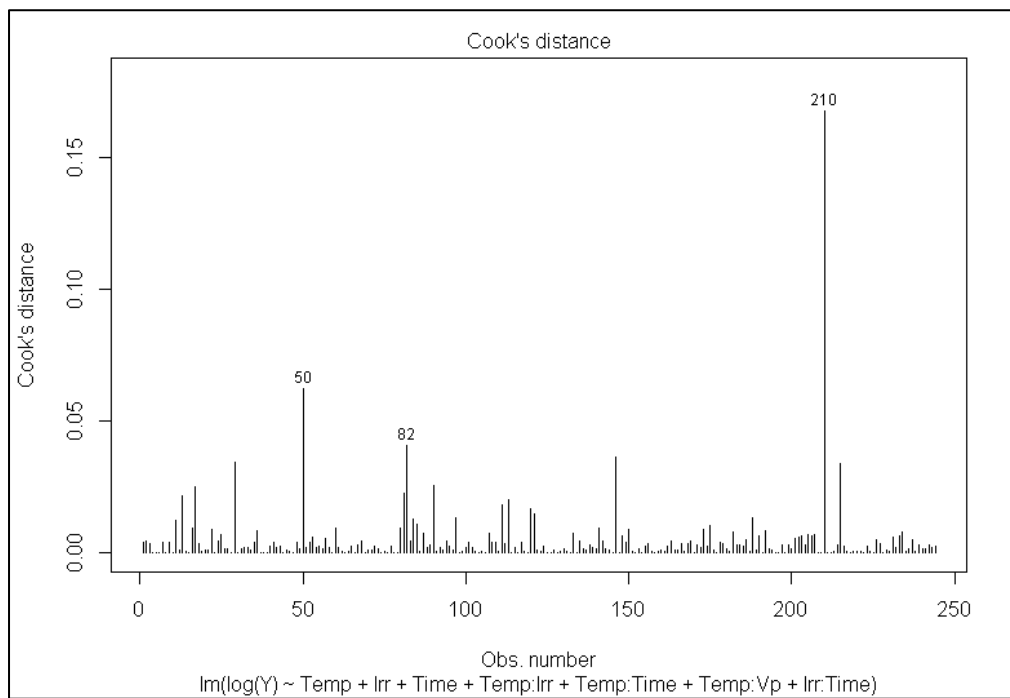
Figure A-II.12 Cook's distance for the 244 observations (Y)
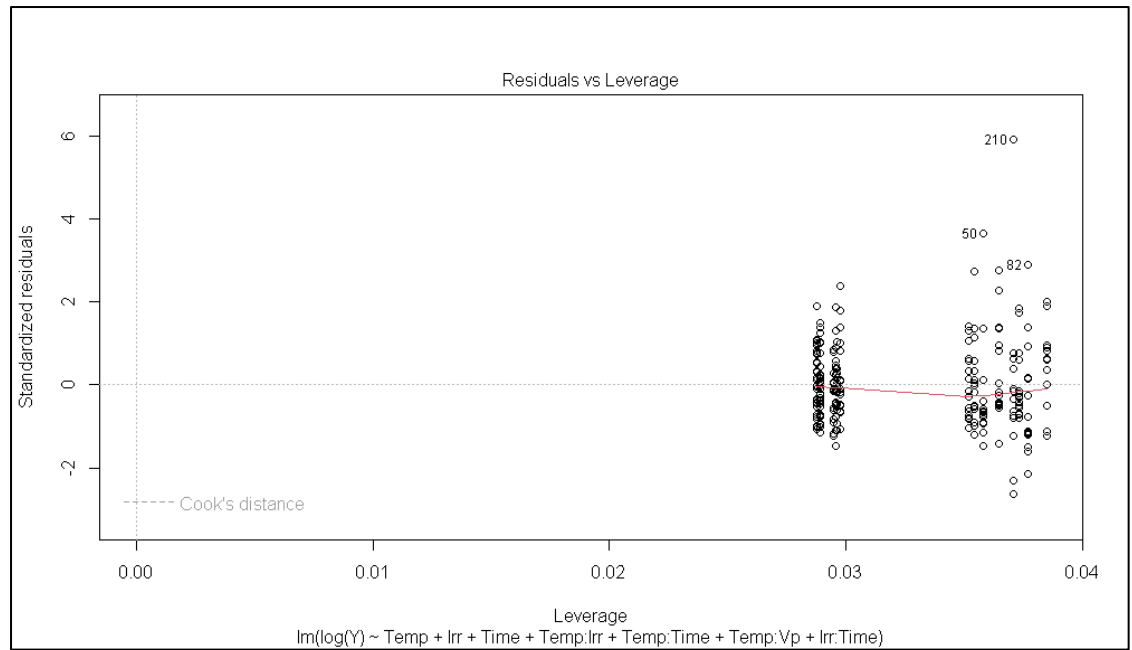
Figure A-II.13 Standardized residuals vs. leverage

Figure A-II.12 reveals that each observation's Cook distance remains below the 0.5 threshold. Moreover, Figure A-II.3 illustrates that the Cook distance, supposed to be represented as a dotted line, lies so far away from the graph that it is not depicted. This evidence points to the absence of influential values, implying that conclusions remain consistent even if certain observations are removed.
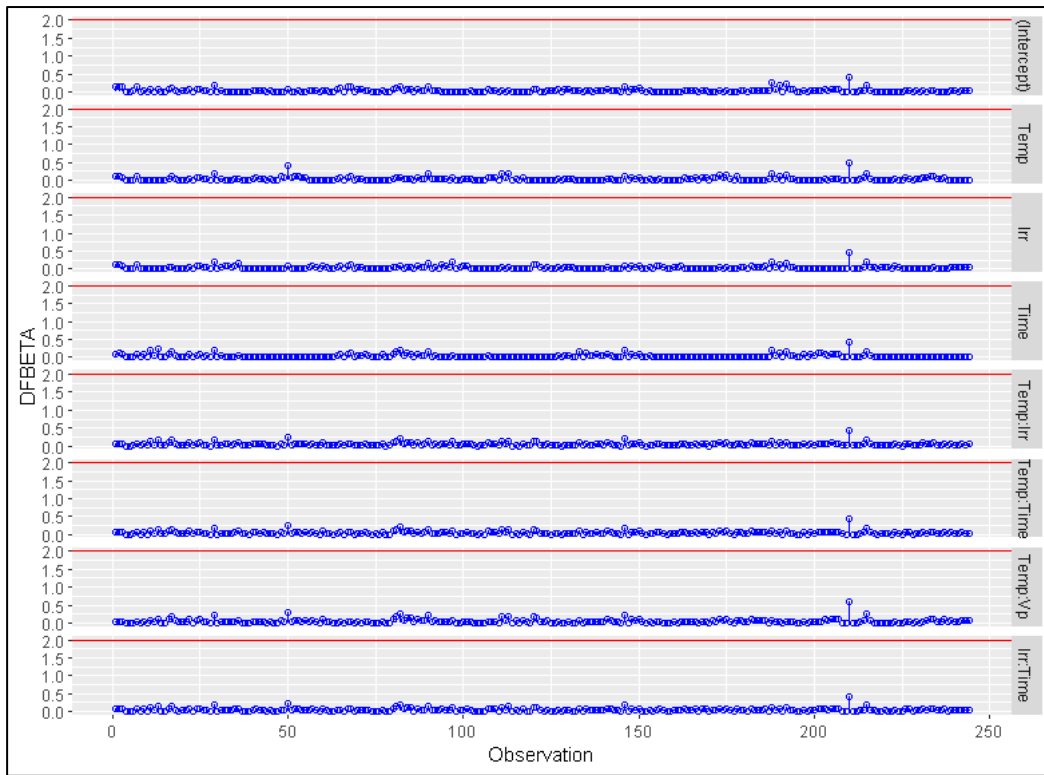
Figure A-II.14 DFBETAS for all observations as a function of each
variable in the MLR model explaining Y

DFBETAS, shown in Figure A-II.14, gauge the impact of individual observations on regression coefficients in terms of standard errors. Notably, none of the variables in the model exceed the threshold value of 2. This finding further supports the absence of influential values in the dataset.

LISTE DE RÉFÉRENCES BIBLIOGRAPHIQUES

Abdi, H., & Williams, L. J. (2010). Tukey's honestly significant difference (HSD) test. *Encyclopedia of research design, 3*(1), 1-5.

Agence de l'Environnement et de la Maîtrise de l'Énergie, A. Repéré le 2023-03-12 à https://expertises.ademe.fr/expertises/economie-circulaire

Al-Ketan, O., Rowshan, R., & Abu Al-Rub, R. K. (2018). Topology-mechanical property relationship of 3D printed strut, skeletal, and sheet based periodic metallic cellular materials. *Additive Manufacturing, 19*, 167-183. doi: https://doi.org/10.1016/j.addma.2017.12.006. Repéré à https://www.sciencedirect.com/science/article/pii/S2214860417303767

Alkadi, F., Lee, J., Yeo, J.-S., Hwang, S.-H., & Choi, J.-W. (2019). 3D printing of ground tire rubber composites. *International Journal of Precision Engineering and Manufacturing-Green Technology, 6*, 211-222.

AMTechnologies. (2022). WHITEPAPERS & CASE STUDIES. Repéré le 15-09-2022 à https://amtechnologies.com/resources/

ASTM-International. (2021). *Standard Test Method for Rubber Property—Durometer Hardness ASTM D2240-15(2021)*. doi: 10.1520/D2240-15R21. Repéré à https://compass.astm.org/document/?contentCode=ASTM%7CD2240-15R21%7Cen-US&proxycl=https%3A%2F%2Fsecure.astm.org&fromLogin=true

ASTM. (2014). *Standard Test Method for Tensile Properties of Plastics D638*.

Attaran, M. (2017). The rise of 3-D printing: The advantages of additive manufacturing over traditional manufacturing. *Business Horizons, 60*(5), 677-688. doi: https://doi.org/10.1016/j.bushor.2017.05.011. Repéré à https://www.sciencedirect.com/science/article/pii/S0007681317300897

AUTODESK. Fusion 360. Repéré à https://www.autodesk.ca/en/products/fusion-360/features

AUTODESK. NASTRAN (Version 17.0.0.21) [FEA Solver]. Repéré à https://help.autodesk.com/view/NSTRN/2017/ENU/?guid=GUID-B7044BA7-3C26-49DA-9EE7-DA7505FD4B2C

Badhotiya, G. K., Avikal, S., Soni, G., & Sengar, N. (2022). Analyzing barriers for the adoption of circular economy in the manufacturing sector. *International Journal of*

Productivity and Performance Management, 71(3), 912-931. doi: 10.1108/IJPPM-01-2021-0021. Repéré à https://doi.org/10.1108/IJPPM-01-2021-0021

Beiderbeck, D., Krüger, H., & Minshall, T. (2020). The future of additive manufacturing in sports. Dans *21st century sports* (pp. 111-132). Springer.

Bleischwitz, R., Welfens, P., & Zhang, Z. (2009). Sustainable Growth and Resource Productivity Economic and Global Policy Issues (ed. Bleischwitz.

Bohlke, T., & Bruggemann, C. (2001). Graphical Representation of the Generalized Hooke's Law. *Technische Mechanik, 21 No. 2* 145-158.

Bonenberger, P. R. (2016). The First Snap-Fit Handbook. Dans P. R. Bonenberger (Éd.), *The First Snap-Fit Handbook (Third Edition)* (pp. I-XXII). Hanser. doi: https://doi.org/10.3139/9781569905968.fm. Repéré à http://www.sciencedirect.com/science/article/pii/B9781569905951500013

Boothroyd, G. (1994). Product design for manufacture and assembly. *Computer-Aided Design, 26*(7), 505-520. doi: https://doi.org/10.1016/0010-4485(94)90082-5. Repéré à https://www.sciencedirect.com/science/article/pii/0010448594900825

Boothroyd, G., & Alting, L. (1992). Design for Assembly and Disassembly. *CIRP Annals, 41*(2), 625-636. doi: https://doi.org/10.1016/S0007-8506(07)63249-1. Repéré à https://www.sciencedirect.com/science/article/pii/S0007850607632491

Caulfield, B., McHugh, P. E., & Lohfeld, S. (2007). Dependence of mechanical properties of polyamide components on build parameters in the SLS process. *Journal of Materials Processing Technology, 182*(1), 477-488. doi: https://doi.org/10.1016/j.jmatprotec.2006.09.007. Repéré à https://www.sciencedirect.com/science/article/pii/S0924013606007886

Cavanaugh, J. E., & Neath, A. A. (2019). The Akaike information criterion: Background, derivation, properties, application, interpretation, and refinements. *WIREs Computational Statistics, 11*(3), e1460. doi: https://doi.org/10.1002/wics.1460. Repéré à https://wires.onlinelibrary.wiley.com/doi/abs/10.1002/wics.1460

Cheah, L., Ciceri, N. D., Olivetti, E., Matsumura, S., Forterre, D., Roth, R., & Kirchain, R. (2013). Manufacturing-focused emissions reductions in footwear production. *Journal of Cleaner Production, 44*, 18-29. doi: https://doi.org/10.1016/j.jclepro.2012.11.037. Repéré à http://www.sciencedirect.com/science/article/pii/S0959652612006300

CLIMATEWATCH. (2019). Dataexplorer. Repéré le 13-07-2022 à https://www.climatewatchdata.org/data-explorer/historical-emissions?historical-emissions-data-sources=cait&historical-emissions-gases=all-ghg&historical-

emissions-regions=All%20Selected&historical-emissions-sectors=total-including-lucf%2Ctotal-including-lucf&page=1#data

Commitment, C. F. S. (2020). *Final Report*. Global Fashion Agenda

Cook, R. D. (2011). Cook's Distance. Dans M. Lovric (Éd.), *International Encyclopedia of Statistical Science* (pp. 301-302). Berlin, Heidelberg: Springer Berlin Heidelberg. doi: 10.1007/978-3-642-04898-2_189. Repéré à https://doi.org/10.1007/978-3-642-04898-2_189

Dassault Systemes. CATIA V5. Repéré à https://www.3ds.com/products-services/catia/

Delpla, V., Kenné, J.-P., & Hof, L. A. (2022). Circular manufacturing 4.0: towards internet of things embedded closed-loop supply chains. *The International Journal of Advanced Manufacturing Technology, 118*(9), 3241-3264. doi: 10.1007/s00170-021-08058-3. Repéré à https://doi.org/10.1007/s00170-021-08058-3

Deshpande, V. S., Ashby, M. F., & Fleck, N. A. (2001). Foam topology: bending versus stretching dominated architectures. *Acta Materialia, 49*(6), 1035-1040. doi: https://doi.org/10.1016/S1359-6454(00)00379-7. Repéré à https://www.sciencedirect.com/science/article/pii/S1359645400003797

Dumas, M., Terriault, P., & Brailovski, V. (2017). Modelling and characterization of a porosity graded lattice structure for additively manufactured biomaterials. *Materials & Design, 121*, 383-392. doi: https://doi.org/10.1016/j.matdes.2017.02.021. Repéré à https://www.sciencedirect.com/science/article/pii/S0264127517301491

Eder-Hansen, J., Chalmer, C., Tarnerberg, S., Tochtermann, T., Seara, J., Boger, S., . . . Jager, K. (2017). *Pulse Of The Fashion Industry 2017*.

Ellen MacArthur Foundation. The circular economy in detail : Deep dive. Repéré le 2023-03-12 à https://ellenmacarthurfoundation.org/the-circular-economy-in-detail-deep-dive

Ellen MacArthur Foundation. (2015). *TOWARDS A CIRCULAR ECONOMY: BUSINESS RATIONALE FOR AN ACCELERATED TRANSITION*.

Ellen MacArthur Foundation. (2017). Circular Design. Repéré le 13-07-2022 à https://archive.ellenmacarthurfoundation.org/explore/circular-design

Ellen MacArthur Foundation, & IDEO. (2018). The Circular Design Guide. Repéré le 13-07-2022 à https://www.circulardesignguide.com/methods

EOS. PA 2200 - Polyamide 12 White. Repéré le 09/09/2022 à https://www.eos.info/en/additive-manufacturing/3d-printing-plastic/sls-polymer-materials/polyamide-pa-12-alumide

Faes, M., Wang, Y., Lava, P., & Moens, D. (2015). Variability in the mechanical properties of laser sintered PA-12 components. *Proceedings of the 26th annual international solid freeform fabrication symposium. Solid freeform fabrication symposium*, 847-856.

Fayolle, B., & Verdu, J. (2005). Vieillissement physique des matériaux polymères. *Techniques de l'ingénieur Corrosion Vieillissement, base documentaire : TIP570WEB*(ref. article : cor108). doi: https://doi.org/10.51257/a-v1-cor108. Repéré à https://www.techniques-ingenieur.fr/base-documentaire/materiaux-th11/materiaux-resistance-a-la-corrosion-et-au-vieillissement-42373210/vieillissement-physique-des-materiaux-polymeres-cor108/

Frulloni, E., Kenny, J., Conti, P., & Torre, L. (2007). Experimental study and finite element analysis of the elastic instability of composite lattice structures for aeronautic applications. *Composite structures, 78*(4), 519-528.

Gedam, V. V., Raut, R. D., Lopes de Sousa Jabbour, A. B., Tanksale, A. N., & Narkhede, B. E. (2021). Circular economy practices in a developing economy: Barriers to be defeated. *Journal of Cleaner Production, 311*, 127670. doi: https://doi.org/10.1016/j.jclepro.2021.127670. Repéré à https://www.sciencedirect.com/science/article/pii/S0959652621018886

George. Papanicolau, Alain. Bensoussan, & Lions, J.-L. (1978). *Asymptotic Analysis for Periodic Structures*. Repéré à https://www.elsevier.com/books/asymptotic-analysis-for-periodic-structures/papanicolau/978-0-444-85172-7

Gewert, B., Plassmann, M. M., & MacLeod, M. (2015). Pathways for degradation of plastic polymers floating in the marine environment. *Environmental Science: Processes & Impacts, 17*(9), 1513-1521. doi: 10.1039/C5EM00207A. Repéré à http://dx.doi.org/10.1039/C5EM00207A

Gibson, I., Rosen, D., & Stucker, B. (2014). *Additive Manufacturing Technologies: 3D Printing, Rapid Prototyping, and Direct Digital Manufacturing*. Springer New York. Repéré à https://books.google.ca/books?id=OPGbBQAAQBAJ

Giurco, D., Littleboy, A., Boyle, T., Fyfe, J., & White, S. (2014). Circular economy: questions for responsible minerals, additive manufacturing and recycling of metals. *Resources, 3*(2), 432-453.

Goodridge, R. D., Hague, R. J. M., & Tuck, C. J. (2010). Effect of long-term ageing on the tensile properties of a polyamide 12 laser sintering material. *Polymer Testing, 29*(4), 483-493. doi: https://doi.org/10.1016/j.polymertesting.2010.02.009. Repéré à https://www.sciencedirect.com/science/article/pii/S0142941810000292

Goodridge, R. D., Tuck, C. J., & Hague, R. J. M. (2012). Laser sintering of polyamides and other polymers. *Progress in Materials Science, 57*(2), 229-267. doi: https://doi.org/10.1016/j.pmatsci.2011.04.001. Repéré à https://www.sciencedirect.com/science/article/pii/S0079642511000648

Guo, J., Bai, J., Liu, K., & Wei, J. (2018). Surface quality improvement of selective laser sintered polyamide 12 by precision grinding and magnetic field-assisted finishing. *Materials & Design, 138*, 39-45. doi: https://doi.org/10.1016/j.matdes.2017.10.048. Repéré à http://www.sciencedirect.com/science/article/pii/S0264127517309759

Guo, Y., Jiang, K., & Bourell, D. L. (2015). Accuracy and mechanical property analysis of LPA12 parts fabricated by laser sintering. *Polymer Testing, 42*, 175-180. doi: https://doi.org/10.1016/j.polymertesting.2015.01.019. Repéré à https://www.sciencedirect.com/science/article/pii/S0142941815000239

Hegab, H., Khanna, N., Monib, N., & Salem, A. (2023). Design for sustainable additive manufacturing: A review. *Sustainable Materials and Technologies, 35*, e00576. doi: https://doi.org/10.1016/j.susmat.2023.e00576. Repéré à https://www.sciencedirect.com/science/article/pii/S2214993723000118

Helou, M., & Kara, S. (2018). Design, analysis and manufacturing of lattice structures: an overview. *International Journal of Computer Integrated Manufacturing, 31*(3), 243-261.

ISO. (2016). *ISO 4892-3:2016 Plastics — Methods of exposure to laboratory light sources — Part 3: Fluorescent UV lamps*. ISO 4892-3:2016. Repéré à https://www.iso.org/standard/67793.html

ISO/ASTM. (2022). *Additive manufacturing - General principles - Fundamentals and vocabulary (ISO/ASTM 52900:2021)*.

Jawahir, I. S., & Bradley, R. (2016). Technological Elements of Circular Economy and the Principles of 6R-Based Closed-loop Material Flow in Sustainable Manufacturing. *Procedia CIRP, 40*, 103-108. doi: https://doi.org/10.1016/j.procir.2016.01.067. Repéré à https://www.sciencedirect.com/science/article/pii/S2212827116000822

Kabalnov, A. S., Wright, J. T., & Kasperchik, V. (2015). *Brevet World*. HEWLETT-PACKARD DEVELOPMENT COMPANY. Repéré à https://patentscope.wipo.int/search/en/detail.jsf?docId=WO2016175748

Khaderi, S. N., Deshpande, V. S., & Fleck, N. A. (2014). The stiffness and strength of the gyroid lattice. *International Journal of Solids and Structures, 51*(23), 3866-3877. doi: https://doi.org/10.1016/j.ijsolstr.2014.06.024. Repéré à https://www.sciencedirect.com/science/article/pii/S002076831400256X

Khajavi, S. H., Partanen, J., & Holmström, J. (2014). Additive manufacturing in the spare parts supply chain. *Computers in Industry, 65*(1), 50-63. doi: https://doi.org/10.1016/j.compind.2013.07.008. Repéré à https://www.sciencedirect.com/science/article/pii/S0166361513001565

Khan, K. A., & Al-Rub, R. K. A. (2018). Modeling Time and Frequency Domain Viscoelastic Behavior of Architectured Foams. *Journal of Engineering Mechanics, 144*(6), 04018029. doi: doi:10.1061/(ASCE)EM.1943-7889.0001448. Repéré à https://ascelibrary.org/doi/abs/10.1061/%28ASCE%29EM.1943-7889.0001448

Khan, K. A., Al Hajeri, F., & Khan, M. A. (2021). Micromechanical modeling approach with simplified boundary conditions to compute electromechanical properties of architected piezoelectric composites. *Smart Materials and Structures, 30*(3), 035013. doi: 10.1088/1361-665x/abdc05. Repéré à http://dx.doi.org/10.1088/1361-665X/abdc05

Kodama, H. (1981). Automatic method for fabricating a three-dimensional plastic model with photo-hardening polymer. *Review of Scientific Instruments, 52*, 1770-1773. doi: 10.1063/1.1136492. Repéré à https://ui.adsabs.harvard.edu/abs/1981RScI...52.1770K

Kreutz, M., Böttjer, A., Trapp, M., Lütjen, M., & Freitag, M. (2022). Towards individualized shoes: Deep learning-based fault detection for 3D printed footwear. *Procedia CIRP, 107*, 196-201. doi: https://doi.org/10.1016/j.procir.2022.04.033. Repéré à https://www.sciencedirect.com/science/article/pii/S2212827122002499

Kumbhar, N. N., & Mulay, A. V. (2018). Post Processing Methods used to Improve Surface Finish of Products which are Manufactured by Additive Manufacturing Technologies: A Review. *Journal of The Institution of Engineers (India): Series C, 99*(4), 481-487. doi: 10.1007/s40032-016-0340-z. Repéré à https://doi.org/10.1007/s40032-016-0340-z

Kumke, M., Watschke, H., & Vietor, T. (2016). A new methodological framework for design for additive manufacturing. *Virtual and Physical Prototyping, 11*(1), 3-19. doi: 10.1080/17452759.2016.1139377. Repéré à https://doi.org/10.1080/17452759.2016.1139377

Lacy, P., & Rutqvist, J. (2015). *Waste to Wealth* (1 éd.). Palgrave Macmillan London. doi: https://doi.org/10.1057/9781137530707

Larson, K. (2017, 09/01). *Can You Estimate Modulus From Durometer Hardness for Silicones? Yes, but only roughly ... and you must choose your modulus carefully!* , (Form No. 11-3716-01 A S2D). Dow Website.

Lavery, G., Pennell, N., & Evans, S. (2014). Food and Beverage Sector Non-Labour Resource Efficiency: Unlocking Cost Savings, Jobs and Environmental Improvements. *Preuzeto*

sa: http://laverypennell.   com/wpcontent/uploads/2014/03/Food-and-Beverage-Resource-Efficiency. pdf.

Lee, M. J., & Rahimifard, S. (2012). An air-based automated material recycling system for postconsumer footwear products. *Resources, Conservation and Recycling, 69*, 90-99. doi: https://doi.org/10.1016/j.resconrec.2012.09.008.   Repéré   à http://www.sciencedirect.com/science/article/pii/S0921344912001693

LehVossGroup. (2019). LUVOSINT TPU X92A-1 NT. Repéré le 09/09/2022 à https://luv-lumas-online-app.azurewebsites.net/api/v1/lumas/gettdsfile/41447859/en/ISO

Lezama-Nicolás, R., Rodríguez-Salvador, M., Río-Belver, R., & Bildosola, I. (2018). A bibliometric method for assessing technological maturity: the case of additive manufacturing. *Scientometrics, 117*(3), 1425-1452. doi: 10.1007/s11192-018-2941-1. Repéré à https://doi.org/10.1007/s11192-018-2941-1

Li, Z., & Bradt, R. C. (1987). The single-crystal elastic constants of cubic (3C) SiC to 1000° C. *Journal of Materials Science, 22*(7), 2557-2559. doi: 10.1007/BF01082145. Repéré à https://doi.org/10.1007/BF01082145

Ligon, S. C., Liska, R., Stampfl, J., Gurr, M., & Mülhaupt, R. (2017). Polymers for 3D Printing and Customized Additive Manufacturing. *Chemical Reviews, 117*(15), 10212-10290. doi: 10.1021/acs.chemrev.7b00074.   Repéré   à https://doi.org/10.1021/acs.chemrev.7b00074

Liu, S., & Welsh, A. H. (2011). Regression Diagnostics. Dans M. Lovric (Éd.), *International Encyclopedia of Statistical Science* (pp. 1206-1208). Berlin, Heidelberg: Springer Berlin   Heidelberg.   doi: 10.1007/978-3-642-04898-2_484.   Repéré   à https://doi.org/10.1007/978-3-642-04898-2_484

Maconachie, T., Leary, M., Lozanovski, B., Zhang, X., Qian, M., Faruque, O., & Brandt, M. (2019). SLM lattice structures: Properties, performance, applications and challenges. *Materials & Design, 183*, 108137. doi: https://doi.org/10.1016/j.matdes.2019.108137. Repéré à https://www.sciencedirect.com/science/article/pii/S0264127519305751

Manoharan, V., Chou, S. M., Forrester, S., Chai, G. B., & Kong, P. W. (2013). Application of additive manufacturing techniques in sports footwear: This paper suggests a five-point scoring technique to evaluate the performance of four AM techniques, namely, stereolithography (SLA), PolyJet (PJ), selective laser sintering (SLS) and three-dimensional printing (3DP), in four important aspects of accuracy, surface finish, range of materials supported and building time for prototyping sports footwear. *Virtual and Physical Prototyping, 8*(4), 249-252.

112

Mathieux, F., Ardente, F., Bobba, S., Nuss, P., Blengini, G. A., Dias, P. A., . . . Pavel, C. (2017). Critical raw materials and the circular economy. *Publications Office of the European Union: Bruxelles, Belgium.*

McDowall, W., Geng, Y., Huang, B., Barteková, E., Bleischwitz, R., Türkeli, S., . . . Doménech, T. (2017). Circular Economy Policies in China and Europe. *Journal of Industrial Ecology, 21*(3), 651-661. doi: https://doi.org/10.1111/jiec.12597. Repéré à https://onlinelibrary.wiley.com/doi/abs/10.1111/jiec.12597
https://onlinelibrary.wiley.com/doi/pdfdirect/10.1111/jiec.12597?download=true

Meththananda, I. M., Parker, S., Patel, M. P., & Braden, M. (2009). The relationship between Shore hardness of elastomeric dental materials and Young's modulus. *Dental Materials, 25*(8), 956-959. doi: https://doi.org/10.1016/j.dental.2009.02.001. Repéré à https://www.sciencedirect.com/science/article/pii/S0109564109001237

Mix, A., & Giacomin, A. (2011). Standardized Polymer Durometry. *Journal of Testing and Evaluation, 39*(4), 696-705. doi: 10.1520/JTE103205. Repéré à https://compass.astm.org/DIGITAL_LIBRARY/JOURNALS/TESTEVAL/PAGES/JTE103205.htm

Mix, A. W., & Giacomin, A. J. (2011). Standardized Polymer Durometry. *Journal of Testing and Evaluation, 39*(4), 696-705. doi: 10.1520/JTE103205. Repéré à http://www.astm.org/cgi-bin/doiLink.cgi?JTE103205

Nordmann, J., Aßmus, M., & Altenbach, H. (2018). Visualising elastic anisotropy: theoretical background and computational implementation. *Continuum Mechanics and Thermodynamics, 30*(4), 689-708. doi: 10.1007/s00161-018-0635-9. Repéré à https://doi.org/10.1007/s00161-018-0635-9

nTopology_Inc. nTop. Repéré le 21/09/2022 à https://ntopology.com/

OCDE. (2015). *Material Resources, Productivity and the Environment.* doi: doi:https://doi.org/10.1787/9789264190504-en. Repéré à https://www.oecd-ilibrary.org/content/publication/9789264190504-en

OCDE. (2022). Utilisation de plastiques par région - projections (Publication no. doi:https://doi.org/10.1787/636cfa71-fr). Consultée le, à https://www.oecd-ilibrary.org/content/data/636cfa71-fr

Osswald, T. A. (2017). Understanding Polymer Processing. Dans T. A. Osswald (Éd.), *Understanding Polymer Processing (Second Edition)* (pp. I-XVI). Hanser. doi: https://doi.org/10.3139/9781569906484.fm. Repéré à https://www.sciencedirect.com/science/article/pii/B9781569906477500012

Overshoot. (2021). Past Earth Overshoot Days. Repéré le 07-01-2022 à https://www.overshootday.org/newsroom/past-earth-overshoot-days/

Pilipović, A., Ilinčić, P., Bakić, A., & Kodvanj, J. (2022). Influence of Atmospheric Conditions on Mechanical Properties of Polyamide with Different Content of Recycled Material in Selective Laser Sintering. *Polymers, 14*(12), 2355. Repéré à https://www.mdpi.com/2073-4360/14/12/2355

Pugalendhi, A., Ranganathan, R., & Chandrasekaran, M. (2020). Effect of process parameters on mechanical properties of VeroBlue material and their optimal selection in PolyJet technology. *The International Journal of Advanced Manufacturing Technology, 108*(4), 1049-1059. doi: 10.1007/s00170-019-04782-z. Repéré à https://doi.org/10.1007/s00170-019-04782-z
https://link.springer.com/content/pdf/10.1007/s00170-019-04782-z.pdf

Puttonen, T., Salmi, M., & Partanen, J. (2021). Mechanical properties and fracture characterization of additive manufacturing polyamide 12 after accelerated weathering. *Polymer Testing, 104*, 107376. doi: https://doi.org/10.1016/j.polymertesting.2021.107376. Repéré à https://www.sciencedirect.com/science/article/pii/S0142941821003214

Q-LAB. Q-SUN XE-3 XENON TEST CHAMBER. Repéré le 18/10/2022 à https://www.q-lab.com/en-gb/products/q-sun-xenon-arc-test-chambers/q-sun-xe-3

Q-LAB. *Sunlight, Weathering & Light Stability Testing -TECHNICAL BULLETIN LU-0822* (nº TECHNICAL BULLETIN LU-0822). Repéré à https://www.q-lab.com/documents/public/cd131122-c252-4142-86ce-5ba366a12759.pdf

Richaud, E., & Verdu, J. (2011). VieiIlissement chimique des polymères Mécanismes de dégradation. *Techniques de l'ingénieur Matériaux : résistance à la corrosion et au vieillissement, base documentaire : TIB373DUO*(ref. article : am3151). doi: https://doi.org/10.51257/a-v2-am3151. Repéré à https://www.techniques-ingenieur.fr/base-documentaire/materiaux-th11/materiaux-resistance-a-la-corrosion-et-au-vieillissement-42373210/vieiilissement-chimique-des-polymeres-am3151/

Rosso, S., Meneghello, R., Biasetto, L., Grigolato, L., Concheri, G., & Savio, G. (2020). In-depth comparison of polyamide 12 parts manufactured by Multi Jet Fusion and Selective Laser Sintering. *Additive Manufacturing, 36*, 101713. doi: https://doi.org/10.1016/j.addma.2020.101713. Repéré à http://www.sciencedirect.com/science/article/pii/S221486042031085X

Rouf, S., Raina, A., Irfan Ul Haq, M., Naveed, N., Jeganmohan, S., & Farzana Kichloo, A. (2022). 3D printed parts and mechanical properties: Influencing parameters, sustainability aspects, global market scenario, challenges and applications. *Advanced Industrial and Engineering Polymer Research, 5*(3), 143-158. doi:

https://doi.org/10.1016/j.aiepr.2022.02.001.   Repéré   à
https://www.sciencedirect.com/science/article/pii/S254250482200001X

Salmi, M. (2021). Additive Manufacturing Processes in Medical Applications. *Materials, 14*(1), 191. Repéré à https://www.mdpi.com/1996-1944/14/1/191

Santander, P., Sanchez, F. A. C., Boudaoud, H., & Camargo, M. (2020). Closed loop supply chain network for local and distributed plastic recycling for 3D printing: a MILP-based optimization approach. *Resources, Conservation and Recycling, 154*, 104531.

Sassanelli, C., Rosa, P., Rocca, R., & Terzi, S. (2019). Circular economy performance assessment methods: A systematic literature review. *Journal of Cleaner Production, 229*, 440-453. doi: https://doi.org/10.1016/j.jclepro.2019.05.019. Repéré à https://www.sciencedirect.com/science/article/pii/S0959652619315355

Sauerwein, M., Bakker, C., & Balkenende, A. (2017). Additive manufacturing for circular product design : A literature review from a design perspective. Dans *PLATE: Product Lifetimes And The Environment: Conference Proceedings of PLATE 2017,* (Vol. 9, pp. 358). IOS Press. doi: 10.3233/978-1-61499-820-4-358

Sauerwein, M., Doubrovski, E., Balkenende, R., & Bakker, C. (2019). Exploring the potential of additive manufacturing for product design in a circular economy. *Journal of Cleaner Production, 226*, 1138-1149. doi: https://doi.org/10.1016/j.jclepro.2019.04.108. Repéré à https://www.sciencedirect.com/science/article/pii/S0959652619311850

Schmidt, J., Dechet, M. A., Gómez Bonilla, J. S., Hesse, N., Bück, A., & Peukert, W. (2019). *Characterization of Polymer Powders for Selective Laser Sintering* présentée à 30th Annual International Solid Freeform Fabrication Symposium Austin, Texas doi: http://dx.doi.org/10.26153/tsw/17314

Seltzer, R., de la Escalera, F. M., & Segurado, J. (2011). Effect of water conditioning on the fracture behavior of PA12 composites processed by selective laser sintering. *Materials Science and Engineering: A, 528*(22), 6927-6933. doi: https://doi.org/10.1016/j.msea.2011.05.045. Repéré à https://www.sciencedirect.com/science/article/pii/S0921509311005946

Shackleford, A. S. D., Williams, R. J., Brown, R., Wingham, J. R., & Majewski, C. (2021). Degradation of Laser Sintered polyamide 12 parts due to accelerated exposure to ultraviolet radiation. *Additive Manufacturing, 46*, 102132. doi: https://doi.org/10.1016/j.addma.2021.102132. Repéré à https://www.sciencedirect.com/science/article/pii/S2214860421002967

Shang, J., Chen, L., Zhang, S., Zhang, C., Huang, J., Wang, X., . . . Ma, X. (2020). Influence of high-heeled shoe parameters on biomechanical performance of young female adults during stair ascent motion. *Gait & Posture, 81*, 159-165. doi:

https://doi.org/10.1016/j.gaitpost.2020.07.065.   Repéré   à
http://www.sciencedirect.com/science/article/pii/S0966636220303076

Sher, D. (2020). Five footwear industry leaders using 3D printing for production today
Repéré le 02/08/2023 à https://www.voxelmatters.com/five-footwear-industry-leaders-using-3d-printing-for-production-today/

Sillani, F., Kleijnen, R. G., Vetterli, M., Schmid, M., & Wegener, K. (2019). Selective laser sintering and multi jet fusion: Process-induced modification of the raw materials and analyses of parts performance. *Additive Manufacturing, 27*, 32-41. doi: https://doi.org/10.1016/j.addma.2019.02.004.   Repéré   à
http://www.sciencedirect.com/science/article/pii/S2214860418308972

Spahiu, T., Almeida, H., Manavis, A., Kyratsis, P., & Jimeno-Morenilla, A. (2021). Industry 4.0 for Sustainable Production in Footwear Industry. Dans J. R. da Costa Sanches Galvão, P. S. Duque de Brito, F. dos Santos Neves, F. G. da Silva Craveiro, H. de Amorim Almeida, J. O. Correia Vasco, L. M. Pires Neves, R. de Jesus Gomes, S. de Jesus Martins Mourato & V. S. Santos Ribeiro (Éds.), *Proceedings of the 1st International Conference on Water Energy Food and Sustainability (ICoWEFS 2021)* (pp. 699-707). Springer International Publishing.

Stahel, W. R. (2020). History of the Circular Economy. The Historic Development of Circularity and the Circular Economy. Dans S. Eisenriegler (Éd.), *The Circular Economy in the European Union: An Interim Review* (pp. 7-19). Cham: Springer International Publishing. doi: 10.1007/978-3-030-50239-3_2. Repéré à https://doi.org/10.1007/978-3-030-50239-3_2

Strömberg, N. (2022). A new multi-scale topology optimization framework for optimal combinations of macro-layouts and local gradings of TPMS-based lattice structures. *Mechanics Based Design of Structures and Machines*, 1-18. doi: 10.1080/15397734.2022.2107538.   Repéré   à
https://doi.org/10.1080/15397734.2022.2107538

Su, A., & Al'Aref, S. J. (2018). Chapter 1 - History of 3D Printing. Dans S. J. Al'Aref, B. Mosadegh, S. Dunham & J. K. Min (Éds.), *3D Printing Applications in Cardiovascular Medicine* (pp. 1-10). Boston: Academic Press. doi: https://doi.org/10.1016/B978-0-12-803917-5.00001-8.   Repéré   à
https://www.sciencedirect.com/science/article/pii/B9780128039175000018

Tan, L. J., Zhu, W., & Zhou, K. (2020). Recent Progress on Polymer Materials for Additive Manufacturing. *Advanced Functional Materials, 30*(43), 2003062. doi: https://doi.org/10.1002/adfm.202003062.   Repéré   à
https://onlinelibrary.wiley.com/doi/abs/10.1002/adfm.202003062

116

Team, R. C. (2022). R: A Language and Environment for Statistical Computing: R Foundation for Statistical Computing. Repéré à https://www.R-project.org/

Teixeira, R., Coelho, C., Oliveira, J., Gomes, J., Pinto, V. V., Ferreira, M. J., . . . Carneiro, O. S. (2021). Towards Customized Footwear with Improved Comfort. *Materials, 14*(7), 1738. Repéré à https://www.mdpi.com/1996-1944/14/7/1738

Teskan. Teskan F-Scan System. Repéré le 01-02-2021 à https://www.tekscan.com/products-solutions/systems/f-scan-system

Thomasson, E., & Michalska, A. (2017, 7 april 2017). Adidas to mass-produce 3D-printed shoe with Silicon Valley start-up. Repéré le 12-09-2022 à https://www.reuters.com/article/us-adidas-manufacturing-idUSKBN1790F6?feedType=RSS&feedName=technologyNews&utm_source=Twitter&utm_medium=Social&utm_campaign=Feed%3A+reuters%2FtechnologyNews+%28Reuters+Technology+News%29

Ticona. (2009). *Design calculations for snap fit joints in plastic parts*.

Wang, G., Wang, P., Zhen, Z., Zhang, W., & Ji, J. (2015). Preparation of PA12 microspheres with tunable morphology and size for use in SLS processing. *Materials & Design, 87*, 656-662. doi: https://doi.org/10.1016/j.matdes.2015.08.083. Repéré à https://www.sciencedirect.com/science/article/pii/S0264127515303324

Wang, Z., Srinivasa, A., Reddy, J. N., & Dubrowski, A. (2022). Topology Optimization of Lightweight Structures With Application to Bone Scaffolds and 3D Printed Shoes for Diabetics. *Journal of Applied Mechanics, 89*(4). doi: 10.1115/1.4053396. Repéré à https://doi.org/10.1115/1.4053396

WorldFootwear.com. (2020). *Word Footwear Yearbook 2020*. Repéré à file:///C:/Users/15146/Downloads/wf20201557987749.pdf

Wörz, A., Wudy, K., Drummer, D., Wegner, A., & Witt, G. (2018). Comparison of long-term properties of laser sintered and injection molded polyamide 12 parts. *Journal of Polymer Engineering, 38*(6), 573-582. doi: doi:10.1515/polyeng-2017-0227. Repéré à https://doi.org/10.1515/polyeng-2017-0227

Wu, Y., Lu, Y., Zhao, M., Bosiakov, S., & Li, L. (2022). A Critical Review of Additive Manufacturing Techniques and Associated Biomaterials Used in Bone Tissue Engineering. *Polymers (Basel), 14*(10). doi: 10.3390/polym14102117

WWF. (2012). *Biodiversity, biocapacity and better choices* (ISBN 978-2-940443-37-6). Repéré à

http://awsassets.panda.org/downloads/1_lpr_2012_online_full_size_single_pages_final_120516.pdf